

2016

Properties and Applications of Self-Assembled Benzophenone Bis-Urea Macrocycles

Arthur Ariston Korous
University of South Carolina

Follow this and additional works at: <https://scholarcommons.sc.edu/etd>

 Part of the [Chemistry Commons](#)

Recommended Citation

Korous, A. A. (2016). *Properties and Applications of Self-Assembled Benzophenone Bis-Urea Macrocycles*. (Master's thesis). Retrieved from <https://scholarcommons.sc.edu/etd/3737>

This Open Access Thesis is brought to you by Scholar Commons. It has been accepted for inclusion in Theses and Dissertations by an authorized administrator of Scholar Commons. For more information, please contact dillarda@mailbox.sc.edu.

**PROPERTIES AND APPLICATIONS OF SELF-ASSEMBLED
BENZOPHENONE *BIS*-UREA MACROCYCLES**

by

Arthur Ariston Korous

Bachelor of Arts
Winthrop University, 2013

Submitted in Partial Fulfillment of the Requirements

For the Degree of Master of Science in

Chemistry

College of Arts and Sciences

University of South Carolina

2016

Accepted by:

Linda Shimizu, Director of Thesis

Sheryl Wiskur, Reader

Lacy Ford, Senior Vice Provost and Dean of Graduate Studies.

ACKNOWLEDGEMENTS

Thanks to Dr. Shimizu for her endless patience and constant help. Thanks to the Shimizu lab group as well for answering my constant stream of questions (especially Sahan Salpage and Ballie DeHaven).

A special thanks goes to USC and NSF for funding this research.

ABSTRACT

Supramolecular chemistry is a vast multidisciplinary field with great potential and application. It is driven by one simple concept, the self-assembly of small building blocks into larger complex architectures without application of external force. This thesis highlights previous applications of supramolecular chemistry in addition to new potential properties and applications. Recently, the Shimizu group reported a self-assembled benzophenone *bis*-urea macrocycle (host **1**) that facilitated the selective oxidation of an encapsulated alkene when UV-irradiated in an oxygen atmosphere to afford products that are typically observed in radical mediated reactions.¹ Surprisingly, the host displayed a stable room temperature radical upon UV irradiation. It is not known if the host **1** radical plays a role in the oxidation of the encapsulated guest. This thesis investigates the structure and properties of host **1**, a ¹⁵N labeled host and a urea protected derivative before and after UV-irradiation through electron paramagnetic resonance (EPR), IR, UV-vis, fluorescence, and computational analysis.

TABLE OF CONTENTS

Acknowledgements	ii
Abstract	iii
List of Figures	v
Chapter 1 Supramolecular Chemistry: Introduction to Chemistry Beyond the Molecule...1	
Chapter 2 Investigation of the Unusual Room Temperature Stable Radical Observed for Assembled Benzophenone Bis-Urea Macrocycle.....	39
Bibliography	111

LIST OF FIGURES

Figure 1.1. (a) Guanine: Cytosine 3 point and Adenine: Thymine 2 point hydrogen bonding interaction. (b) DNA helical assembly as dictated by base pair assembly motif.....3

Figure 1.2. (a) Schematic representation of van der Waals forces. Space filling models of (b) n-butane, (c) 2-methylpropane, and (d) n-dodecane that highlight differences in overlap that contribute to the induced electrical interactions.....7

Figure 1.3. Hydrogen bonding interactions vary in their geometry as seen with (a) the linear geometry exemplified by $\text{HCH}\cdots\text{HF}$, (b) trigonal planar by $\text{H}_2\text{CO}\cdots\text{HF}$, (c) carboxylic acid dimer of *p*-tolueic acid, and (d) the three centered interactions of ureas....9

Figure 1.4. (a) Schematic representation of dipole-dipole attractive interactions. (b) Interaction and orientation between 2-propanone molecules via dipole-dipole forces.....9

Figure 1.5. Schematic representation of (a) hexafluorobenzene-benzene adopting a sandwich conformation, (b) benzene-benzene in an edge-to-face conformation, and (c) benzene-benzene in a staggered conformation.11

Figure 1.6. Schematic representation of (a) ion-ion interactions of NaCl and CaCO_3 salts and (b) ion-dipole interaction between water and sodium ions.....12

Figure 1.7. Representation of the (a) zinc-oxygen framework seen in Fisher's MOF and the (b) nickel-oxygen octahedral seen in Chang's MOF.....14

Figure 1.8. (a) Lock and key model demonstrated by substrate and size/shape specific enzyme active site and (b) schematic representation of assembly of complementary building blocks.....15

Figure 1.9. Meijer's (a) ureidotriazine building blocks that assemble through a 4-point hydrogen bonding and solvophobic assembly motif into (b) chiral helical complexes.....16

Figure 1.10. Schematic representation of how dipole-dipole interactions can influence supramolecular assembly into (a) sandwich and (b) staggered conformations. Perpendicular geometries are also possible.18

Figure 1.11. (a) Cram's supramolecular dimer that assembles through binding of methyl groups on adjacent rings (b) Rebek's supramolecular dimeric capsule that assembles

through a bifurcated hydrogen bonded motif. (c) Gibbs octa acid dimer used by Ramamurthy as a nanoscale supramolecular capsule.....21

Figure 1.12. (a) Wasielewski's DABCO chlorophyll trimer and (b) Fujita's tetrameric cage.....22

Figure 1.13. Schematic representations of (a) covalent polymers and (b) supramolecular polymers.....24

Figure 1.14. Schematic representation of (a) DeSantis' cyclic building block consisting of alternating D and L peptides and (b) Ghadiri's cyclic alternating polypeptide consisting of 8 peptides that assemble into hollow nanotubular complexes.....25

Figure 1.15. (a) Zimmerman's ureido-naphthyridine oligomer and (b) Bouteiller's bis-urea based polymer27

Figure 1.16. Schematic representation and assembly of (a) Karle's cysteine-based bis-urea macrocycles and (b) Shimizu's bis-urea macrocycles28

Figure 1.17. Schematic representation of (a) the dimerization within assembled host **1** cavity and (b) product distribution for the selective dimerization of coumarin, 6-methylcoumarin, and 7-methylcoumarin.....29

Figure 2.1. Judicious choice of pyridyl ligands by the Fujita group afford smaller and larger cages. a) Smaller of the two cages resulting from the assembly of two 1,3,5-tris(4-pyridylmethyl)benzene with three Pd(NO₃)₂ molecules.¹² b) Larger cages resulting from the assembly of tridentate ligands, with varying length modifications from aromatic groups, with six Pd(NO₃)₂ molecules.....42

Figure 2.2. Benzophenone has been shown to absorb 320-370 nm light for n-π* transitions and 240-300 nm light π-π* transitions. Upon absorption, benzophenone is excited from the singlet ground state to the singlet excited state. The singlet excited then undergoes intersystem crossing to the more stable triplet excited state. The triplet excited state can then transfer energy to a suitable acceptor molecule.....44

Figure 2.3. (a) Structure of host **1** macrocycle and its hydrogen bonded assembly motif and (b) host **1** cavity dimensions. (c) Structure of bis-urea phenyl ether macrocycle (host **2**).....46

Figure 2.4. (a) Schematic representation of host **1** guest loading and conversion, (b) isomerization of *trans*-β-methylstyrene,²⁴ (c) selective oxidation of 2-methyl-2-butene, (d) and selective oxidation of cumene facilitated by host **1**.....47

Figure 2.5. Geer's EPR analysis before and after 1h UV irradiation of (a) host **1** empty, (b) host **1**•2-methyl-2-butene, and (c) host **1**•2cumene.....48

Figure 2.6. The excitation of benzophenone to the ketyl radical state with the corresponding energetic states. Benzophenone upon UV irradiation is excited to a singlet excited state. This state then undergoes intersystem crossing to the triplet excited state. If there is a suitable proton in close proximity then the di radical will abstract the proton resulting in a benzophenone ketyl radical in a doublet excited state.....52

Figure 2.7. Crystal structure of assembled host **1** with 90% order of DMSO molecules pointing in the same direction. (a) Space fill model of DMSO from crystal structure highlighting its molecular dipole, (b) host **1** crystal structure with DMSO removed showing the partial charges associated with the urea functionality and (c) host **1**•DMSO structure front view with partial charges aligned with ordered DMSO guest molecules...58

Figure 2.8. Front and top view of host **1** X-ray crystal structure (a) before and (b) after 30 min UV irradiation.....59

Figure 2.9. EPR analysis on host **1**•DMSO, purified by three recrystallization cycles, before and after 30 min UV irradiation.....61

Figure 2.10. Host **1** (empty) EPR analysis before and after 30 min UV irradiation under Argon atmosphere after the (a) 1st, (b) 2nd, and (c) 3rd recrystallization cycles.....62

Figure 2.11. Host **1**•DMSO dark quenching EPR analysis over nine days.....64

Figure 2.12. (a) Structure of host **1a**, (b) Dewal and Smith's host **1a** crystal structure showing a staggered columnar assembly with disordered chloroform molecules in the interstitial space and (c) EPR comparison between UV irradiated host **1** and host **1a**.....66

Figure 2.13. (a) PXRD comparison of host **1** (DMSO) and host **1** (precipitate) and (b) EPR comparison of unassembled, precipitate, and assembled host **1** after UV irradiation.....67

Figure 2.14. (a) Host **1** and its ¹⁵N labeled analogue with the (b) resulting EPR spectra after 30 min UV irradiation.....70

Figure 2.15. EPR comparison at 20, 50, and 100 °C for host **1** (empty) and ¹⁵N labeled host **1**.....72

Figure 2.16. IR comparison of solid host **1** (empty) before (black line) and after (red line) UV irradiation.....74

Figure 2.17. UV-vis comparison of solid host **1** (empty) before (black line) and after (red line) UV irradiation. UV irradiated host **1** shows similar λ_{max} values at 304 and 355 nm but may display a new band with λ_{max} at 588 nm.....76

Figure 2.18. Emission spectra comparison of solid host **1** (empty) before (black line) and after (red line) UV irradiation. Scan range was 375 to 525 nm using λ_{ex} =355 nm as the excitation wavelength.....77

Figure 2.19. (a) Schematic representation of benzophenone radical generation with the corresponding excited states and (b) the energetic states computationally compared between benzophenone and host 1	80
Figure 2.20. Energetics of ground singlet, singlet excited, triplet excited, and doublet excited states for a.) benzophenone and b.) host 1	82
Figure 2.21. (a) Schematic representation of sample preparation and magnetic data from SQUID analysis for (b) ambient light exposed host 1 •DMSO complex, (c) UV irradiated host 1 •DMSO complex, (d) and UV irradiated host 1 (empty) complex.....	84
Figure 2.22. Comparison of product distribution of 1-methylcyclohexene oxidation via photooxygenation and OCl ⁻ /H ₂ O ₂	86
Figure 2.23. Desorption of 1-methylcyclohexene from host 1 nanochamber via TGA. Host: guest ratio was determined to be 2:1.....	87
Figure 2.24. Desorption of 1-methylcyclohexene from host 1 nanochamber via TGA. Host: guest ratio was determined to be 2:1.....	88
Figure 2.25. ¹ H-NMR (300 MHz, CDCl ₃) of 4,4'-bis (bromomethyl) benzophenone....	92
Figure 2.26. ¹³ C-NMR (75 MHz, CDCl ₃) of 4,4'-bis (bromomethyl) benzophenone.....	93
Figure 2.27. ¹ H-NMR (300 MHz, CDCl ₃) of host 1a	94
Figure 2.28. ¹ H-NMR (300 MHz, δ ₆ -DMSO) of ¹⁵ N labeled host 1	95
Figure 2.29. ¹ H-NMR (300 MHz, δ ₆ -DMSO) of ¹⁵ N labeled host 1a	96
Figure 2.30. ¹ H-NMR (300 MHz, δ ₆ -DMSO) of ¹⁵ N labeled host 1	97
Figure 2.31. ¹³ C-NMR (75 MHz, δ ₆ -DMSO) of ¹⁵ N labeled host 1	98

CHAPTER 1

SUPRAMOLECULAR CHEMISTRY: INTRODUCTION TO CHEMISTRY BEYOND THE MOLECULE

1.1 Abstract

Supramolecular chemistry is a vast multidisciplinary field with great potential and application. It is driven by one simple concept, the self-assembly of small building blocks into larger complex architectures without application of external force. This chapter discusses the non-covalent interactions that drive self-assembly and highlights how these forces can be applied in supramolecular design. Supramolecular assemblies resulting from van der Waals forces, hydrogen bonding, and dative bonds are discussed. Simple architectures are achieved from the assembly of two, three and four units forming dimers, trimers and tetramers respectively. Assemblies that have application in guest encapsulation, molecular recognition, and selective transformation are also highlighted. These examples have inspired much of our current research. The Shimizu group utilizes *bis*-urea macrocycles consisting of two ureas and two C-shaped spacers that predictably assemble in columnar nanotubes through hydrogen bonding. These materials can be tuned by modifying the C-shape spacers between the ureas. The examples discussed within this chapter show applications of previously reported supramolecular complexes and highlights the utility of tunable supramolecular assemblies with multiple applications such as *bis*-urea macrocycle systems.

1.2 Introduction

The assembly of small units into larger complexes is a process that has been studied by scientists long before it was its own subdivision of chemistry. Self-assembly describes the formation of discrete architectures from building blocks that can range in size from atoms and molecules up to macroscopic units without help or guidance from an exterior source.¹ Early examples of assembly were typically observed in biological systems such as the pairing of nucleotide bases and the interactions that dictate their assembly. It is well known that nucleotide bases can interact with their complementary base pairs via hydrogen bonding interactions.^{2,3} When these base pairs are included in a DNA backbone strand, they cause the strand to hydrogen bond to a partner strand. The aryl stacking of these hydrogen bonded base pairs then forms DNA with its classical double helix architecture (Figure 1.1.). While it has been known for quite some time that smaller units can self-assemble into functional materials, the field of supramolecular chemistry wasn't defined until 1969 by Lehn as the "chemistry beyond the molecule".⁴

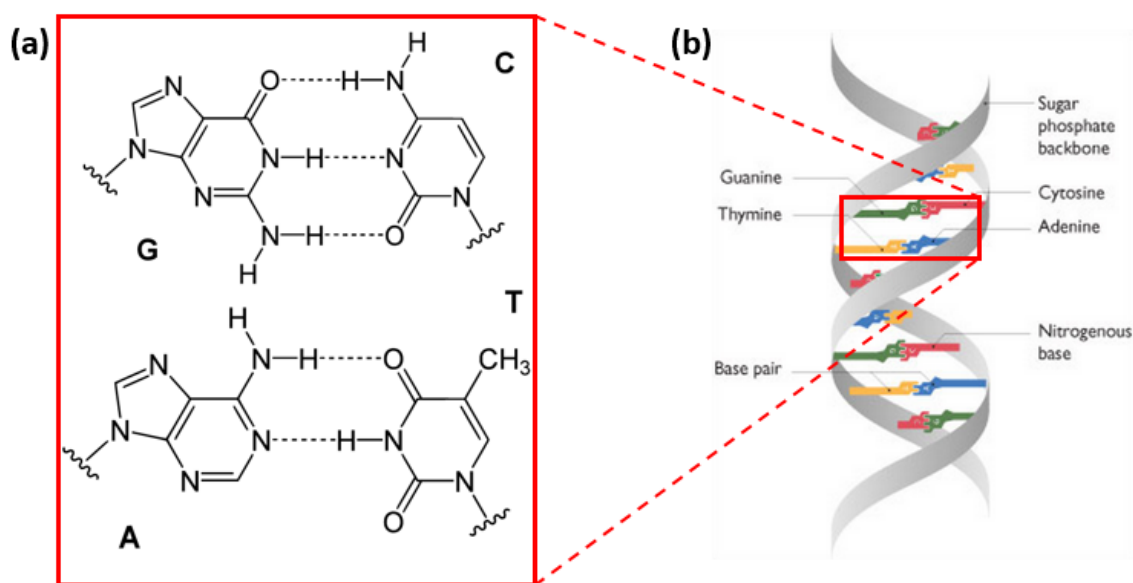


Figure 1.1. (a) Guanine: Cytosine 3 point and Adenine: Thymine 2 point hydrogen bonding interaction. (b) DNA helical assembly as dictated by base pair assembly motif.

The above biological example highlights the important key concept of the assembly of smaller units into larger complexes via non-covalent interactions. What is particularly interesting about non-covalent interactions is how the forces are capable of dictating the assembly of small building blocks into large ordered complexes despite being weak interactions. Non-covalent interactions such as hydrogen bonding, π - π stacking, or ion pairing have been used to build self-assembled structures from two or more monomers.⁵⁻⁷ The zipping of DNA also highlights how supramolecular assembly can be utilized in the formation of large intricate systems without complex synthesis. The controlled self-assembly of small molecules with well-defined association properties is an easier and more economical way than the direct synthesis of a similar complex covalent structure.⁸

The self-assembly process can occur without any external force to give thermodynamically stable systems.^{9,10} This supramolecular process can occur between two or more of the same type of molecule or govern the assembly of several different types of molecules into an intricate ordered structure. We will consider these systems more in section 1.5. Biological systems can also form assemblies that are less thermodynamically stable with help, in the form of chaperones etc.^{11,12} The environment in which assembly occurs requires further consideration as it can compete with the forces that stabilize supramolecular assemblies. Non-covalent bonds significantly depend on surrounding conditions (e.g. polarity of the solvent, pH, temperature) giving the chance for external control of self-assembly and de-assembly.⁸ These processes can occur on the atomic, molecular or macromolecular scale. Even children have experiences with these processes, as soap bubbles are an example of self-assembling molecules. Unfortunately, there does not seem to be a universal set of rules that governs self-assembly over the entire atomic to

macromolar length scale. There are however general guidelines for molecular self-assembly based off of our understanding of the weak intermolecular forces that drive supramolecular assembly, which is of primary importance to this project.¹³⁻¹⁶

In section 1.3, we will discuss the typical strength of these weak interactions and how they are influenced by solvent and environment. By understanding both how these forces can govern self-assembly and the conditions in which they are optimal, supramolecular chemists can begin to employ weak noncovalent interactions in the construction of supramolecular compounds to afford functional materials.¹⁷ Size, shape, physical properties, and the strength of the intermolecular forces by which individual building blocks interact also requires significant consideration. Despite the challenges, many supramolecular assemblies with beautiful architectures have been reported in the literature from small dimeric capsules with cavities 420 \AA^3 to large supramolecular polymers with 1.9×10^{-3} -mol repeat units.^{18,19} This chapter will focus on the factors that guide self-assembly and discusses a handful of simple, small supramolecular complexes.

1.3. Strength of Intermolecular Interactions

Intermolecular forces and covalent bonds can both be used to hold groups of atoms together, but they differ in character and strength. A typical covalent bond involves the sharing of electrons between adjacent atoms and is generally much stronger than the intermolecular forces by which supramolecular assembly occurs apart from ionic forces. Strengths of covalent bonds range from 57 kcal/mol for a typical C-I bond to 200 kcal/mol for a C-C triple bond. To understand how weaker intermolecular forces govern assembly, it is important to understand their strengths and the patterns by which they interact.

Similarly, supramolecular interactions also differ in strength from strong metal ligand interactions, ranging from 10-30 kcal/mol, to hydrogen bonds and Van der Waals forces, which can be very weak for atoms and small molecules (>1 kcal/mol) or near zero for hydrogen bonds in water. To obtain stable supramolecular complexes from these forces we must understand their strength and additivity, directional nature and the optimal conditions under which these forces function. With a good understanding of these factors, we can employ noncovalent interactions to design functional self-assembling materials.

Of all the intermolecular forces, van der Waals are the most common and exist between any interacting chemical species. These forces are driven by induced electrical interactions between two or more chemical species that are within close proximity (Figure 1.2a).⁶ Despite these forces being individually weak, they are additive and can be quite strong between large linear molecules which can fit together well. The strength of these forces are highly dependent on the overlap of interacting molecules. This trend can be seen through comparison of boiling points between butane (b.p = -1 °C) and 2-methylpropane (b.p = -11.7 °C) versus n-dodecane (214-218 °C). The branching caused by the methyl group in 2-methylpropane (Figure 1.2c), when compared to butane (Figure 1.2b), reduces overlap resulting in less induced electrical interactions with adjacent molecules. The additive nature of van der Waals forces is also obvious when considering n-dodecane. The long linear structure of this molecule allows for overlap resulting in significant induced electrical interactions, which is demonstrated through its high boiling point. One important characteristic of this force, from a supramolecular chemist's point of view, is the lack of directionality. Designs that rely on this force must accommodate shape selectivity and fit.

Van der Waals forces contribute towards assembly of many supramolecular systems and are compatible with many other intermolecular forces that display directional character.

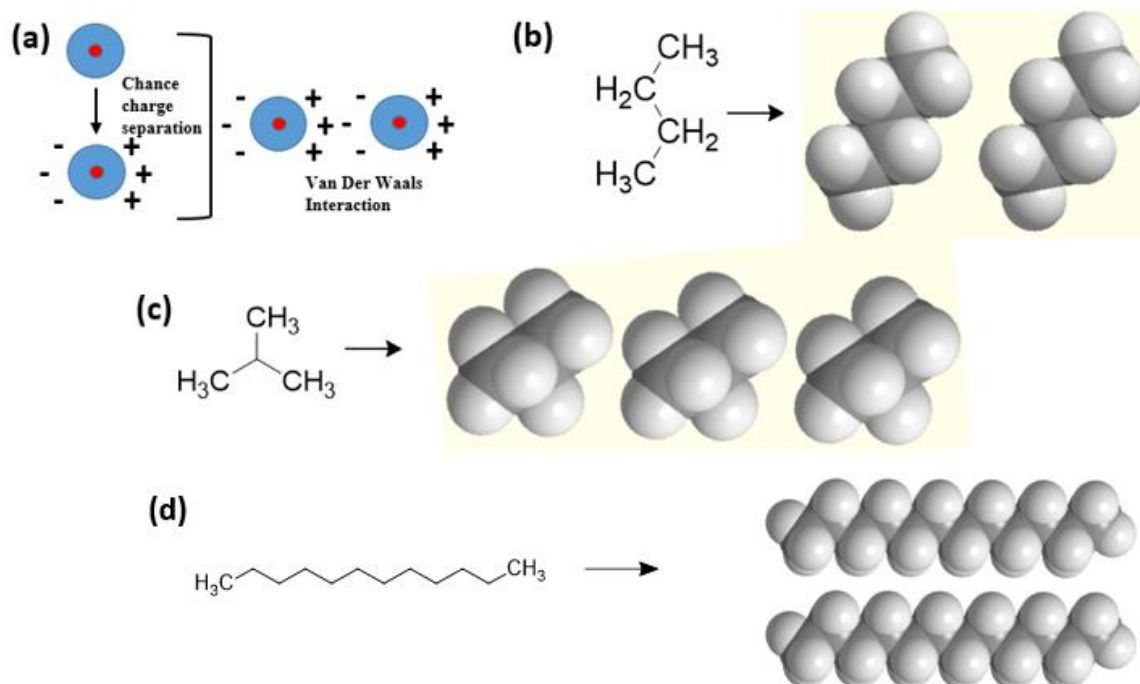


Figure 1.2. (a) Schematic representation of van der Waals forces. Space filling models of (b) n-butane, (c) 2-methylpropane, and (d) n-dodecane that highlight differences in overlap that contribute to the induced electrical interactions

Hydrogen bonds play an important role in supramolecular chemistry. They are characterized by an electrostatic attraction between hydrogens bound to an electronegative atom (typically N, O, F, S) also-called a hydrogen bond donor (X-H) and a lone pair of an electronegative atom in close proximity, which is often referred to as the hydrogen bond acceptor (X:). The strengths of hydrogen bonds are generally correlated with the acidity of the hydrogen bond donor and basicity of the hydrogen bond acceptor.¹⁶ Therefore the hydrogen bond donors range from strong donors such as F-H and O-H to extremely poor donors such as C-H. Conversely, acceptors with strong negative character make the best hydrogen bond acceptors ($^-\text{OH} > ^-\text{COO}^- > \text{H}_2\text{O} > \text{C-F}$). Hydrogen bonds are also dependent

on the surrounding environment. For example, individual hydrogen bonds are stronger in the gas phase or in non-polar solvents (5-40 kcal/mol) than they are in solvents, such as water, that compete for hydrogen bonds (0 kcal/mol).¹⁶

An important property of hydrogen bonding is its directionality, which makes it particularly useful for the supramolecular chemist. Angles of single hydrogen bonds range from linear (180°), as seen in HCN---HF, to trigonal planar (120°) for H₂CO---HF (Figure 1.3).¹³ The angular geometry of hydrogen bonds can be distorted with minimal external force so linear hydrogen bonds must be characterized under conditions that minimize these forces. Therefore, HCN---HF hydrogen bonds were characterized under low pressure in the gas phase using rotational spectroscopy.¹³ Molecules that utilize multiple hydrogen bonds, such as carboxylic acid dimers, have been observed through crystallography. As demonstrated by Takwale et. al., *p*-toluic acid crystal analysis shows the simultaneous hydrogen donor and acceptor character of carboxylic acids resulting in planar dimers consisting of oppositely oriented acids (Figure 1.3c).²⁰ Hydrogen bonding interactions can vary further when considering molecules with hydrogen bonding donors and acceptors on opposite sides of the molecule. For example, ureas interact with each other through a three point bifurcated hydrogen bonding motif.²¹ Directionality of hydrogen bonding is especially relevant during the design stage of supramolecular chemistry because hydrogen bonds govern assembly in a predictable manner. So far, the vast majority of self-assembling systems incorporate some hydrogen bonds interactions due to their directionality and specificity.¹³

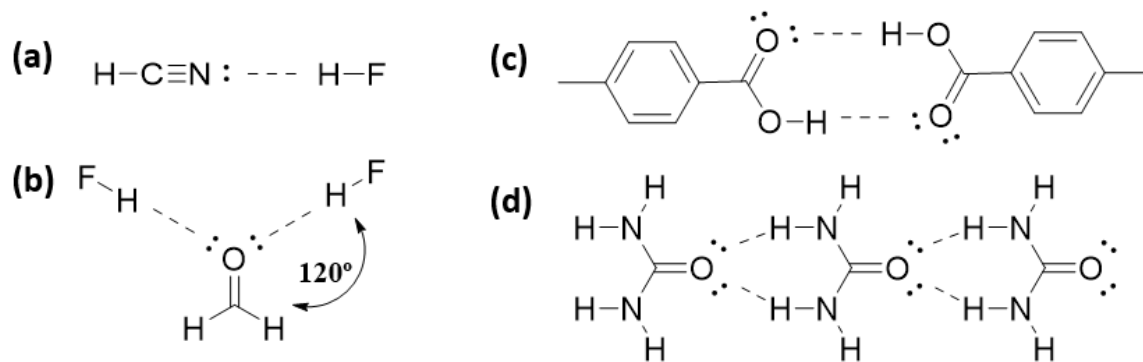


Figure 1.3. Hydrogen bonding interactions vary in their geometry as seen with (a) the linear geometry exemplified by HCH---HF, (b) trigonal planar by H₂CO---HF, (c) carboxylic acid dimer of *p*-tolueic acid, and (d) the three centered interactions of ureas.

Dipole-dipole interactions are also common in supramolecular chemistry. When there is an unequal sharing of electrons between atoms, the molecule will possess both partial positive and partial negative regions resulting in a molecule that expresses a dipole.²² Upon orientation of a partial positive region of one molecule to partial negative regions of another, an attractive interaction exists (Figure 1.4a). This electrostatic interaction falls off with distance. Dipole-dipole strengths typically range from 1-20 kcal/mol. For example, propanone dimers are stabilized by a dipole-dipole interaction that is 5.25 kcal/mol strong (Figure 1.4b).²³ Because this force is dependent on dipole orientation, they are directional and useful during the design step in supramolecular chemistry.

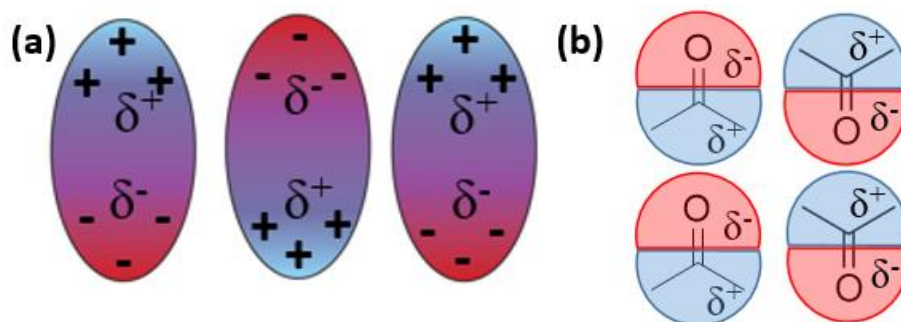


Figure 1.4. (a) Schematic representation of dipole-dipole attractive interactions. (b) Interaction and orientation between 2-propanone molecules via dipole-dipole forces.

Aromatic stacking interactions are attractive noncovalent interactions that exist between aromatic rings. The attractive force is a result of quadrupole interactions between delocalized electrons in p-orbitals.²⁴ Consider one of the simplest aromatic compounds, benzene. While benzene does not display a dipole moment, it does have a quadrupole moment.²⁵ In other words, benzene can be viewed as a charge sandwich where the middle has positive character while the top and bottom have negative character. Upon interaction with another aromatic ring, these charges are displaced resulting in an induced dipole. Aromatic stacking interactions can be seen in sandwich, edge-to-face, and staggered orientations (Figure 1.5). There is ongoing debate about the nature of these interactions and their relative geometry and strengths.²⁶

Aromatic interactions are believed to arise from multiple attractive and repulsive interactions including intermolecular forces such as van der Waals, hydrophobic interactions, and electrostatic interactions.²⁷ More recent literature argues that electron substituent effects play a major role in aromatic interaction.²⁸ This can be seen since certain orientations can be favored when considering how the quadrupolar moment varies with aromatic functionality. Dougherty et. al. demonstrated through Hartree-Fock calculations that benzene and hexafluorobenzene adopts a sandwich conformation that is stabilizing by approximately 3.7 kcal/mol (Figure 1.5a).²⁹ Due to the electronegative nature of fluorine and their location in the plane of the molecule, significant negative character lies in the center of the charge sandwich. This allows for a stable sandwich conformation between hexafluorobenzene and benzene.

Edge-to-face aromatic interactions were first observed by Cox et. al. through single crystal analysis of benzene (Figure 1.5b).³⁰ These types of interactions are especially important in peptides and proteins because they greatly influence the folding of peptide chains and the resulting protein conformations.^{31,32} For the simple benzene-benzene edge-to-face interaction, Spirko determined this interaction to be stabilizing by 1.7 kcal/mol using nonempirical modeling (NEMO) studies.³³ Staggered aromatic interactions of two benzene units have also been studied (Figure 1.5c). Spirko, using NEMO studies, reported that staggered aromatic interactions are stabilizing by 1.2 kcal/mol for two interacting benzene units.³³ Even though aromatic interactions manifest in various orientations that provide different amounts of stability, aromatic stacking, similar to hydrogen bonding, provides ample opportunity for control over supramolecular assembly.

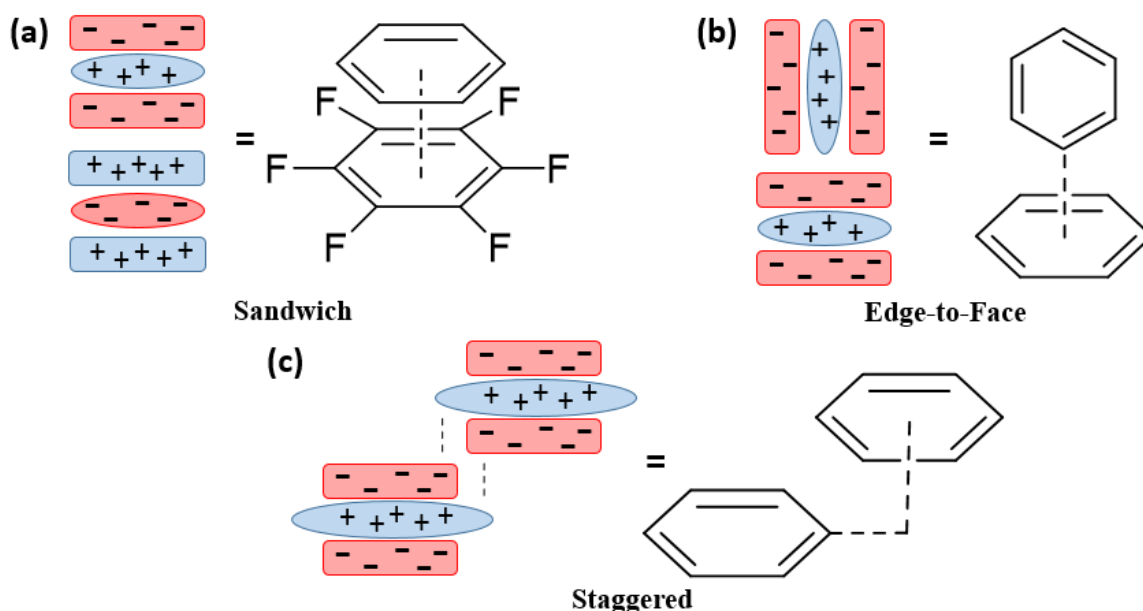


Figure 1.5. Schematic representation of (a) hexafluorobenzene-benzene adopting a sandwich conformation, (b) benzene-benzene in an edge-to-face conformation, and (c) benzene-benzene in a staggered conformation.

Ionic interactions are stronger than the other interactions presented so far and can be as strong as 60 kcal/mol for NaCl as measured through activity coefficient calculations.³⁴ They are characterized by a charged ion interacting with either a molecule that expresses a dipole or another oppositely charged ion. As seen in Figure 1.6b, an example of an ion-dipole interaction can be seen between positively charged sodium and the partially negative region of water's dipole.³⁵ This is different than the stronger ion-ion interaction that is characterized by two oppositely charged ions that are bound together (Figure 1.6a). While these forces are particularly strong, their strength is largely dependent on environment. Solvents with significant Lewis acid or base character can interact with ions in solution causing competition between ion-ion and ion-dipole interactions.³⁶ Solvents that possess hydrogen bonding, such as water and ethanol, are particularly good at stabilizing ions, making the ion-dipole interaction more favorable. Despite this, the competition provided by certain solvents provides the benefit of reversibility for ion interactions. This means that under certain solvents, these strong ionic interactions can be switched from free ions to ionic bonds. Since these interactions are similar in strength to covalent bonds but are easily reversible, they are widely used in supramolecular assembly.

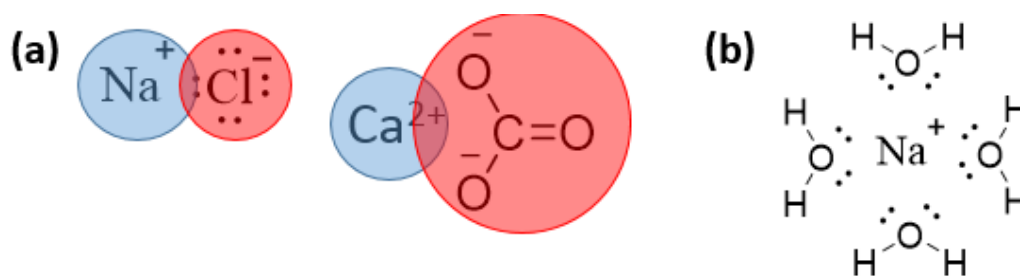


Figure 1.6. Schematic representation of (a) ion-ion interactions of NaCl and CaCO_3 salts and (b) ion-dipole interaction between water and sodium ions.

Metal-ligand interactions describe the coordination of metals to ligands by the donation of two electrons in the formation of a dative bond. These bonds range from 60-190 kcal/mol but are reversible at higher temperatures. The use of metal-ligand interactions provides two major advantages. Metal-ligand dative bonds are thermodynamically strong interactions but also have varying degrees of lability that allows for a range of kinetic stabilities. Also, transition metal ions often have specific geometric requirements in their coordination sphere, which gives supramolecular chemists some control over shape and assembly.³⁷ Their strong stability usually means that when they are employed for supramolecular assembly, the assembly is carried out at higher temperature, where these bonds are 'reversible' to get the thermodynamic product. It is important to mention that thermodynamic stability is a function of change in free energy while kinetic stability is a function of rate of reaction. The necessity for elevated temperatures to control dative bonds has previously been observed in metal-organic framework (MOF) design and assembly. For example, Fischer required diethylformamide heated to 60 °C to facilitate nucleation of a $Zn_4O(bdc)_3$ MOF ($bdc = 1,4$ -benzenedicarboxylate).³⁸ In another example, Chang required microwave irradiation at 220 °C to selectively grow one of a possible two architectures; a tetragonal $[Ni_{22}(C_5H_6O_4)_{20}(OH)_4(H_2O)_{10}] \cdot 38 H_2O$ MOF ($C_5H_6O_4 =$ glutarate).³⁹ The interactions that dictate the assembly of the mentioned MOFs have been highlighted in Figure 1.7. Metal-ligand interactions are highly used in supramolecular chemistry due to their strength, geometry, and reversibility.

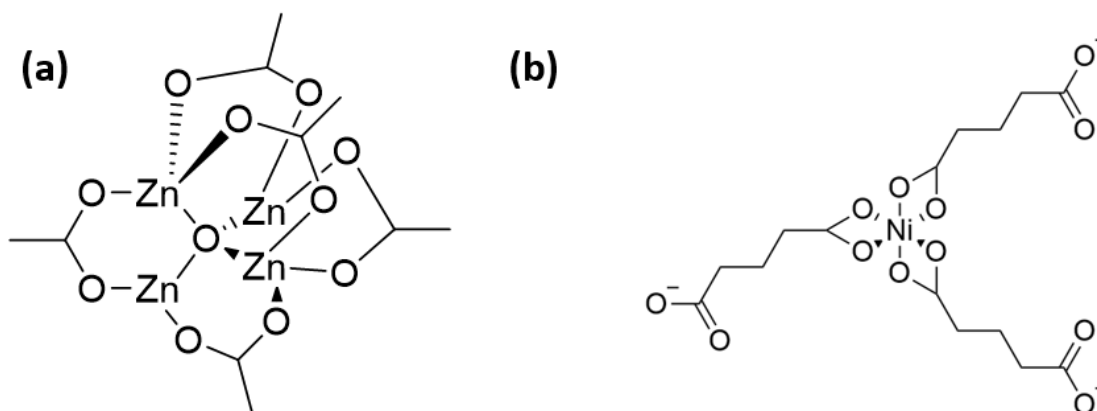


Figure 1.7. Representation of the (a) zinc-oxygen framework seen in Fisher's MOF and the (b) nickel-oxygen octahedral seen in Chang's MOF.

1.4. Building Block Requirements

In order for self-assembly to occur, individual building blocks must be matched to one other in both shape and size and contain complementary functional groups to form the non-covalent interactions just discussed. The lock and key model, as demonstrated by enzyme and substrate, provides a good analogy for understanding how size and shape influences the interactions between building blocks (Figure 1.8). In 1894, Fischer described this model as a complementary steric interaction between enzyme and substrate.⁴⁰ In other words, the size, shape and position of the binding sites within the active site are ideal for specific substrate recognition. Supramolecular assembly is similar in that complexes can only be formed from building blocks that have size and shape compatibility. The fit provides the foundation by which weak intermolecular forces can govern the self-assembly of individual building blocks into ordered supramolecular complexes.

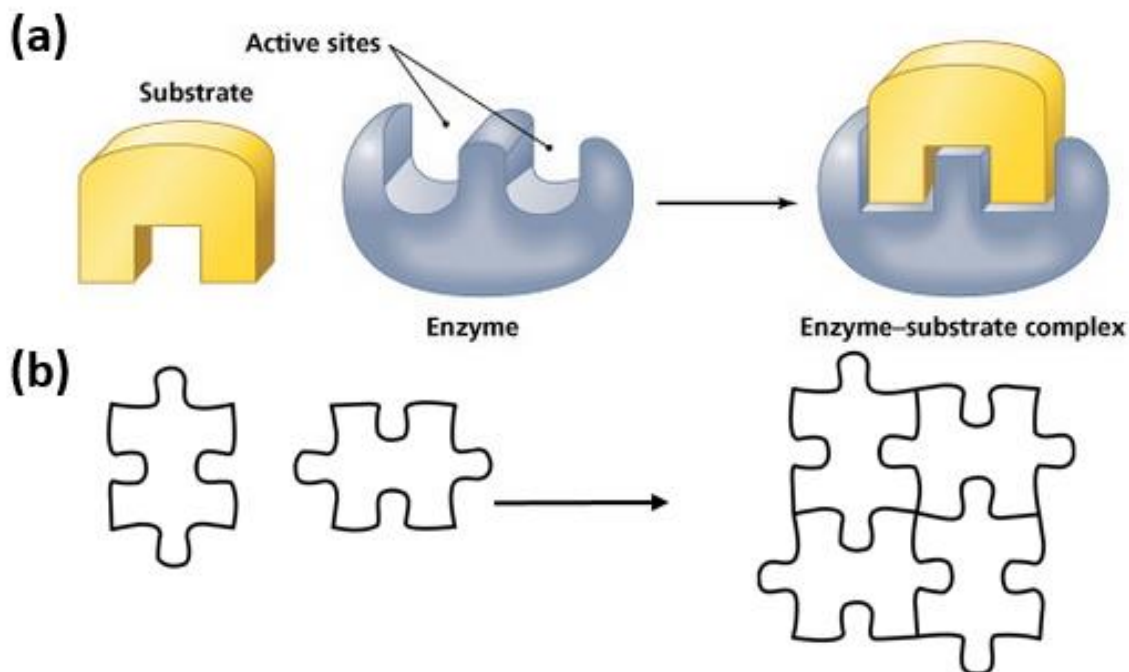


Figure 1.8. (a) Lock and key model demonstrated by substrate and size/shape specific enzyme active site and (b) schematic representation of assembly of complementary building blocks.

As mentioned previously, building blocks self-assemble as a result of non-covalent intermolecular interactions. Understanding these interactions is essential in the design of building blocks that assemble into supramolecular complexes. There are three important factors to consider about the forces that govern assembly: (1) strength; (2) reversibility; and (3) directionality. As highlighted earlier, the strengths of many non-covalent interactions used by supramolecular chemists are generally much weaker ranging from > 1 kcal/mol for dispersion forces, to 5-10 kcal/mol for a hydrogen bond, to 60 kcal/mol for an ion-ion interaction to 190 kcal/mol for metal-ligand interaction. Despite many of these interactions being individually weak, they are very capable of governing self-assembly, especially, when they work in tandem with one another. For example, Meijer and co-workers were able to develop supramolecular polymers that assemble through extensive

hydrophobic interactions in combination with hydrogen bonding (Figure 1.9).⁴¹ In this particular example, ureidotriazine building blocks bind through a 4-point hydrogen bonding interaction to adjacent building blocks. The association constant was estimated through ¹H-NMR integration studies, using varying concentration of monomer, as $K_{\text{ass}} = 2 \times 10^4 \text{ M}^{-1}$ in chloroform.⁴² This example highlights how multiple intermolecular forces can be applied in the design of supramolecular complexes that adopt unique architectures, such as a chiral helical structure (Figure 1.9b). Many other supramolecular complexes that assemble through additive and cooperative non-covalent interactions have also been reported in the literature that have applications in gel design,⁴³ organic semiconductors,⁴⁴ and theranostics.⁴⁵

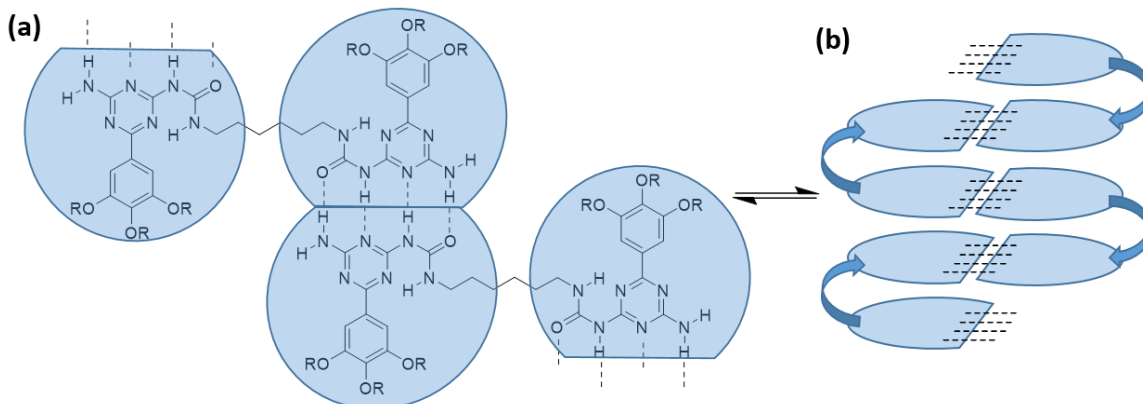


Figure 1.9. Meijer's (a) ureidotriazine building blocks that assemble through a 4-point hydrogen bonding and solvophobic assembly motif into (b) chiral helical like complexes.

We will now consider the reversible process that guides the formation of a single thermodynamically more stable product while sampling many other less stable intermediates. In a covalent synthesis, bond formation is generally irreversible and attributed to enthalpy and kinetic stability of the product. Supramolecular assembly is different in that complexes are constantly equilibrating to balance enthalpy and entropy. This quality gives supramolecular complexes a very big advantage: reversibility.

Reversibility of self-assembly allows an improperly formed assembly or mismatch of subunits to be eliminated from the final structure through self-correction.⁴⁶ In other words, supramolecular materials have “self-healing” properties and generally adopt the most thermodynamically favorable conformation. However, this reversibility of non-covalent bonds is also the main weakness of at least artificial self-assembled structures.¹⁴ Supramolecular assemblies may be quite sensitive to their environment and factors such as temperature, solvent, and pH greatly influence assembly. While intricate architectures can be achieved through assembly, they can undergo the reverse process and disassemble. A non-covalent synthesis provides the challenge of manipulating multiple equilibria in supramolecular design and synthesis. In order to effectively design supramolecular systems, one must understand how intermolecular forces influence the geometry and orientation of building blocks during the assembly process in addition to the strengths and optimal conditions for these forces.

In addition to the strength, the directionality of intermolecular forces guides the intricate self-assembled secondary and tertiary structures. Just like covalent bonds, where the electrons are shared between adjacent atoms, intermolecular forces are directional in how they interact. When designing building blocks, directionality must be considered in order to access specific supramolecular architectures. Not all of the previously discussed non-covalent interactions are constrained to specific geometries and orientations otherwise called directional interactions. For example, although molecules that interact via dipole-dipole forces tend to align the positive and negative ends of the dipole towards each other, there are many geometrical alignments that can satisfy these conditions and they do not specify a single lowest energy orientation. For example Figure 1.10 shows a simple oval

species with a dipole could be ordered in several geometries within a single plane including sandwiched or staggered orientations. Additionally, non-planar and even perpendicular geometries are also possible. Directional forces are particularly useful since geometric and spatial control of interacting species can be optimized.⁴⁷ In addition to directionality, the surrounding environment must provide conditions by which these intermolecular forces are capable of interacting. The remainder of this chapter focuses on supramolecular complexes that have been reported as a result of directional intermolecular forces between building blocks.

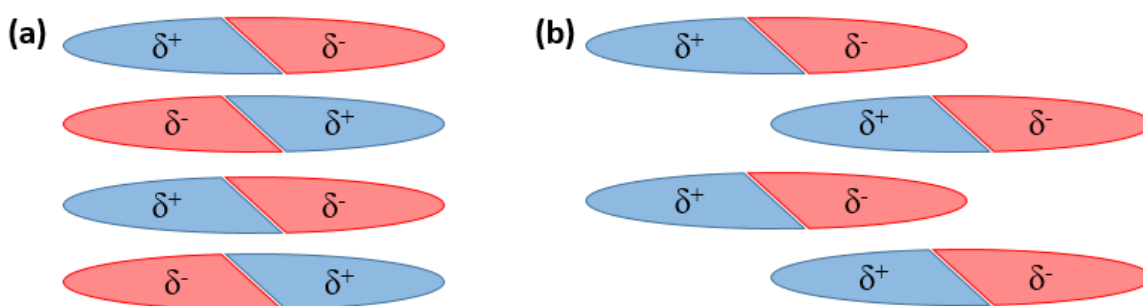


Figure 1.10. Schematic representation of how dipole-dipole interactions can influence supramolecular assembly into (a) sandwich and (b) staggered conformations. Perpendicular geometries are also possible.

1.5. Examples of Supramolecular Assembly

Many supramolecular complexes have been prepared with unique shape, size and functionality for applications in chemistry, biology, material science and electronics. Indeed, one goal of supramolecular chemistry is to develop “intelligent” materials with tailor-made properties that change and adapt themselves in response to the surroundings.⁴⁶ Supramolecular assemblies have been achieved with various degrees of assembly ranging from homodimers, heterodimers, and trimers all the way up to oligomers and

supramolecular polymers with complex architectures. It is impossible to talk about all of the previously reported supramolecular complexes but we will highlight a series of assemblies that differ in size, shape, degree of assembly, and complexity of architecture. The remainder of this chapter discusses supramolecular assemblies with architectures as simple as dimers to more complex architectures such as nanotubes.

Let us consider the simplest supramolecular assembly motif the homodimer, which is characterized by the assembly of two identical building blocks to afford supramolecular complexes that can be a velcroplex, sphere, or a cylinder.⁴⁸⁻⁵⁰ For example, Cram reported the assembly of two identical porphyrin like rings that interact via dipole-dipole, van der Waal's, and solvophobic interactions in the formation of dimers. This type of assembly was defined as velcroplexes (Figure 1.11).⁴⁸ What is particularly interesting about this system is how its assembly motif displays host: guest character. Each porphyrin like ring contains two protruding methyl groups that bind to methyl sized cavities of adjacent rings. Assembly of these rings was facilitated in polar solvents with ΔG values for dimer formation varying greatly from 1 to 9 kcal/mol.

Supramolecular dimerization has also been applied in the design of dimeric cavities capable of guest encapsulation. Figure 1.11b shows a supramolecular dimer, designed by Rebek that assembles through a belt of eight bifurcated hydrogen bonds to form a cylindrical capsule. This capsule possesses a tapered cavity with polar character of 420 \AA^3 capable of binding a variety of guests.⁴⁹ The walls of the cylindrical confinement also provide a physical barrier that temporarily isolates guest molecules from the outside environment. Other supramolecular capsules capable of shielding guest molecules from the surrounding environment have been developed that can bind guests, alter their

conformation, absorption or emission properties and even modulate their reactivity.⁵⁰ Ramamurthy designed a water soluble deep cavity (Figure 1.11c), based off of Gibb's octa acid design, capable of assembling via templation in the presence of a suitable guest or guests.⁵¹ Just as Rebek's system protects the encapsulated molecule from the surrounding environment, Ramamurthy's complex protects the templating guest or guests from the surrounding aqueous environment. In addition to providing protection, this capsule is also a confined nanoscale reactor that can facilitate selective reactions upon its guests. Within this cavity, the excited-state behavior and reactivity of eight different α -alkyl dibenzyl ketones was studied. Upon irradiation in hexane or buffer solution, each of these ketones is known to undergo type 1 Norrish reactions. These reactions are characterized by cleavage of aldehydes or ketones into two radical intermediates upon irradiation. These radical intermediates can yield a mixture of products. However, upon inclusion within Gibb's eggshell followed by subsequent irradiation, reactants underwent processes such as type 2 Norrish reactions and ketone rearrangement. This example highlights how inclusion within a nanoreactor with defined properties can greatly influence reactivity resulting in products not typically seen from bulk solution reactions.

Supramolecular systems consisting of more than two building blocks have also been reported. For example, Wasielewski designed a supramolecular trimer complex consisting of 1,4-diazabicyclo[2.2.2]octane (DABCO) and chlorophyll (Ch1) trefoils that assemble via metal ligand interactions (Figure 1.12a).⁵² DABCO has previously been used to assemble a wide variety of supramolecular porphyrin systems, in which metal-ligand binding between two porphyrin metal centers and the two nitrogens of one DABCO molecule generate dimeric sandwiches.^{53,54} This system assembles in a similar manner.

Two porphyrin moieties from one building block form dative bonds with zinc within the chlorophyll group to connect with adjacent building blocks to form a supramolecular trimer with a hexagonal geometry. This assembly is also being studied for light harvesting capabilities and facilitates dual singlet-singlet annihilation energy transfer processes that suggest two separate time scale energy transfers within the molecule.⁵²

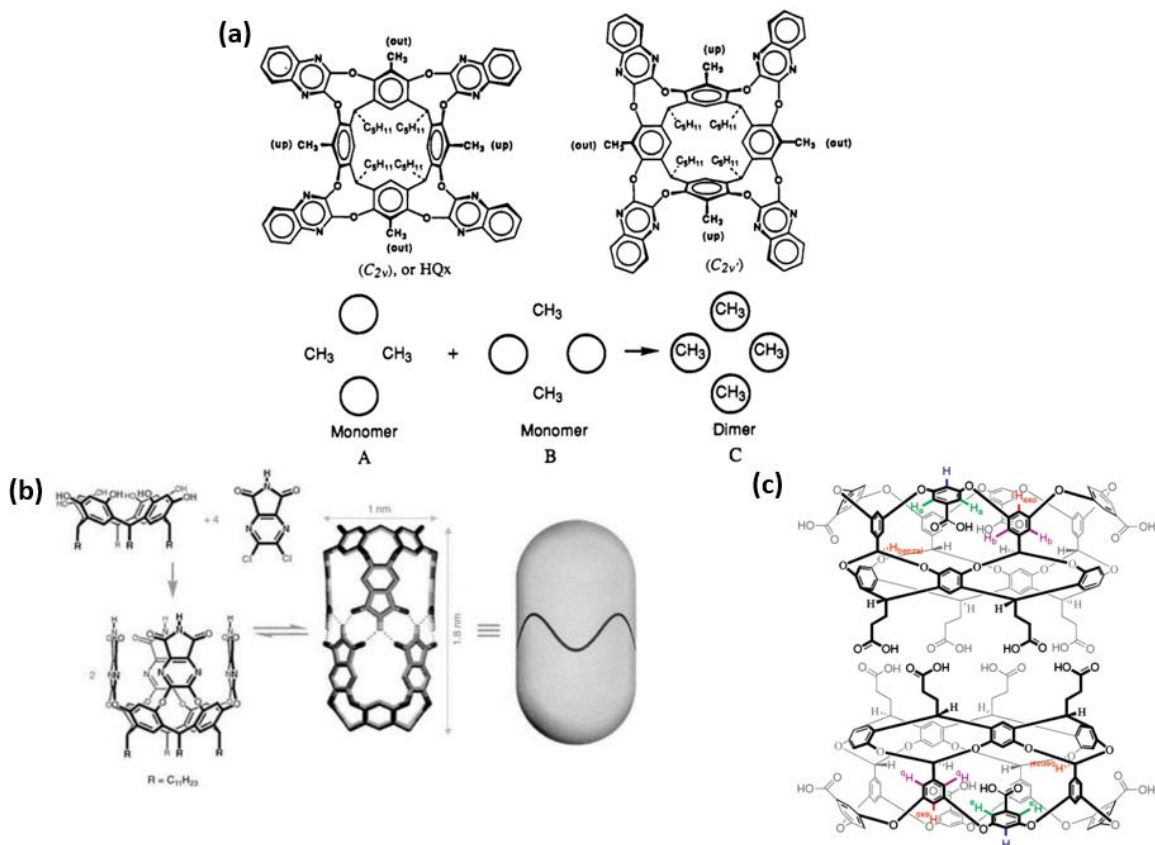


Figure 1.11. (a) Cram's supramolecular dimer that assembles through binding of methyl groups on adjacent rings (b) Rebek's supramolecular dimeric capsule that assembles through a bifurcated hydrogen bonded motif. (c) Gibbs octa acid dimer used by Ramamurthy as a nanoscale supramolecular capsule.

*Permission to reprint for the above figures granted by John Wiley and Sons

Supramolecular assemblies consisting of more than three building blocks have also been reported. For example, Fujita's hollow supramolecular tetramer (Figure 1.12b) consisting of four pyridyl ligands assembled through six palladium metal ions results in an octahedral cage like structure.⁵⁵ The large empty space is capable of encapsulating a handful of guest molecules, specifically four adamantyl carboxylate ions. This complex has also been applied in the acceleration of room temperature Diels-Alder reactions.⁵⁶ The confined space of this octahedral cage promotes the stereoselectivity of reactions that occur within its confined space. This example highlights one of the major goals sought after by supramolecular complexes, the design of a confined reaction environment capable of facilitating selective reactions. Supramolecular assemblies resulting from higher degrees of assembly, such as pentamers⁵⁷ and hexamers,⁵⁸ have also been reported, but are beyond the scope of this chapter.

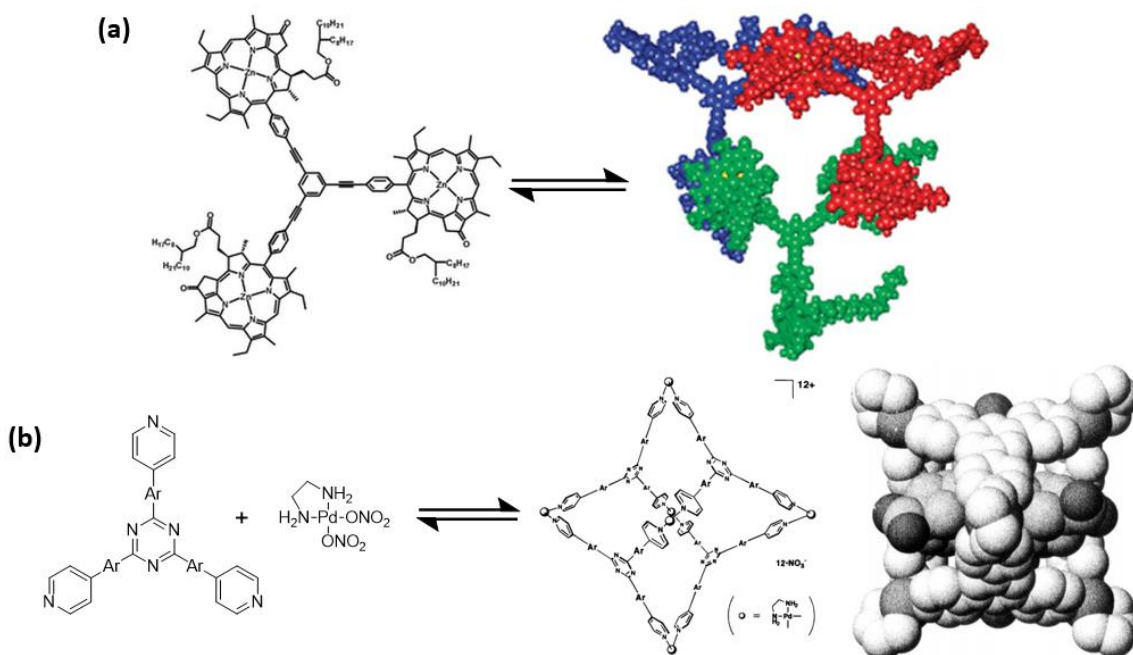


Figure 1.12. (a) Wasielowski's DABCO chlorophyll trimer and (b) Fujita's tetrameric cage
*Permission to reprint granted by John Wiley and Sons

1.6 Supramolecular Polymers

Supramolecular chemistry is a multidisciplinary field that embodies expertise from many different areas such as polymer chemistry. Supramolecular polymers, which are polymers held together by directional and reversible secondary interactions (Figure 1.13b), have led to supramolecular complexes with quite intriguing architectures. In 2001, Lehn proposed the following definition for these systems: Supramolecular polymers are defined as polymeric arrays of monomeric units that are brought together by reversible and highly directional secondary interactions, resulting in polymeric properties in dilute and concentrated solutions, as well as in the bulk. The monomeric units of the supramolecular polymers themselves do not possess a repetition of chemical fragments. The directionality and strength of the supramolecular bonding are important features of systems that can be regarded as polymers and that behave according to well established theories of polymer physics.⁵⁹ Complexes with as low as 20 repeat units have been reported in the literature as a supramolecular polymer.⁶⁰ Degree of polymerization for supramolecular polymers is completely dependent on the relationship between strength of the association constant and concentration of the monomer. One strategy to ensure that the association constant between monomers is strong enough for polymerization is to utilize a strong assembly motif, such as one based off of pyridyl and carboxylic acid interaction. Coleman utilized this interaction in the design of a poly(ethylene-co-methacrylic acid) poly(2-vinylpyridine) copolymer and valued the association constant at $K_a = 500 \text{ M}^{-1}$.⁶¹ The field in which supramolecular chemistry and polymer science meet has developed into a vast area of research; ranging from the study of interacting biomacromolecules, such as DNA and proteins, to the self-assembly of large synthetic molecules into well-defined architectures.⁵⁹

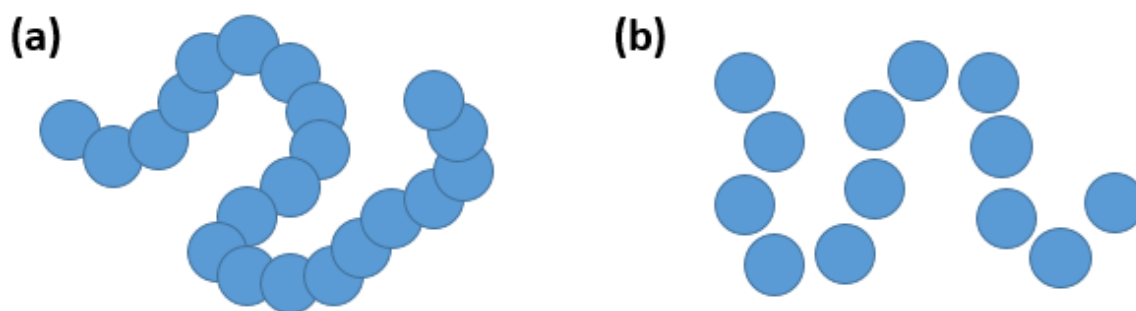


Figure 1.13. Schematic representations of (a) covalent polymers and (b) supramolecular polymers

Supramolecular polymers are especially interesting because they have been used in the design of supramolecular complexes that adopt quite complex architectures. Helices,^{62,63} nanorods,⁶⁴ and nanotubes^{65,66} have all been reported. Hollow nanotubular assemblies are of particular interest and have inspired much of our current work. They have potential applications in inclusion chemistry, catalysis, molecular electronics and molecular separation technology.⁶²⁻⁶⁶ These structures can be accessed supramolecularly through the assembly of cyclic peptides via β -sheetlike hydrogen-bonding patterns.⁶⁷ This strategy was first recognized in 1974 by De Santis *et. al.* through ring-stacking of heterochiral cyclic peptides.⁶⁸ De-Santis describes macrocyclic polypeptide building blocks that consists of L,D alternating peptides in which the C=O and N-H from the amide groups are facing in opposite directions (Figure 1.14). Hydrogen bonding through these opposite facing functional groups drives the assembly of these macrocyclic polypeptides into hollow nanotubular structures.

This strategy was also applied by Ghadiri through the self-assembly of cyclic peptide building blocks into nanotubes.^{69,70} Ghadiri's macrocyclic building block design consists of an eight-residue cyclic peptide with the following sequence: cyclo [-(D-Ala-Gle-D-Ala-Gln)₂]. The eight-residue building block can adopt a low energy ring-shaped

flat conformation in which the backbone amide functionalities lie approximately perpendicular to the plane of the structure. The perpendicular orientation of the amide functionalities is ideal for hydrogen bonded guided assembly into hollow nanotubular assemblies. Assembly of these macrocycles could be triggered by controlled acidification of a basic solution of the peptide building blocks to afford nanotubular assembly. Temperature studies in chloroform gave an estimated association constant of $\sim 2500 \text{ M}^{-1}$.⁷⁰

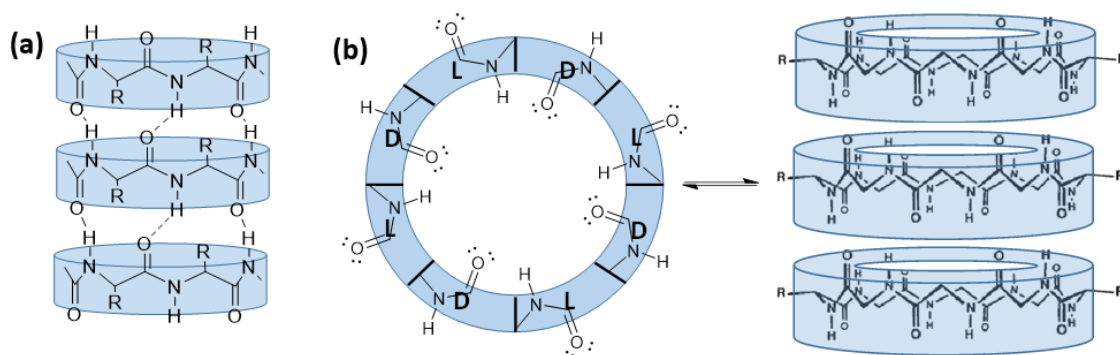


Figure 1.14. Schematic representation of (a) DeSantis' cyclic building block consisting of alternating D and L peptides and (b) Ghadiri's cyclic alternating polypeptide consisting of 8 peptides that assemble into hollow nanotubular complexes

1.7. Bis-Urea Based Supramolecular Oligomers and Polymers

The predictable manner in which amide functional groups hydrogen bond is an effective tool, as just demonstrated, towards the design of supramolecular complexes. Other functional groups, such as urea, also possess predictable hydrogen bonding tendencies. Ureas are known to form head-to-tail arrays based on 3-center hydrogen bonds from the NH's of one urea to the carbonyl oxygen of an adjacent urea.^{71,72} Urea N-H groups and urea oxygens are also great hydrogen bond donors and hydrogen bond acceptors which is demonstrated by their α and β values ($\alpha = 3.0$, $\beta = 8.2$).⁷³ Given their strong and directional assembly, it is not surprising that ureas have been incorporated into many kinds

of supramolecular building blocks and used for the formation of tapes, helices, columns, ribbons etc.

One area of research that *bis*-urea functionality has received attention in is supramolecular oligomer and polymer design. For example, Zimmerman designed a soluble ureido-naphthyridine oligomer that assembles via an eight point hydrogen bonding network where ureas act as hydrogen bond donors (Figure 1.15a). The association constant of hydrogen bonding assembly motif was experimentally calculated through NMR dilution studies in 1:9 δ_6 -DMSO : CDCl_3 to be $K_a > 4.5 \times 10^5 \text{ M}^{-1}$.⁷⁴ This example highlights how the low solubility of urea can cause problems when trying to obtain urea driven supramolecular assembly. The ureido-naphthyridine building blocks were modified with functional groups, such as tosyl, that promote solubility. Bouteiller also designed a *bis*-urea monomer that assembles into long cylindrical wire architecture via urea's predictable hydrogen bonding pattern (Figure 1.15b).⁷⁵ This system readily dissolves at room temperature in common solvents, such as chloroform, and forms visco elastic solutions. The length of this supramolecular polymer can be adjusted by slightly modifying the solvent conditions. The association constant was determined to be $K_n = 1.0 \times 10^5 \text{ L/mol}$ in CDCl_3 .

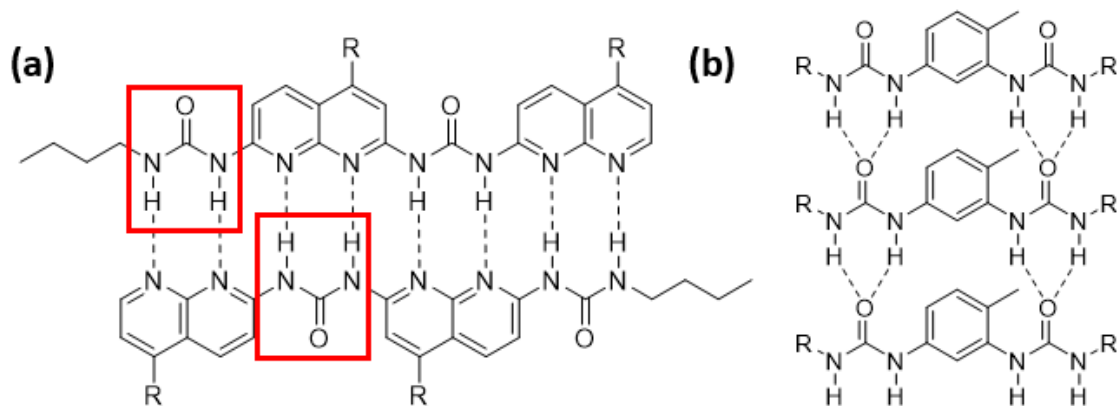


Figure 1.15. (a) Zimmerman's ureido-naphthyridine oligomer and (b) Bouteiller's bis-urea based polymer

1.8. Bis-Urea Macrocycles

The predictable hydrogen bonding tendencies of *bis*-ureas have also been applied in the design of macrocycles that assemble into columns similar to the previously mentioned alternating cyclic peptides used by DeSantis and Ghadiri. This strategy was first recognized by Karle in the design of cysteine-based *bis*-urea macrocycles that assemble into nanotubes (Figure 1.16a).⁷⁶ Assemblies derived from cyclic *bis*-urea building blocks of 16, 18, and 24 membered ring sizes were synthesized, assembled from a chloroform/methanol mixture, and characterized via X-ray crystallography. The assembly motif is characterized by a three point hydrogen bonding network through a urea backbone with the ureas facing the same direction in the tubular assembly. What is particularly interesting is assemblies derived from 18 and 24 membered rings are capable of specific guest binding as seen by their encapsulation of oxalic and succinic dianions.

The Shimizu group has identified *bis*-urea macrocycles that assemble reliably into columnar structures.⁷³ The first and simplest of these macrocycles contained two urea groups connected through two *meta*-xylene spacers. These macrocycles readily assemble

into columnar nanotubes via the three centered urea interactions. The resulting assembly is also further stabilized by off-set aryl stacking interactions and the opposite facing orientation of ureas, which minimizes repulsive dipole-dipole interactions. The simple design of the *bis*-urea macrocycle design enables the control of the size, shape, and interior functionality of the nanotubular structure simply by changing the c-shape spacer of the individual macrocycle building blocks. As a result, these macrocycles have expanded to include many variations ranging in cavity size, functionality, application, and properties (Figure 1.16b).

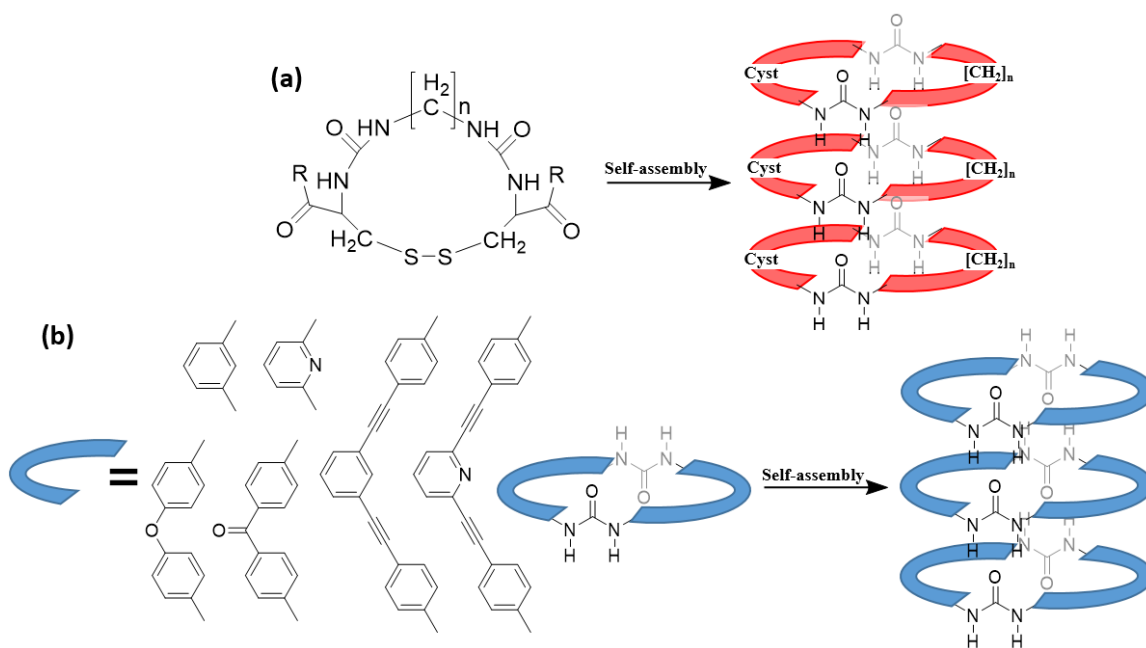


Figure 1.16. Schematic representation and assembly of (a) Karle's cysteine-based *bis*-urea macrocycles and (b) Shimizu's *bis*-urea macrocycles

Variations of Shimizu's *bis*-urea macrocycle design have been used for a wide range of application such as guest absorption,⁷⁷ metal ion recognition,⁷⁸ and selective photodimerization.^{79,80} The application of assembled *bis*-urea phenylethylnylene macrocycle (host **1.1**) for the selective dimerization of coumarin and coumarin derivatives

highlights the power of a confined supramolecular architectures (Figure 1.17a). Coumarin, 6-methylcoumarin, and 7-methylcoumarin all load into assembled host **1.1** with a 1:1 host: guest ratio that is required for dimerization. UV irradiation of host **1.1** coumarin complex facilitates the selective dimerization resulting in the formation of mostly anti head to head dimers (Figure 1.17b). The dimerization of coumarin and 7-methylcoumarin are both converted to the *anti*-head to head dimer with 97% selectivity. The dimerization of 6-methylcoumarin shows preference for the same dimer but with slightly lower selectivity of 84%.⁷⁹

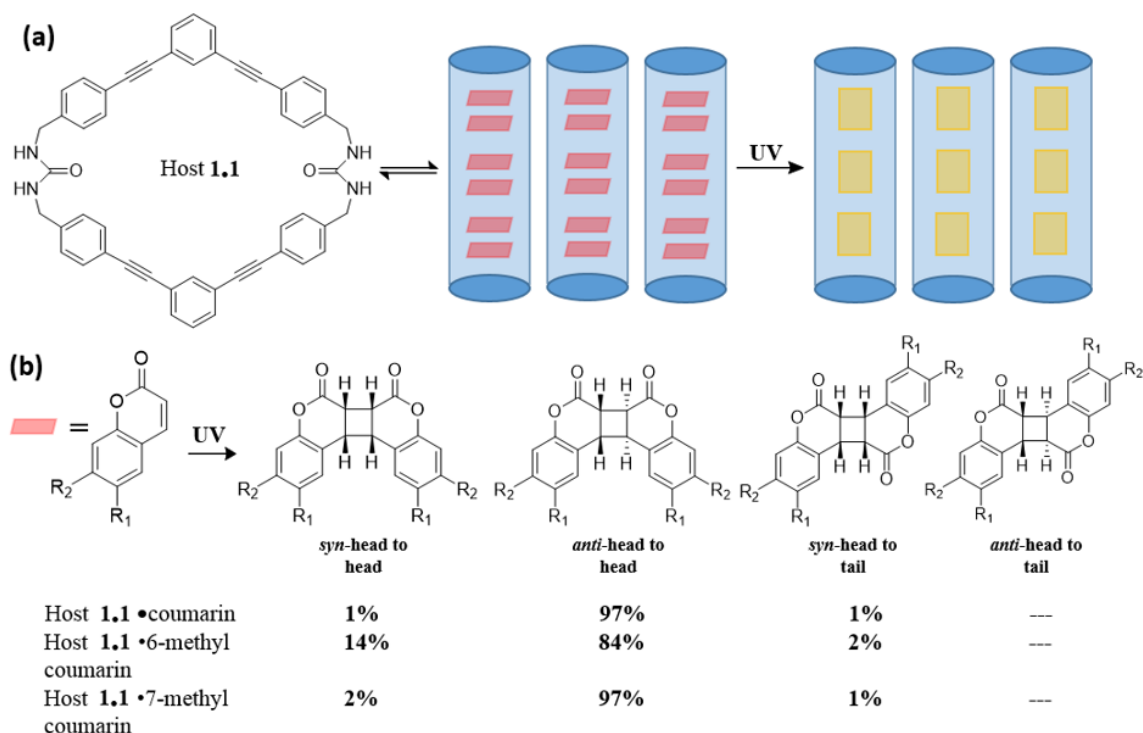


Figure 1.17. Schematic representation of (a) the dimerization within assembled host **1.1** cavity and (b) product distribution for the selective dimerization of coumarin, 6-methylcoumarin, and 7-methylcoumarin.

One variation of Shimizu's *bis*-urea macrocycle has benzophenone, a well-known, triplet sensitizer, incorporated into its design. Assembled benzophenone *bis*-urea

macrocycle (host **1**) has previously been used for isomerization and selective oxidation of encapsulated guests.^{81,82} Dewal demonstrated that the confined environment of assembled host **1** facilitates the *cis-trans* photoisomerization of encapsulated *trans*- β -methylstyrene upon UV irradiation (Figure 1.17).⁸¹ The isomerization of *trans*- β -methylstyrene is known to only occur in the presence of a triplet sensitizer.^{83,84} Host **1** has also been applied for selective oxidations of encapsulated guests via singlet oxygen. Molecular oxygen, which is in the triplet state in its stable form, can easily be excited to singlet oxygen when it comes in contact with a triplet sensitizer under UV irradiation.⁸⁵ Singlet oxygen, unlike ground state molecular oxygen, is highly reactive and interacts with encapsulated guests within assembled host **1** cavity. Geer demonstrated that UV-irradiation of the host **1**•2-methyl-2-butene complex resulted in the selective oxidation via singlet oxygen with 80% conversion into the allylic alcohol, 3-methyl-2-buten-1-ol, with 90% selectivity. UV-irradiation of host **1**•cumene complex also results in 69% conversion into α,α' -dimethyl benzyl alcohol with 63% selectivity. What is particularly interesting about the oxidation products is that these products are typically only seen as a result of radical mechanisms. Perhaps the host **1** complex possessed radical character that participated mechanistically in host: guest reactions! Electron paramagnetic resonance (EPR) was used to analyze host **1** and verified the presence of radical character although simple detection of a radical does not ‘prove’ that this species participates mechanistically in the oxidation reaction. Therefore, we attempted to investigate the origin and characterization of this radical. Chapter 2 of this thesis outlines experiments concerning host **1** radical and discusses our current findings.

1.9. Summary and Conclusions

Supramolecular chemistry, defined by Lehn as “chemistry beyond the molecule”, is the study of the self-assembly of small building blocks into larger more complex architectures without application of external force. This field is unique in that supramolecular complexes are achieved using weaker reversible intermolecular forces. This provides the possibility of designing intricate functional materials without the use of complex covalent synthesis. However, careful planning during the design stage is required to effectively utilize intermolecular forces in the design of supramolecular architectures. This requires extensive knowledge of the forces by which assembly is achieved. The strength, directionality, and conditions under which each intermolecular force is optimal have all been highlighted. Additionally, supramolecular complexes resulting from the entire spectrum of intermolecular forces with varying degrees of assembly and functionality have also been discussed. Dimers, capsules, trimers, cages, oligomers, polymers, columnar, and nanotubular assemblies along with properties that can't be observed from the individual building blocks have all been highlighted. *Bis-urea* macrocycles are of particular interest to our research. As first demonstrated by Karle, *bis-urea* macrocycles are capable of predictable assembly into columnar nanotubes with defined cavities that are capable of selective guest binding. Karle's research has provided inspiration for early examples of Shimizu's *bis-urea* macrocycles, which has since expanded to include many *bis-urea* macrocycle variations with a multiplicity of functionality and applications.

In this thesis, we investigate the unique properties observed of the benzophenone *bis-urea* macrocycle (host **1**). Specifically, chapter 2 investigates the unusual stable room

temperature radical observed for host **1**. As previously demonstrated by Dewal and Geer, host **1** is capable of facilitating host: guest reactions such as the isomerization of β -methylstyrene and the selective oxidation of 2-methyl-2-butene and cumene.^{80,81} Selective oxidation of both 2-methyl-2-butene and cumene via singlet oxygen resulted in products typically generated via radical processes. This suggests that host **1** possesses radical character that participates mechanistically in host: guest reactions resulting in the selectivity observed for the mentioned selective oxidations. Host **1** was analyzed by electron paramagnetic resonance (EPR) and the resulting spectra revealed that host **1** possesses radical character. In order to understand if and how this radical drives selectivity, a better understanding of the unusually stable radical is required along with characterization. Chapter 2 highlights the experiments performed thus far on the unusual radical observed for host **1**.

1.10 References

1. Ercolani, G. *J. Phys. Chem. B* **1998**, *102*, 5699-5703.
2. Seeman, N. C. *Angew. Chem.*, **1998**, *110*, 3408-3428.
3. Seeman, N. C. *Angew. Chem.*, **1998**, *37*, 3220-3238.
4. Lehn, J. -M. *Angew. Chem. Int. Ed. Engl.*, **1988**, *27*, 89-112.
5. Schneider, H. -J.; Yatsimirsky, A. *Principles and Methods in Supramolecular Chemistry*, VCH, Weinheim, **2000**.
6. Steed, J. W.; Atwood, J. L. *Supramolecular Chemistry*, Wiley, Chichester, **2000**.
7. Lehn, J.-M. *Supramolecular Chemistry: Concepts and Perspectives*, VCH, Weinheim, **1995**.
8. Rehm, T.; Schmuck, C. *Chem. Commun*, **2008**, 810-813.
9. Tsivadze, A. Y.; Ionova, G. V.; Kostrubov, Y. N. *Russ. Chem. Rev.* **2007**, *76*, 213-233.
10. Marie, R-L.; Christian, P. *Science China Chem.* **2013**, *56*, 24-32.
11. Chi, X.; Xu, D.; Yan, X.; Chen, J.; Zhang, M.; Hu, B.; Yu, Y.; Huang, F. *Polym. Chem.*, **2013**, *4*, 2767-2772.
12. Park, S.; Li, X.; Kim, H. M.; Singh, C. R.; Tian, G.; Hoyt, M. A.; Lovell, S.; Battaile, K. P.; Zolkiewski, M.; Coffino, P.; Roelofs, J.; Cheng, Y.; Finley, D. *Nature*, **2013**, *479*, 512-516.
13. Glusker, J. P. *Top. Curr. Chem.*, **1998**, *198*, 1-56.
14. Israelachvili, J. *Intermolecular & Surface Forces*, Academic Press, London, 2nd edn, **1992**.
15. Kelly, T. R.; Kim, M. H. *J. Am. Chem. Soc.*, **1994**, *116*, 7072-7080.

16. Jeffrey, G. A., *An Introduction to Hydrogen Bonding*, Oxford University Press, New York, **1997**.
17. Legon, A. C.; Millen, D. J. *Chem. Soc. Rev.*, **1987**, *16*, 467-498.
18. Rebek, Jr. J. *Chem. Commun.*, **2007**, 2777-2789.
19. Wang, F.; Ma, N.; Chen, Q.; Wang, W.; Wang, L. *Langmuir* **2007**, *23*, 9540-9542.
20. Takwale, M. G.; Pant, L. M., *Acta. Crystallogr. Sect. B*, **1971**, *27*, 1152-1158.
21. Shimizu, L. S.; Salpage, S. R.; Korous. A. A. *Acc. Chem. Res.*, **2014**, *47*, 2116-2127.
22. Schneider, H. J. *Angew. Chem. Int. Ed.* **2009**, *48*, 3924-3977.
23. Allen, F. H.; Baalham, C. A.; Lommerse, J. P. M.; Raithby, P. R. *Acta Crystallogr. Sect. B.* **1998**, *54*, 320-329.
24. Hunter, C. A.; Sander, J. K. M. *J. Am. Chem. Soc.*, **1990**, *112*, 5525-5534.
25. Battaglia, M. R.; Buckingham, A. D.; Williams, J. H. *Chem. Phys. Lett.*, **1981**, *75*, 421-423.
26. Waters, M. L. *Curr. Opin. Chem. Biol.*, **2002**, *6*, 736-741.
27. Hunter, C. A.; Lawson, K. R.; Perkins, J.; Urch, C. J. *J. Chem. Soc. Perkin. Trans. 2*, **2001**, 651-669.
28. Hwang, J.; Li, P.; Carroll, W. R.; Smith, M. D.; Pellechia, P. J.; Shimizu, K. D. *J. Am. Chem. Soc.* **2014**, *136*, 14060-14067.
29. West, J.; Mecozzi, S.; Dougherty, D. A. *J. Phys. Org. Chem.* **1997**, *10*, 347-350.
30. Cox, E. G.; Cruickshank, D. W. J.; Smith, J. A. S. *Proc. R. Soc. London*, **1958**, *247*, 1-21.

31. Burley, S. K.; Petsko, F. A. *Science* **1985**, 229, 23-28.
32. Burley, S. K.; Petsko, G. A. *Adv. Protein Chem.* **1988**, 39, 125-189.
33. Spirko, V.; Engkvist, O.; Soldan, P.; Selzle, H. L.; Schlag, E. W.; Hobza, P., *J. Chem. Phys.* **1999**, 111, 572-582.
34. Lewis, G. N.; Randall, M. *J. Am. Chem. Soc.* **1921**, 43, 1112-1154.
35. Gokel, G. W.; Barbour, L. J.; Ferdani, R.; Hu, J. X. *Accounts Chem. Res.* **2002**, 35, 878-886.
36. Krygowski, T. M.; Fawcett, W. R. *J. Am. Chem. Soc.* **1975**, 97, 2143-2148.
37. Lauher, J. W. *J. Am. Chem. Soc.*, **1978**, 100, 5305-5315.
38. Hermes, S.; Witte, T.; Hikov, T.; Zacher, D.; Bahnmueller, S.; Langstein, G.; Huber, L. Fischer, R. A., *J. Am. Chem. Soc.* **2007**, 129, 5324-5325.
39. Jung, S. H.; Lee, J-H.; Forster, P. M.; Ferey, G.; Cheetham, A. K.; Chang, J-S. *Chem. Eur. J.* **2006**, 12, 7899-7905.
40. Koshland, D. E. *Angew. Chem. Int. Ed. Engl.* **1995**, 33, 2375-2378.
41. Hirschberg, J. H. K.; Brunsveld, L.; Ramzi, A.; Vekemans, J. A.; Sibesma, R. P.; Meijer, E. W. *Nature*, **2000**, 407, 167-170.
42. Beijer, F. H.; Kooijman, J.; Spek, A. L.; Sijbesma, R. P.; Meijer, E. W. *Angew. Chem. Int. Edn. Engl.*, **1998**, 37, 75-78.
43. Sangeetha, N. M.; Maitra, U. *Chem. Soc. Rev.* **2005**, 34, 821-836.
44. Sergeev, S.; Pisula, W.; Geerts, Y. H. *Chem. Soc. Rev.* **2007**, 36, 1902-1929.
45. Li, Z.; Barnes, J. C.; Bosoy, A.; Stoddard, J. F.; Zink, J. I. *Chem Soc. Rev.* **2012**, 41, 2590-2605.

46. Beer, P. D.; Gale, P. A.; Smith, D. K. *Supramolecular Chemistry*, Oxford University Press, **1998**.
47. Murray-Rust, P.; Glusker, J. P. *J. Am. Chem. Soc.*, **1984**, *106*, 1018-1025.
48. Cram, D. J.; Choi, H-J.; Bryant, J. A.; Knobler, C. B. *J. Am. Chem. Soc.* **1992**, *114*, 7748-7765.
49. Rebek, Jr, J. *Chem. Commun.*, **2007**, 2777-2789.
50. Vriezema, D. M.; Aragoes, M. C.; Elemans, J. A.; Cornelissen, J. J.; Rowan, A. E.; Nolte, R. J. *Chem. Rev.* **2005**, *105*, 1445-1490.
51. Gibb, C. L. D.; Sundaresan, A. K.; Ramamurthy, V.; Gibb, B. C. *J. Am. Chem. Soc.* **2008**, *130*, 4069-4080.
52. Gunderson, V. L.; Conron, S. M. M.; Wasielewski, M. R. *Chem. Commun.*, **2010**, *46*, 401-403.
53. Flamigni, L.; Ventura, B.; Oliva, A. I.; Ballester, P. *Chem.-Eur. J.*, **2008**, *14*, 4214-4224.
54. Hunter, C. A.; Meah, M. N.; Sanders, J. K. M. *J. Am. Chem. Soc.*, **1990**, *112*, 5773-5780.
55. Fujita, M.; Oguro, D.; Miyazawa, M.; Oka, H.; Yamaguchi, K. Ogura, K. *Nature* **1995**, *378*, 469-471.
56. Kusukawa, T.; Nakai, T.; Okano, T.; Fujita, M. *Chem. Lett.* **2003**, *32*, 284-285.
57. Haycock, R. A.; Yartsev, A.; Michelsen, U.; Sundstrom, V.; Hunter, C. A. *Angew. Chem. Int. Ed.*, **2000**, *39*, 3616-3619.
58. Moorthy, J. N.; Natarajan, R.; Venugopalan, P. *Angew. Chem. Int. Ed.*, **2002**, *14*, 4317-4320.

59. Brunsveld, L.; Folmer, B. J. B.; Meijer, E. W.; Sijbesma, R. P. *Chem. Rev.* **2001**, *101*, 4071-4097.
60. Li, G.; McGown, L. B. *Science* **1994**, *264*, 249-251.
61. Lee, J. Y.; Painter, P. C.; Coleman, M. M. *Macromolecules* **1988**, *21*, 954-960.
62. Appella, D. H.; Christianson, L. A.; Klein, D. A.; Powell, D. R.; Huang, X.; Barchi, J. J.; Gellman, S. H. *Nature*, **1997**, *387*, 381-384.
63. Nelson, J. C.; Saven, J. G.; Moore, J. S.; Wolynes, P. G., *Science*, **1997**, *277*, 1793-1796.
64. Sakai, N.; Majumdar, N.; Matile, S. *J. Am. Chem. Soc.* **1999**, *121*, 4294-4295.
65. Clark, T. D.; Buriak, J. M.; Kobayashi, K.; Isler, M. P.; McRee, D. E.; Ghadiri, M. R. *J. Am. Chem. Soc.* **1998**, *120*, 8949-8962.
66. Semetey, V.; Didierjean, C.; Briand, J-P.; Aubry, A.; Guichard, G. *Angew. Chem.*, **2002**, *114*, 1975-1978.
67. Nelson, J. C.; Saven, J. G.; Moore, J. S.; Wolynes, P. G. *Science*, **1997**, *277*, 1793-1796.
68. De Santis, P.; Morosetti, S.; Rizzo, R. *Macromolecules*, **1974**, *7*, 52- 58.
69. Clark, T. D.; Buriak, J. M.; Kobayashi, K.; Isler, M. P.; McRee, D. E.; Ghadiri, M. R. *J. Am. Chem. Soc.* **1998**, *120*, 8949-8962.
70. Ghadiri, M. R.; Granja, J. R.; Milligan, R. A.; McRee, D. E.; Khazanovich, N. *Nature*, **1993**, *366*, 324-327.
71. Etter, M. C.; Urbanczyk-Lipkowska, Z.; Zia-Ebrahimi, M.; Panunto, T. W. *J. Am. Chem. Soc.*, **1990**, *112*, 8415-8426.
72. Etter, M. C.; Panunto, T. W. *J. Am. Chem. Soc.*, **1988**, *110*, 5896-5897.

73. Shimizu L. S.; Smith, M. D.; Hughes, A. D.; Shimizu, K. D. *Chem. Commun.*, **2001**, 1592-1593.
74. Mayer, M. F.; Nakashima, S.; Zimmerman, S. C. *Org. Lett.*, **2005**, *14*, 3005-3008.
75. Simic, V.; Bouteiller, L.; Jalabert, M. *J. Am. Chem. Soc.*, **2003**, *125*, 13148-13154.
76. Ranganathan, D.; Lakshmi, C.; Karle, I. L. *J. Am. Chem. Soc.* **1999**, *121*, 6103-6107.
77. Roy, K.; Wibowo, A. C.; Pellechia, P. J.; Ma, S.; Geer, M. F.; Shimizu, L. S. *Chem. Mater.* **2012**, *24*, 4773-4781.
78. Roy, K.; Wang, C.; Smith, M. D.; Pellechia, P. J.; Shimizu, L. S. *J. Org. Chem.* **2010**, *75*, 5453-5460.
79. Dawn, S.; Dewal, M. B.; Sobransingh, D.; Paderes, M. C.; Wibowo, A. C.; Smith, M. D.; Krause, J. A.; Pellechia, P. J.; Shimizu, L. S. *J. Am. Chem. Soc.* **2011**, *133*, 7025-7032.
80. Dawn, S.; Salpage, S. R.; Koscher, B. A.; Bick, A.; Wibowo, A. C.; Pellechia, P. J.; Shimizu, L. S. *J. Phys. Chem. A* **2014**, *118*, 10563-10574.
81. Dewal, M. B.; Xu, Y.; Yang, J.; Mohammed, F.; Smith, M. D.; Shimizu, L. S. *Chem. Commun.* **2008**, 3909-3911.
82. Geer, M. F.; Walla, M. D.; Solnstev, K. M.; Strassert, C. A.; Shimizu, L. S. *J. Org. Chem.* **2013**, *78*, 5568-5578.
83. Arai, T.; Sakuragi, J. Tokumaru, K. *Bull. Chem. Soc. Jpn.*, **1982**, *55*, 2204-2207.
84. Rocklye, M. G.; Salisbury, K. *J. Chem. Soc., Perkin. Trans.* **1972**, *2*, 158215-85.
85. Foote, C. S. *Acc. Chem. Res.* **1968**, *1*, 104-110.

CHAPTER 2

INVESTIGATION OF THE UNUSUAL ROOM TEMPERATURE STABLE RADICAL OBSERVED FOR ASSEMBLED BENZOPHENONE BIS-UREA MACROCYCLES

2.1 Abstract

Stable organic radicals at room temperature are rare in nature. Significant stabilization from hyperconjugation, resonance and sterics is typically required for organic radicals to be stable at room temperature. Recently, the Shimizu group reported a self-assembled benzophenone *bis*-urea macrocycle (host **1**) that facilitated the selective oxidation of an encapsulated alkene when UV-irradiated in an oxygen atmosphere to afford products that are typically observed in radical mediated reactions.¹ Surprisingly, the host displayed a stable room temperature radical upon UV irradiation. It is not known if the host **1** radical plays a role in the oxidation of the encapsulated guest. This chapter investigates the structure and properties of host **1**, a ¹⁵N labeled host and a urea protected derivative before and after UV-irradiation through electron paramagnetic resonance (EPR), IR, UV-vis, fluorescence, and computational analysis. EPR analysis confirmed a single broad uncoupled signal after UV-irradiation with a G-value of 2.0060 +/- 0.0001, which was unusually stable and persisted up to eight days after UV irradiation. UV-vis spectra possibly has a very weak λ_{max} at 588 nm⁻¹, which might corresponds to ketyl radical; however, the intensity is exceedingly small (0.01). Thus more studies are necessary.

EPR comparison of host **1** to a ¹⁵N labeled analogue, computational analysis, and the appearance of a new λ_{max} at 588 nm all point to a benzophenone ketyl type radical as the likely source of the EPR signal in the UV-irradiated host **1** crystals. Understanding the nature of this radical could provide valuable information towards the selective oxidation demonstrated by assembled host **1**. Additionally, better characterization of host **1** radical would expand upon what is known about stable organic radicals.

2.2.1 Introduction

Supramolecular complexes with controlled assembly and defined cavities have been employed as confined environments for selective reactions,²⁻⁴ as functional materials for absorption and sequestration of reactive species and intermediates,⁵⁻⁷ and as molecular machines and electronic materials.⁸⁻¹⁰ A supramolecular approach may use significantly less chemical synthesis versus a comparable covalently bound complex. Also advantageous is that supramolecular approaches are potentially responsive to solvent environment, temperature, and guest encapsulation.¹¹

Accessing supramolecular complexes with specific properties requires careful consideration of the size, shape, and the forces by which the individual building blocks will assemble. For example, supramolecular binding of larger guests requires building blocks that predictably assemble into cavities that are complimentary in size and shape to the target guests. This is highlighted by Fujita's supramolecular cage, which was discussed in Chapter 1 (section 1.5, page 20). Fujita's tetrameric cages are formed by pyridyl ligands that coordinate to the two vacant sites of Pd (II) complexes with roughly 90°. ¹² The Fujita group expanded on this design by using extended pyridine ligands in the design of a tetrameric cage with specific size dimensions capable of binding guests of compatible size. Figure 2.1 illustrates these differences by comparing a cage formed from the smaller pyridine ligand (a) versus a larger cage formed with an extended tridentate ligand (b). A comparison of the cavity size is indicated by the size of the guests that each cage can encapsulate. The first cage binds guests such as 2-phenylpropanoate, 1-adamantyl carboxylate, and 4-methoxyphenylacetate.¹² These guests range in size 2-phenylpropanoate, up to the a largest, 4-methoxyphenylacetate, a difference of $\sim 102 \text{ \AA}^3$

versus 156 \AA^3 respectively. The guest 4-methoxyphenylacetate is especially important because it gives an indication of cage cavity size because it binds in a 1:1 host guest ratio. By using a tridentate ligand with aromatic extensions, the cavity of the cage can be significantly expanded allowing for encapsulation of bigger or a larger amount of smaller guests. This larger cage is capable of binding four 4-adamantyl carboxylate molecules which are $\sim 123 \text{ \AA}^3$ each.¹³ This example highlights how cavity dimensions of a supramolecular complex can be tuned through ligand choice and modification.

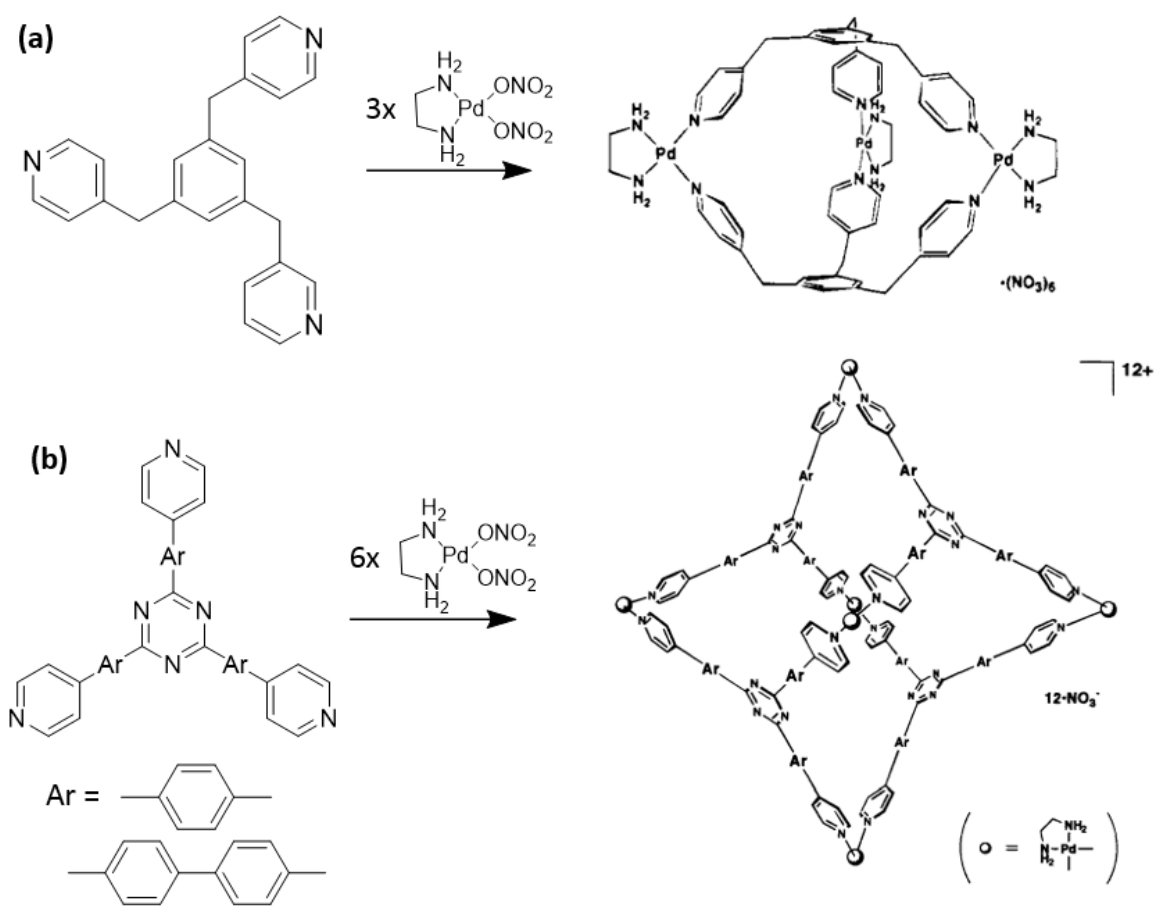


Figure 2.1. Judicious choice of pyridyl ligands by the Fujita group afford smaller and larger cages. a) Smaller of the two cages resulting from the assembly of two 1,3,5-tris(4-pyridylmethyl)benzene with three $\text{Pd}(\text{NO}_3)_2$ molecules.¹² b) Larger cages resulting from the assembly of tridentate ligands, with varying length modifications from aromatic groups, with six $\text{Pd}(\text{NO}_3)_2$ molecules.¹³

*Permission granted by American Chemical Society and Nature Publishing Group

Beyond simply binding guests or stabilizing reactants, supramolecular complexes can facilitate organic, inorganic and photochemical reactions.¹⁴⁻¹⁹ As highlighted by Fujita's cages, supramolecular complexes are capable of binding specific guests. In addition to guest binding, certain supramolecular complexes are capable of facilitating host: guest reactions upon encapsulated guests. The type of reactions can be modified by the functionality of the supramolecular complex. As this thesis is focused on photochemical processes, specifically triplet energy transfer processes, we will discuss examples of supramolecular complexes that incorporate triplet sensitizers either within their framework or as encapsulated guest molecules. For example, Ramamurthy utilized the Gibb's octa acid egg shell design that self assembles in the presence of a hydrophobic guests.⁴ Fluorenone, a triplet sensitizer guest capable of encapsulation, was bound from an aqueous solution by the egg shell host which is then capable of transferring triplet energy to other guests in solution upon UV irradiation. The inclusion of a triplet sensitizer guests was applied in the isomerization of stilbenes. Calzaferri *et al.* also demonstrated triplet energy transfer with a supramolecular $[\text{Ru}-(\text{bpy})_2(\text{bpy}-\text{ph}_4-\text{Si}(\text{CH}_3)_3)]^{2+}$ complex.²⁰ The supramolecular complex is capable of absorbing oxazine 1 dyes within its chambers which are then subjected to triplet-singlet excitation energy transfer from the Ru^{+2} complex to included dye guests. Mascio *et al.* also used a tetaruthenated porphyrin supramolecular complex to decompose DNA model compounds such as 2'-deoxyguanosine via a singlet oxygen mediated mechanism.²¹ These examples demonstrate how supramolecular assembly can be used to facilitate triplet energy transfer and facilitate reactions. By designing complexes that possess triplet sensitizer character and/or are capable of binding

a triplet sensitizer, a supramolecular assembly can then be applied to selective triplet energy processes.

Shimizu's self-assembling *bis*-urea macrocycle are tunable and can also be modified to incorporate triplet energy transfer. Benzophenone, a well-known triplet sensitizer, is present as the C-shaped spacer in the benzophenone *bis*-urea macrocycle (host **1**). As medium energy triplet sensitizers, benzophenone can absorb UV irradiation and be excited to a singlet excited state. Benzophenone has been shown to absorb 320-370 nm light for $n-\pi^*$ transitions and 240-300 nm light $\pi-\pi^*$ transitions (Figure 2.2).²² The first excited state then undergoes intersystem crossing (ISC) to the more stable triplet excited state. This energetic state is then capable of transferring its triplet energy of 69 kcal/mol to a suitable acceptor molecule.²³ This chapter will highlight the previous applications of assembled host **1** and discuss research concerning unusually stable radical observed for assembled host **1**.

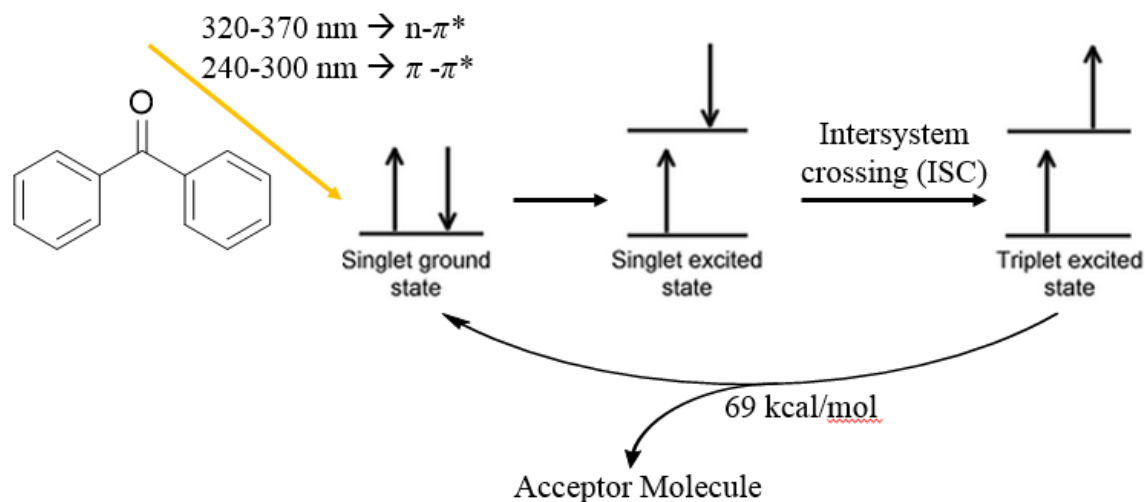


Figure 2.2. Benzophenone has been shown to absorb 320-370 nm light for $n-\pi^*$ transitions and 240-300 nm light $\pi-\pi^*$ transitions. Upon absorption, benzophenone is excited from the singlet ground state to the singlet excited state. The singlet excited then undergoes intersystem crossing to the more stable triplet excited state. The triplet excited state can then transfer energy to a suitable acceptor molecule.

2.2.2 Background and Significance

The Shimizu group investigated the assembly and utility of *bis*-urea macrocycles, which consist of two urea groups and two C-shaped spacers.²⁴ Important design features include macrocyclic building blocks with C-shaped spacers of different size and functionality that predictably assemble into nanotubular assemblies through the urea three centered hydrogen bonding motif.²³ Dewal *et al.* first synthesized a variation of this design, a *bis*-urea macrocycle that utilizes two benzophenone C-spacers (host **1**).²⁵ Benzophenone was incorporated into the macrocyclic design due to its photophysical properties. Benzophenones have previously been used for polymerization initiation,²⁶ photodimerization,²⁷ and singlet oxygen transformations.²⁸ The *bis*-urea macrocyclic units assemble as designed into columnar structures (Figure 2.3) *via* a bifurcated hydrogen bonding network with each individual macrocycle unit spaced 4.74 Å apart. In addition to hydrogen bonding interactions, the columnar structures are further stabilized by edge to face aryl-stacking interactions. Assembled host **1**'s cavity is small with dimensions of 3.7 Å x 2.7 Å corresponding to the intramolecular distances between H8-H8* and H7-H7* respectively. The crystallization solvent DMSO filled the channel in a 1:1 macrocycle:guest ratio. The solvent could be removed from the host **1**•DMSO crystal by heating (RT to 180°C with a ramp of 4°C/min) in the TGA, leaving the empty host **1**, whose nanochannel was capable of binding a series of other guests such as tetrahydrofuran, ethyl acetate, 2-methyl-2-butene, cumene and others.^{1,25}

Work from our group demonstrated that the benzophenone moiety in the framework of the nanotube could be used to facilitate selective triplet sensitized processes (Figure 2.4c,d).^{24,28,29} Dewal demonstrated that the confined environment of assembled host **1**

facilitated the *cis-trans* photoisomerization of encapsulated *trans*- β -methylstyrene upon UV irradiation.²⁴ The isomerization of *trans*- β -methylstyrene is known to only occur in the presence of a triplet sensitizer.^{30,31} This isomerization was also attempted within assembled *bis*-urea phenyl ether macrocycle **2** (Figure 2.3c), which does not incorporate a triplet sensitizer. Although both host **1** and **2** absorb the *trans*- β -methylstyrene in similar ratios, the *cis-trans* photoisomerization was only observed in the channel of host **1** but not in host **2**, which lacks the triplet sensitizer. The successful isomerization of *trans*- β -methylstyrene within host **1**'s cavity demonstrated that the sensitizer of host **1** is capable of transferring energy directly to included guests (Figure 2.4b).

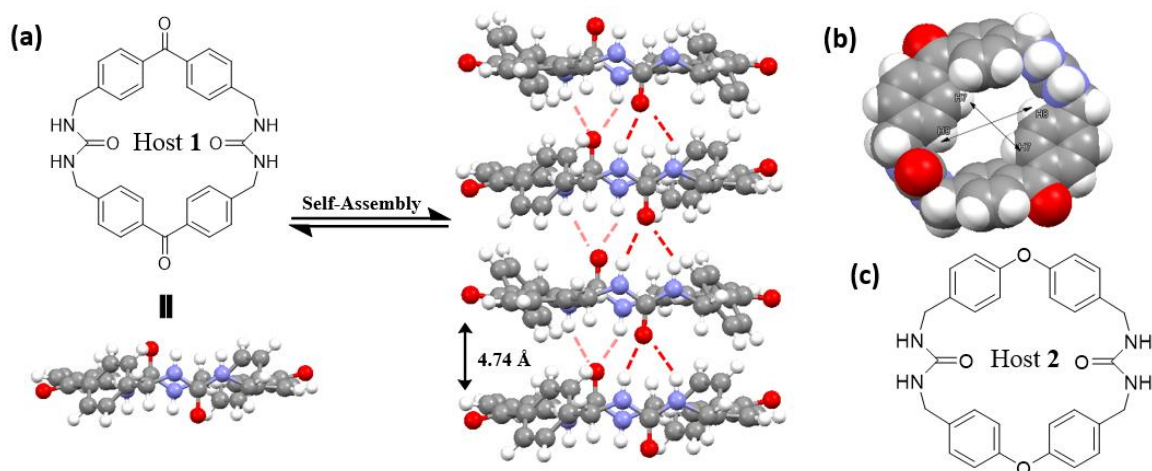


Figure 2.3. (a) Structure of host **1** macrocycle and its hydrogen bonded assembly motif and (b) host **1** cavity dimensions. (c) Structure of *bis*-urea phenyl ether macrocycle (host **2**)

Geer *et al.* further investigated the properties of this host and examined its utility to promote other triplet sensitized processes. They demonstrated that host **1** is capable of facilitating selective oxidation reactions. First, they showed that UV-irradiation of host **1** in oxygenated deuterated chloroform generated singlet oxygen, a very reactive oxidant,

which was characterized based on its near IR emission spectra of singlet oxygen produced from host **1** crystals excited at $\lambda_{\text{max}}=345$.²⁸ They next investigated the oxidation of encapsulated guests containing allylic or benzylic sites when the solid complexes were UV-irradiated under an oxygen atmosphere. Suitable guests for the small channel of the host included both 2-methyl-2-butene and cumene, which formed solid host:guest complexes. UV-irradiation of the host **1**•2-methyl-2-butene complex resulted in the selective oxidation with 80% conversion into the allylic alcohol, 3-methyl-2-buten-1-ol, with 90% selectivity. UV-irradiation of host **1**•cumene complex also results in 69% conversion into α,α' -dimethyl benzyl alcohol with 63% selectivity. The cumene oxidation is typically observed as a radical process in seen the case of Mayer's *cis*-[RuIV(bpy)₂(py)(O)]²⁺ and Zhang's CuO nanoparticle facilitated oxidations.^{32,33}

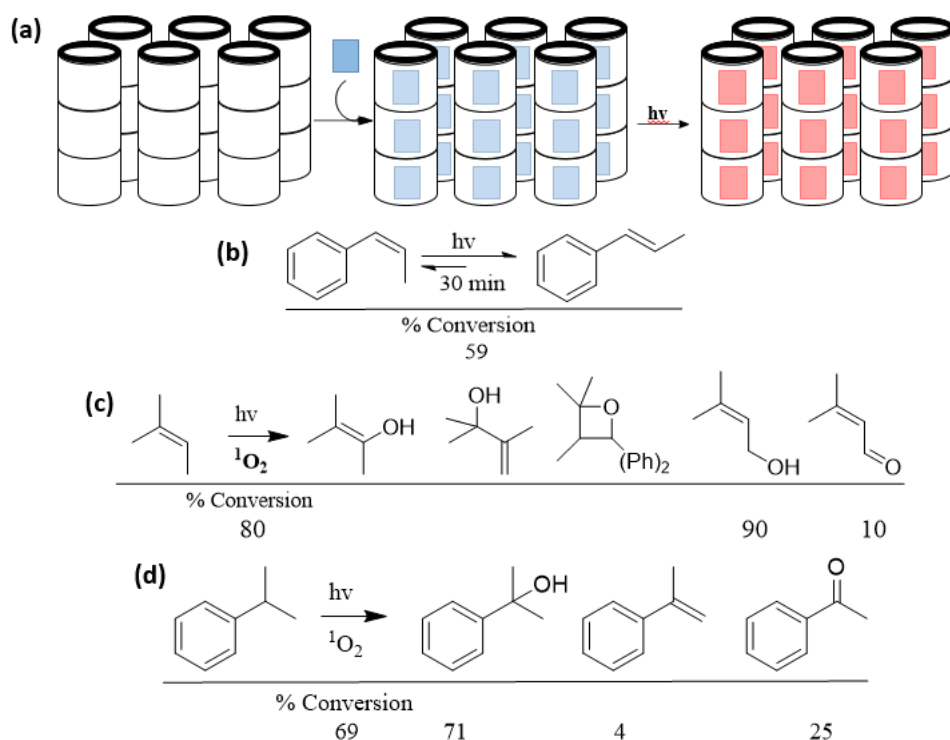


Figure 2.4. (a) Schematic representation of host **1** guest loading and conversion, (b) isomerization of *trans*- β -methylstyrene,²⁴ (c) selective oxidation of 2-methyl-2-butene, (d) and selective oxidation of cumene facilitated by host **1**.^{28,29}

Because these oxidations typically occur *via* radical mechanisms, Geer investigated if the host and host•guest complexes exhibit radical character. Host **1** (empty), host **1**•2-methyl-2-butene, and host **1**•cumene were probed by electron paramagnetic resonance (EPR) analysis and showed radical character under ambient light conditions. EPR is a type of spectroscopy that detects unpaired electrons. Upon UV irradiation, each of these signal were intensified (Figure 2.5).²⁸ The empty host **1** complex showed positive EPR signal (RT under O₂ (g)), with a single uncoupled peak. The observed *g*-value, which is the measurement of the radicals response to an applied magnetic field, at ambient light exposure was *g* = 2.0049 a very similar spectra was observed after 1h UV irradiation (365 nm) with *g* = 2.0051 (Figure 2.5a). Host **1**•2-methyl-2-butene and host **1**•cumene both showed similar EPR signals after ambient light exposure. The signals were significantly enhanced upon UV irradiation and affording a broad uncoupled signal with a *g*-Value of *g* = 2.0051 (Figure 2.5b and c respectively).

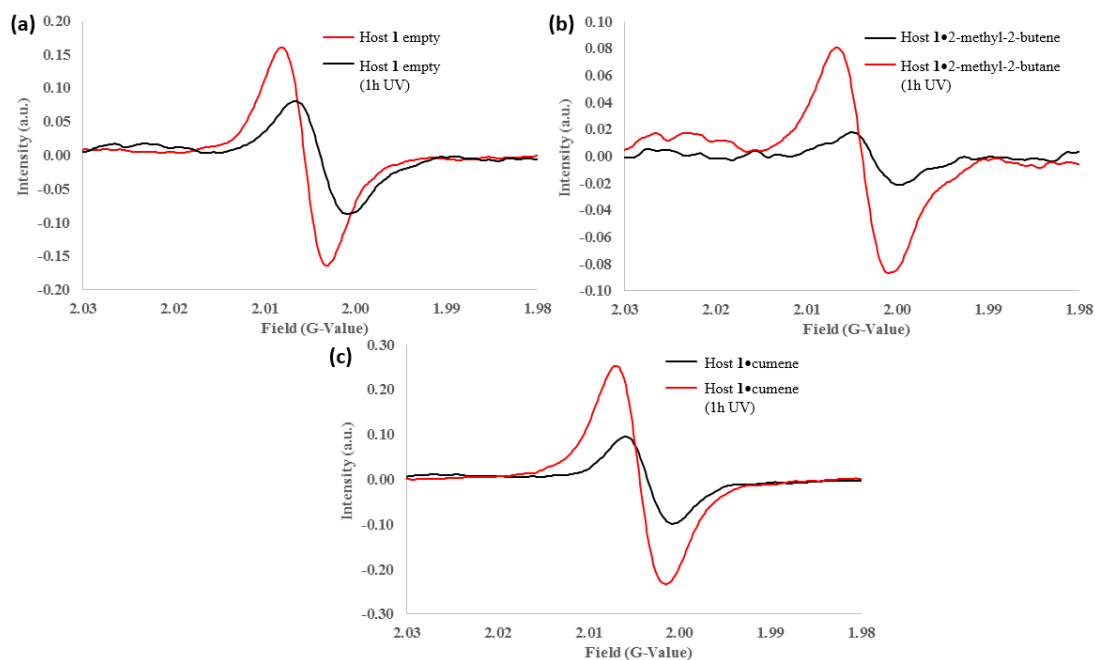
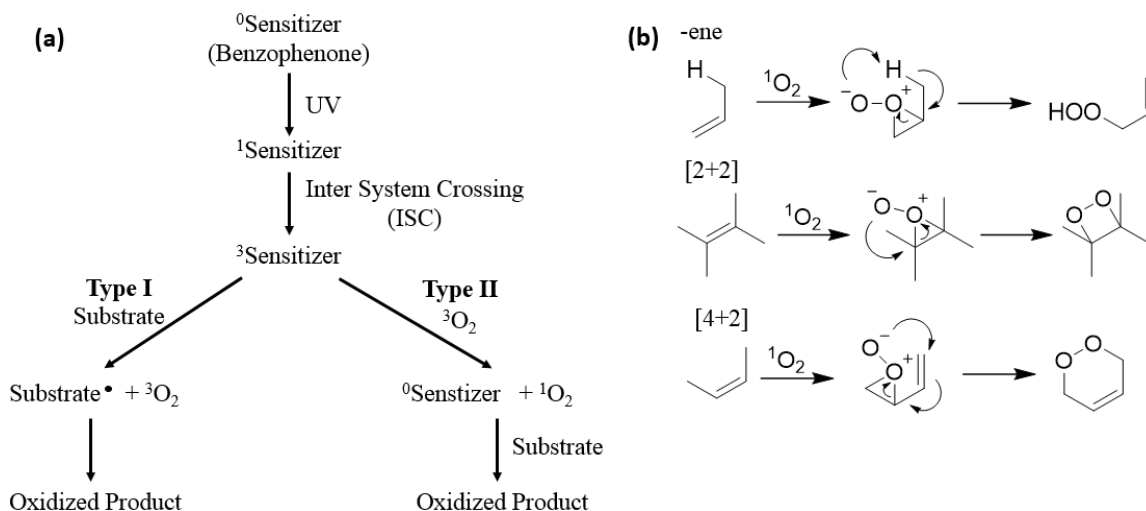


Figure 2.5. Geer's EPR analysis before and after 1h UV irradiation of (a) host **1** empty, (b) host **1**•2-methyl-2-butene, and (c) host **1**•2cumene

These EPR findings as well as the intriguing selectivity observed in the oxidations raises the question of what is the mechanism of oxidation within the channels of host **1**. Could host **1** be participating mechanistically in the oxidation reaction? One possible pathway for singlet oxygen mediated oxidation proceeds by a type 1 mechanism described by Foote (Scheme 2.1).^{34,35} Such a process would be characterized by hydrogen abstraction from included guest to host **1** resulting in resonance-stabilized radical. This radical could then react with triplet oxygen followed by hydrogen reabstraction back from host to guest resulting in the final alcohol. An alternative possibility is the confinement assisted singlet oxygen-ene mechanism (Scheme 2.1b). Such a singlet oxygen-ene pathway begins with the olefin reacting with singlet oxygen and typically result in peroxides that require reduction to the corresponding alcohols.³⁶ In Geer's case, the observed products required no reduction suggesting that the formation of the alcohol occurred without going through a peroxide precursor. Alternatively, the peroxide might be quickly reduced within the host under the reaction conditions. Closer investigation of the mechanistic aspects of this unusually selective process could provide insight for the design of other industrially useful catalysts capable of controlling the selectivity of oxidation reactions. Section 2.3 outlines experiments concerning the radical character of assembled host **1** with the intent of understanding if the radical character is related to host: guest reaction selectivity.



Scheme 2.1. Reaction pathways of Type I and Type II singlet oxygen mechanism. (a) Type I reactions are characterized by energy transfer from an excited sensitizer to substrate which forms a radical substrate. The radical substrate then reacts with triplet (ground state) oxygen to form an oxidized product. Type II reactions differ in that the excited sensitizer transfers its energy to triplet oxygen to form singlet oxygen. Singlet oxygen then reacts with the substrate to yield oxidized product. (b) Representation of the -ene , [2+2], and [4+2] singlet oxygen pathways.

2.3.1 Research Design and Methods

Stable organic room temperature radicals are rare and are limited to examples such as triarylmethyl,³⁷ nitroxide,³⁸ thiazyl,³⁹ and verdazyl radicals.⁴⁰ Host **1** consists of two benzophenone units and two ureas, neither of which is known to show radical character at room temperature. The stable organic radicals from the literature are not structurally similar to host **1** and possible radical centers like benzophenone and urea are only observable at extremely low temperature.^{41,42} This makes the stable room temperature radical observed for assembled host **1** intriguing. In such a simple molecule, there are relatively few choices. The radical center could be located at the benzophenone, at the ureas or at the aryl methylenes. Previously, benzophenone radicals have been reported in literature through radical trapping with nitroxides,^{43,44} through H-abstraction,⁴⁵ and at low

temperature.⁴⁶ Benzophenone, upon UV irradiation, is excited to a short lived singlet state that rapidly undergoes intersystem crossing to a triplet excited state. If there is a suitable proton in close proximity, benzophenone in the triplet excited state will typically abstract a hydrogen atom resulting in a benzophenone ketyl radical that is in the doublet excited state (Figure 2.6).⁴⁷ Benzophenone ketyl radicals have previously been observed through time resolved ESR detection at 77K as a doublet with a value of $g = 2.003 \pm 0.001$.⁴⁸ These radicals have been observed at room temperature after single electron reduction from potassium followed by single crystal x-ray crystallography.⁴⁹ Alternatively, urea radicals have been reported by Bowers via EPR analysis at 77K with a g-value of 2.0061.⁵⁰ Urea based radicals have not been observed at room temperature; however, the extended urea hydrogen bonding pattern in the assembled host may play a role in the radical stability.

The experiments outlined in the following section addresses some key questions about this radical including reproducibility, inclusion of benzophenone within a macrocycle unit's relation to radical stability, correlation between assembly and radical stability, the lifetime, temperature effects, attempts at characterization, and potential magnetic properties. By probing the nature and origin of the usually stable room temperature radical observed for host **1**, we hope to understand if and how this radical participates mechanistically in reactions that occur within its nanochannel.

2.3.2 Methods for probing the radical center

EPR analysis is notorious for being extremely sensitive to impurities. Thus our first goal was to reproduce Geer's reported EPR data for host **1**. Host **1** (empty) was analyzed via EPR after each of three recrystallization purification cycles using the same experimental parameters outlined by Geer's initial results. Additionally, we tested if

DMSO inclusion has an effect on radical signal. We also investigated more closely the time required for EPR signal quenching to further probe the lifetime of the observed radical. The examination of EPR at periodic intervals after excitation of assembled host **1** until the signal was quenched provided insight to the lifetime of the radical after UV excitation. Since radical character for host **1** was only observable upon irradiation, techniques like UV, IR, and fluorescence spectroscopy were used to compare host **1** before and after irradiation to look for changes in the structure.

To provide further insight into radical characterization, the stability of the benzophenone doublet excited state was probed by computational analysis to compare the energetic states of the parent benzophenone and the benzophenones within a single host **1** macrocycle unit. Differences in energetic states in addition to the gaps between energy states were calculated and compared for both systems. Using the information gathered from computational analysis, we drew conclusions about whether inclusion within a single macrocycle unit makes higher energetic states of benzophenone more energetically favorable. A host **1** ketyl radical calculated to be more stable than benzophenone would suggest that inclusion within the macrocycle has a stabilizing effect on the radical.

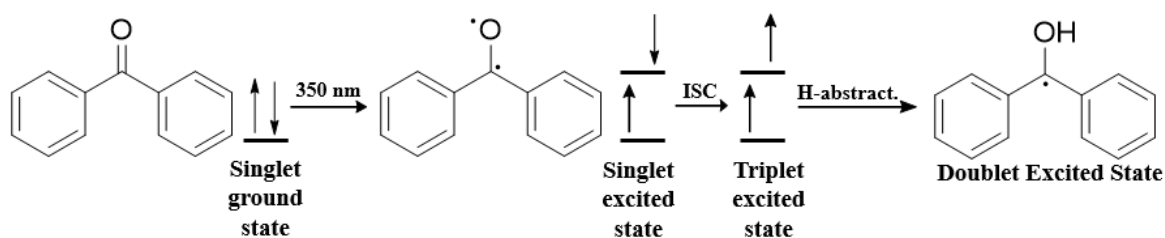


Figure 2.6. The excitation of benzophenone to the ketyl radical state with the corresponding energetic states. Benzophenone upon UV irradiation is excited to a singlet excited state. This state then undergoes intersystem crossing to the triplet excited state. If there is a suitable proton in close proximity then the di radical will abstract the proton resulting in a benzophenone ketyl radical in a doublet excited state.⁴⁶

What factors contribute to the unusual stability of the host **1** radical? Potentially, the supramolecular assembly could influence the radical lifetime, in this case the columnar structure and further packing of the columns to afford the crystalline host **1**. As seen with nitroxyl radicals such as TEMPO, significant radical stabilization is provided by sterics from four methyl groups. Does assembly and/or crystal packing provide a similar type of stability for host **1**? To address these questions, we must first review the solid-state structure and packing of the host.²⁴ As seen in the crystal structure (Figure 2.3), a distance of 4.74 Å separates the carbonyl groups of adjacent macrocycle units. The urea nitrogens between neighboring nanotubes are also spaced 3.41 Å apart.²⁸ This long range order positions the benzophenone carbonyl oxygen close to the two methylene hydrogens of neighboring macrocycle units at 2.44 Å and 2.81 Å respectively. Similar to how the methyl groups provide steric stability to the nitroxyl radical seen in TEMPO, the nanotubular assembly may provide stability to host **1** radical. Our goal was to probe the structure and origin of the radical to see if it might be located at the benzophenone, at the ureas or at the aryl methylenes through the H-abstraction process. Additionally, the effects of the nanotubular assembly described above on host **1** radical stability was also be investigated.

EPR analysis was performed to compare host **1a** (protected host **1**), unassembled host **1** (in solution), precipitated host **1** (pre-crystallization), and assembled host **1**. Protected host **1** lacks the necessary hydrogen bond donors needed for the three point bifurcated hydrogen bond network seen for host **1**'s nanotubular assembly and has a different assembly motif. The precipitated host **1**, which is host **1** recovered from the deprotection step, should have an alternate or several alternate crystal forms and not only the nanotubular assembly, though it may be present. Thus, it serves to test if the specific

nanotube assembly motif is needed for radical stabilization. This precipitate was first analyzed via PXRD to analyze its crystalline character and compare it to the assembled host **1**.

In addition to IR, UV-vis and fluorescence studies, isotopic labeling were used in an effort to characterize host **1** radical. Free radicals respond differently to the applied magnetic field used in EPR between isotopically labeled radicals and non-labeled radicals. Isotopic labeling has previously been used for radical characterization.^{51,52} While labeled benzophenone derivatives are not readily available, ¹⁵N labeled urea is commercial. Therefore, ¹⁵N labeled host **1** derivative was targeted for synthesis and analysis by EPR spectroscopy. If host **1** radical is urea nitrogen centered or if an H-abstraction leads to a radical on the neighboring methylene group, we expected to observe a change or noticeable broadening of signal for the ¹⁵N labeled host. The remainder of this chapter discusses the synthesis and characterization of host **1** in addition to our investigation of the unusually stable room temperature radical observed for host **1** through the experiments described above.

2.3.3 Methods for probing magnetic properties of host 1

The search for magnetic open framework structures has become a major objective due to their potential applications in the development of low density magnetic materials, magnetic sensors and intelligent or multifunctional materials.⁵³ Because of the many potential uses of these magnetic materials, there is currently special interest in designing materials whose magnetic properties can be accessed by application of external light. Previous examples of photoswitchable materials include Irie and Matsuda's photochromic spin coupler that readily interconverts between singlet and triplet states,⁵⁴ Iwamura's

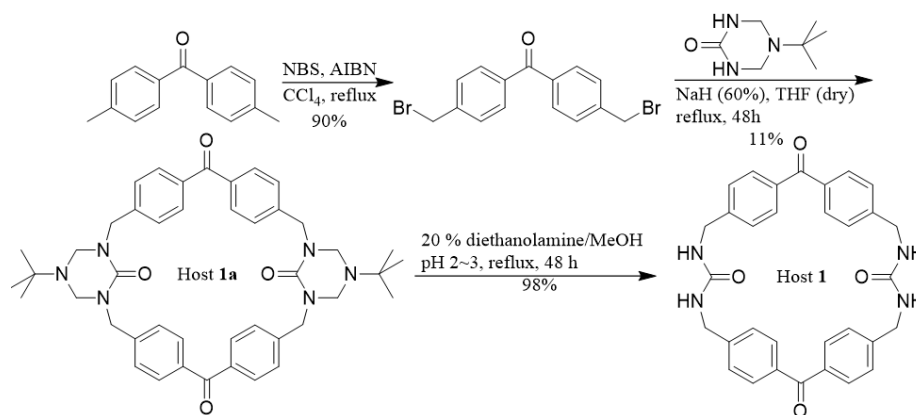
diradical consisting of two stable nitroxide radicals connected through an isomerizable bridge,⁵⁵ and Hashimoto's Cobalt-Iron Cyanide Prussian blue analog that undergoes ferromagnetic modulation as a result of an internal photochemical redox reaction.⁵⁶ There are even fewer examples of supramolecular photomagnetic materials, none of which are purely organic. Currently, Veciana's ferrocene-based polychlorotriphenylmethyl radical system is the only supramolecular photoswitchable material in literature.⁵⁷

Should the assembled host **1**•DMSO complex form significant amount of radicals, it could be a candidate for a photoswitchable magnetic material. In order for our complex to be a supramolecular magnetic material, both synthetic tailoring of open-shell building blocks that allow both proper control over their supramolecular assembly and the establishment of correct magnetic interactions are required. Crystal engineering through hydrogen-bonding interactions has proven to be a powerful method for achieving both conditions.⁵⁸ Besides the structural control offered by hydrogen bonding (as discussed in Ch. 1), hydrogen bonds have also been shown to favor magnetic exchange interactions between bound radical molecules of α -nitronyl nitroxides, α -imino nitroxides, or tert-butyl nitroxide derivatives.⁵⁹⁻⁶² In addition to host **1** being a possible supramolecular magnetic photoswitchable material, it may also be switchable via guest inclusion. Currently, only one purely organic solvent switchable magnetic material has been reported in the literature.⁶³ This complex consists of a series of carboxylic-substituted polychlorinated triphenylmethyl radicals assembled through hydrogen bonding that can reversibly bind a handful of common solvents. What is particularly intriguing about their system is how the rigidity of their assembly weakens when the complex is empty of solvent. Host **1** was probed for magnetic properties using superconducting quantum interference device

(SQUID) analysis as discussed in section 2.11. Such measurements also help to quantify the amount of radical formed in the solid sample.

2.4 Synthesis and characterization of host 1

Benzophenone bis-urea macrocycle (host **1**) was prepared *via* the three step synthesis used by Dewal (Scheme 2.2).²⁴ First, commercially available 4,4'-dimethylbenzophenone was brominated using a free radical bromination with *N*-bromosuccinimide in the presence of a catalytic amount of azobisisobutyronitrile (AIBN) in carbon tetrachloride at reflux to afford the 4,4'-bis(bromomethyl)benzophenone. The resulting dibromide was purified via silica gel column chromatography using 1:9 ethyl acetate: hexane as mobile phase. Pure dibromide was cyclized with triazinanone in THF (dry) using sodium hydride (60% suspension in oil) as base. The crude protected macrocycle was purified via silica gel column chromatography using 1:19 methanol: ethyl acetate as mobile phase. Pure protected macrocycle was deprotected using acidified (pH 2~3) 20% diethanolamine in methanol resulting in host **1** as a white precipitate.



Scheme 2.2. Synthesis of *bis*-urea benzophenone macrocycle (host **1**). Reagents and Conditions: 4,4-dimethylbenzophenone was brominated using *N*-bromosuccinimide (NBS) and 2,2'-azobis(isobutyronitrile) (AIBN) in CCl₄ at reflux to produce 4,4'-*bis*-(bromomethyl)benzophenone. The dibromide was reacted with triazinanone and NaH in dry THF at reflux to yield the protected macrocycle (host **1a**), which was deprotected in acidified diethanol amine/methanol mixture resulting in the *bis*-urea benzophenone macrocycle (host **1**).

Crystals were obtained by dissolving pure host **1** in hot DMSO (130 °C, 80 mg/ 40 mL) followed by slow cooling (1 °C/hr) to room temperature. Rod shaped crystals suitable for X-ray crystallography were obtained in 4 days. Figure 2.7 illustrates the columnar structures obtained by the assembly of **1** through the ureas via a bifurcated hydrogen bonding network, similar to Dewal's crystal data. However, we observed that the DMSO guests were highly ordered with about 90% of DMSO guest molecules pointing in the same direction while filling the channel in a 1:1 host:guest ratio (Figure 2.7). This was different than the earlier structure in which a 50:50 distribution of DMSO guest molecules was found. The polar nature of host **1**'s nanochamber is ideal for DMSO binding because it complements its molecular dipole. The ureas of host **1** are highly polarized with the urea NH's showing a partial positive and the carbonyl oxygen showing a partial negative charge at the and a partial positive at the urea hydrogens (Figure 2.7a). This charge distribution is responsible for host **1** nanotubular hydrogen assembly through the urea backbone but it could also contribute to the strong interaction to DMSO guests. Due to the electronegativity of oxygen, DMSO possesses a partial negative charge at the oxygen while the methyl groups have a partial positive charge (Figure 2.7b). When DMSO is loaded host **1**'s nanochamber, the molecular dipoles of host **1** and DMSO align resulting in host: guest complex with DMSO tightly bound (Figure 2.7c). Additionally, the highly ordered nature of DMSO within host **1** chamber is a result of a dipole-dipole interaction between the methyl groups of one guest to sulfur of an adjacent one. The DMSO guests were removed

from the crystal by heating (RT to 180°C with ramp of 4 °C/min) via thermogravimetric analysis (TGA), leaving an empty nano-chamber capable of binding a series of other guests.

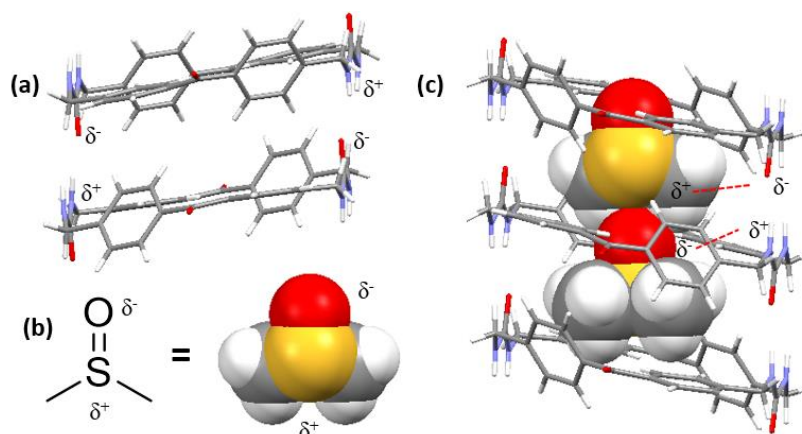


Figure 2.7. Crystal structure of assembled host **1** with 90% order of DMSO molecules pointing in the same direction. (a) Space fill model of DMSO from crystal structure highlighting its molecular dipole, (b) host **1** crystal structure with DMSO removed showing the partial charges associated with the urea functionality and (c) host **1**•DMSO structure front view with partial charges aligned with ordered DMSO guest molecules.

2.5 Host **1** crystal structure comparison after UV-irradiation.

EPR analysis performed by Geer revealed that assembled host **1** possesses radical character. The intensity of the observed radical signal was significantly higher after UV irradiation. Therefore, we wanted to test if the crystal structure of UV irradiation host **1** showed structural changes that could identify the radical center. A single host **1**•DMSO crystal, purified via three recrystallization cycles, was submitted for X-ray crystal analysis (Figure 2.8a). This same crystal was then UV irradiated for 30 min as previously described and submitted again for X-ray crystal analysis (Figure 2.8b). No differences in crystal structure were observed suggesting that either radical concentration is too low to be detected or that crystal structure comparison isn't adequate for detecting host **1** radical. A crystallographic approach to characterizing reactive intermediates or unstable radicals is uncommon.⁶⁴ Detecting electron density changes caused by a single electron is extremely

difficult, especially if the population of radical is low. The identical structure of host **1** crystal before and after 30 UV irradiation indicates that electron density changes are too minimal to be detectable by X-ray crystallography. An alternative approach would be to look for conformational changes in the single crystal structure that result from radical formation.

As mentioned previously, the benzophenone moiety could be a potential radical center. Figure 2.6 highlights that benzophenone ketyl radicals are formed after hydrogen abstraction from a suitable proton source. The methylene groups could be a potential proton source for host ketyl radical formation. However, analysis of host **1** crystal after UV irradiation was identical showing no conformational changes relating to the methylene hydrogen atoms. Future methods to increase the percentage of radical include using a more powerful UV source or longer UV exposure times. If host **1** radical population can be increased to a detectable amount, then it could be possible to observe structural host **1** ketyl radical via X-ray crystallography.

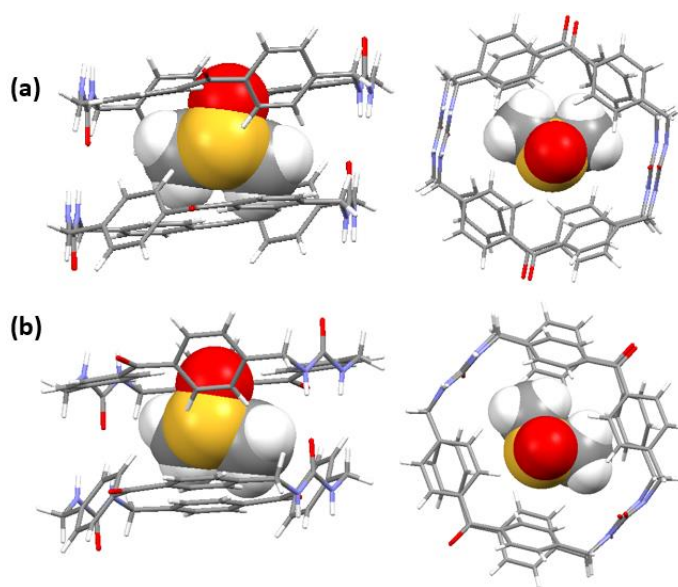


Figure 2.8. Front and top view of host **1** X-ray crystal structure (a) before and (b) after 30 min UV irradiation.

2.6. Evaluation of host 1 EPR data

With crystals in hand, we set out to repeat and confirm the EPR experiments from Geer. EPR spectroscopy is a versatile nondestructive analytical technique capable of detecting the presence of free radicals. However, this technique is especially sensitive to impurities. To test that the observed radical is not due to some impurity, host **1** was analyzed via EPR after each of three recrystallization cycles. Recrystallization was performed by first dissolving host **1** (20 mg) in hot DMSO (10 mL) at 130 °C in a sealed pressure tube. Host **1** solution was then filtered via Millipore vacuum filtration to remove unwanted particles. The solution was placed back into an oil bath at 130 °C and was allowed to slow cool at a rate of 1° C/hour to room temperature. The colorless needle crystals were collected via Millipore vacuum filtration and washed with methylene chloride (25 mL) to remove any excess DMSO. To verify the purity of host **1** after each recrystallization cycle, the sample was analyzed via ¹H-NMR with the understanding that NMR is likely only sensitive enough to identify an impurity of >2-3% . Crystals were then heated to 180 °C using a ramp of 4 °C/min via TGA to remove DMSO from host **1** nanochamber. After each recrystallization cycle, the host **1**•DMSO crystals were freshly evacuated by TGA to yield the empty host (5 mg) that were immediately loaded into an EPR tube and purged with argon gas for 5 min. EPR spectra was then recorded. Sample was then UV irradiated for 30 min in a Rayonet reactor equipped with 16 x 120 W lamps (350 nm). The EPR spectra was again recorded.

The initial freshly recrystallized host **1** (empty) EPR analysis is shown in Figure 2.9a and shows no signal after ambient light exposure (Figure 2.9, black lines). This is different than Geer's EPR analysis which showed a single broad uncoupled signal at $g =$

2.0049 upon ambient light exposure albeit with very low intensity.²⁸ However, similar to Geer, we observed a broad 20 gauss uncoupled signal (as measured from the beginning of the signal to the center) for host **1** (Figure 2.9, red line) at $g = 2.0061$, suggesting an organic radical has indeed been generated. Next, the sample was recrystallized from host DMSO and the experiment repeated. Again, initially host **1** showed no radical signal under ambient conditions (Figure 2.10b, black); however, after UV-irradiation, a broad signal was observed with $g = 2.0059$ (Figure 2.10b, red). This sample was recrystallized a third time, the DMSO was removed by TGA, and the EPR measured under ambient conditions. Again, no signal was observed (Figure 2.10c, black). After UV-irradiation, the broad signal with $g = 2.0061$ was again observed. Given that an identical signal was observed after each recrystallization at $g = 2.0060 \pm 0.0001$, we conclude that host **1** (empty) possesses radical character only after UV irradiation.

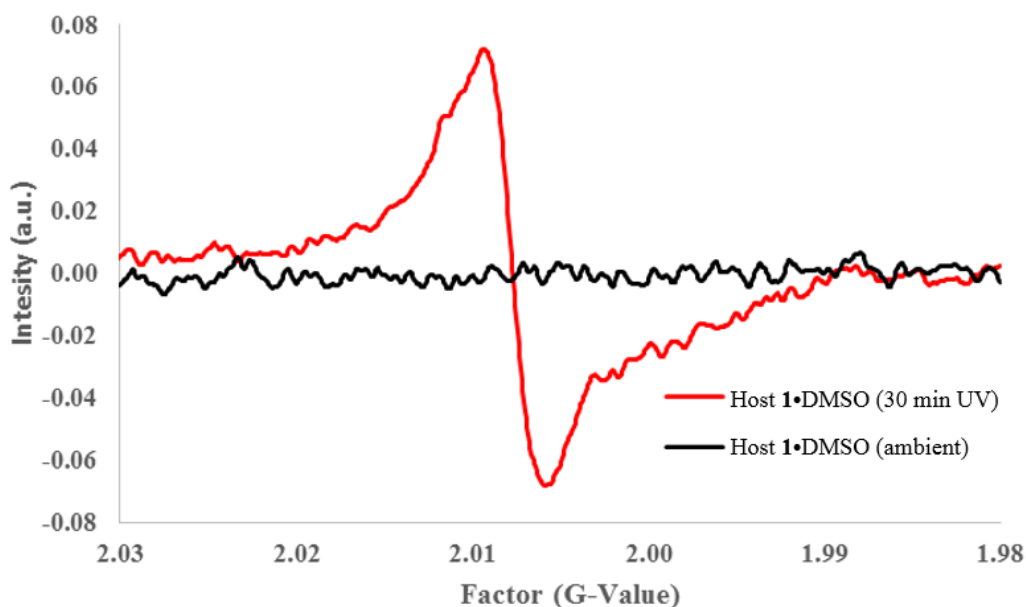


Figure 2.9. EPR analysis on host **1**•DMSO, purified by three recrystallization cycles, before and after 30 min UV irradiation.

2.7. Host 1•DMSO EPR

Geer probed empty host **1**, host **1**•2-methyl-2-butene, and host **1**•cumene complexes by EPR analysis (Figure 2.4) and demonstrated that guest inclusion has no effect on radical host **1** character.²⁸ We sought to analyze host **1**•DMSO to test if it also shows UV-initiated radical formation. Host **1**•DMSO crystals (10 mg), purified via three recrystallization cycles, were placed in an EPR tube and purged with argon gas for 5 minutes. EPR analysis was then performed. Sample was then transferred to the Rayonet reactor and UV irradiated for 30 mins. EPR analysis was again performed. Similar to host **1** (empty), no signal was observed for host **1**•DMSO after ambient light exposure (Figure 2.9, black line). Upon UV exposure, a single broad uncoupled signal was observed at $g = 2.0060$ (Figure 2.9, red line). Much like host **1**•2-methyl-2-butene, and host **1**•cumene complexes analyzed by Geer, the guest DMSO in the host **1**•DMSO complex does not appear to influence the radical character observed upon UV irradiation of host **1**.

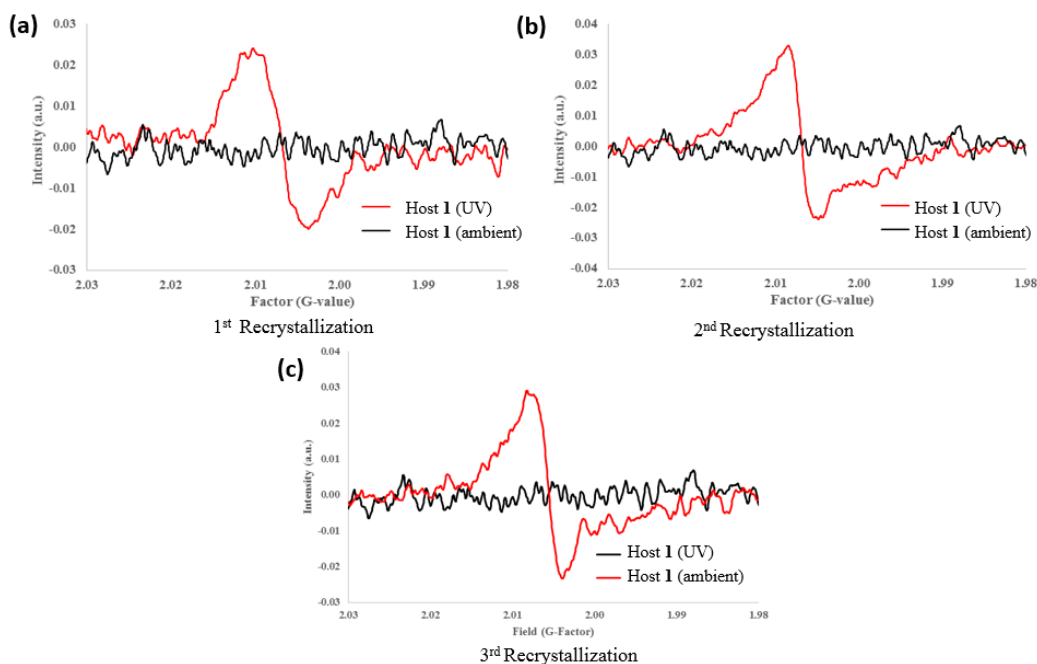


Figure 2.10. Host **1** (empty) EPR analysis before and after 30 min UV irradiation under Argon atmosphere after the (a) 1st, (b) 2nd, and (c) 3rd recrystallization cycles.

2.8. Dark Quenching of Host 1 Radical

The host **1**•DMSO radical generated by UV exposure has been shown to quench over an unknown amount of time in the dark.²⁸ In an effort to understand the lifetime of the radical, host **1**•DMSO was monitored via EPR from 0 h to 10 days in the dark. Host **1**•DMSO crystals (5 mg), purified via one recrystallization cycle, were collected, washed, and dried on a Millipore vacuum filtration apparatus. Sample was then washed with methylene chloride (25 mL) and dried on the filter apparatus for an additional 10 min. The sample was then purged with argon for 5 min then transferred to the Rayonet UV reactor and irradiated for 30 min. The EPR spectra was recorded then the sample was wrapped in aluminum foil and stored in the dark. Every 24 hours, sample was loaded into the EPR sample holder in the dark with any exposed parts of the EPR tube wrapped in foil. EPR spectra was recorded in the dark and once again wrapped in foil and stored in the dark. This process was repeated until the EPR signal was completely quenched (Figure 2.11). A very slight signal was observed after 8 days; however, no signal was observed after 9 days. Therefore, we conclude that host **1** (DMSO) radicals are remarkable stable and persist for ~8 days after UV exposure with G values of $g = 2.0065 \pm 0.0001$.

The signal persisted for a total of 8 days which is slightly longer than previously reported. Assuming that the signal is a result of host **1** ketyl radical, host **1** radical lifetime is significantly longer than the lifetime estimated previously for literature examples of benzophenone ketyl radicals of 2.0 ns \pm 0.1 in cyclohexane solution and > 5 ns in gas phase for benzophenone ketyl radicals. In general, the solid state and or the specific columnar assembly may be contributing to this stabilization.

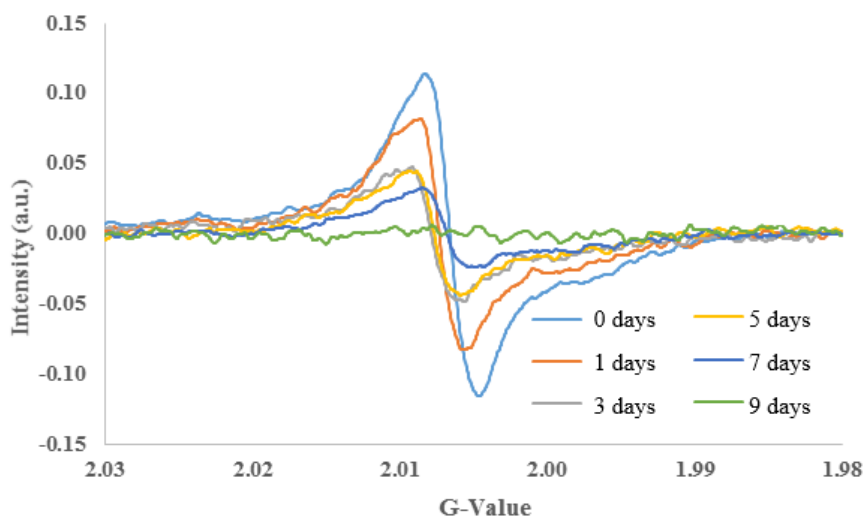


Figure 2.11. Host **1** •DMSO dark quenching EPR analysis over nine days

2.9. Investigation of the influence of assembly on radical stability

To investigate if the unusual stability of the radical displayed by host **1** complex was correlated to assembly, we next compared host **1** and the protected host **1a** by EPR spectroscopy. Host **1a** lacks the necessary hydrogen bond donors needed for nanotubular as seen in Figure 2.12a. The structure of host **1a** was obtained by Dewal and Smith from chloroform and is shown in Figure 2.12b.²⁴ Host **1a** assembly differs from host **1** in that assembly doesn't result from a hydrogen bond network through a urea backbone. Instead, assembly results from a series of dipole-dipole interactions between adjacent host **1a** macrocycle units. These interactions in addition to the steric bulk of the t-butyl groups cause host **1a** to adopt a tilted columnar assembly with disordered chloroform molecules occupying the interstitial space. As host **1a** does not adopt the same columnar assembly as observed for host **1** yet contains the benzophenone moiety, we were curious if it would display detectable radical formation upon UV-irradiation. Powder host **1a** (5 mg) was placed into an EPR tube and purged with argon for 5 min. Sample was then UV irradiated

for 30 min using a Rayonet reactor equipped with 16 x 120 W lamps (350 nm) followed by EPR analysis. Figure 2.12c shows that no EPR signal indicative of radical character was observed for host **1a** at room temperature.

Benzophenone ketyl radical species typically exhibit high reactivity and are too reactive to survive for an extended period of time.⁴⁷ Previous analysis of benzophenone ketyl radical systems required stabilization of the ketyl radical species using low temperatures.^{46,47} Could the columnar assembly motif of host **1** be stabilizing a benzophenone ketyl type radical? To gauge the effect of assembly on radical stability, we investigated the EPR of host **1** in solution (unassembled), pre recrystallization, and columnar assembled (crystalline) host **1** after UV irradiation.

The unassembled host **1** was analyzed by dissolving host **1** (1 mg, 1.88×10^{-3} mmol) in DMSO (1 mL). Host **1** solution was then UV irradiated for 30 min at 350 nm then immediately analyzed via EPR. No signal was observed indicating that unassembled host **1** has no radical character. Alternatively, the lifetime of a protected host **1** (host **1a**) radical might be significantly reduced due to the lack assembly. Next, freshly deprotected host **1** was precipitated from the acidified diethanolamine deprotection step outlined in Scheme 2.2 and analyzed by PXRD analysis to probe its crystalline. Figure 2.13a displays the ordered powder diffraction pattern of precipitated host **1** with the assembled host **1**•DMSO. In comparing the two spectra, one observes that the peaks of the precipitate are broaden and shifted. Key low angle peaks at 7.60, 13.24, 15.28 and 20.28 two theta in the columnar assembled host **1** are much sharper and correlate to host **1** nanotubular assembly (Figure 2.17a). As mentioned, host **1** (precipitate) possesses shifted broader peaks at 12.88, 13.64, 16.08, 19.12, 19.72, 20.60, 22.72, 25.08, 25.88, 27.08, 29.84, 32.60, and 34.60. These

differences indicate that precipitated host **1** possesses a different crystal form than columnar assembled host **1**. In addition, it is likely that the precipitated host is a mixture of several crystal forms.

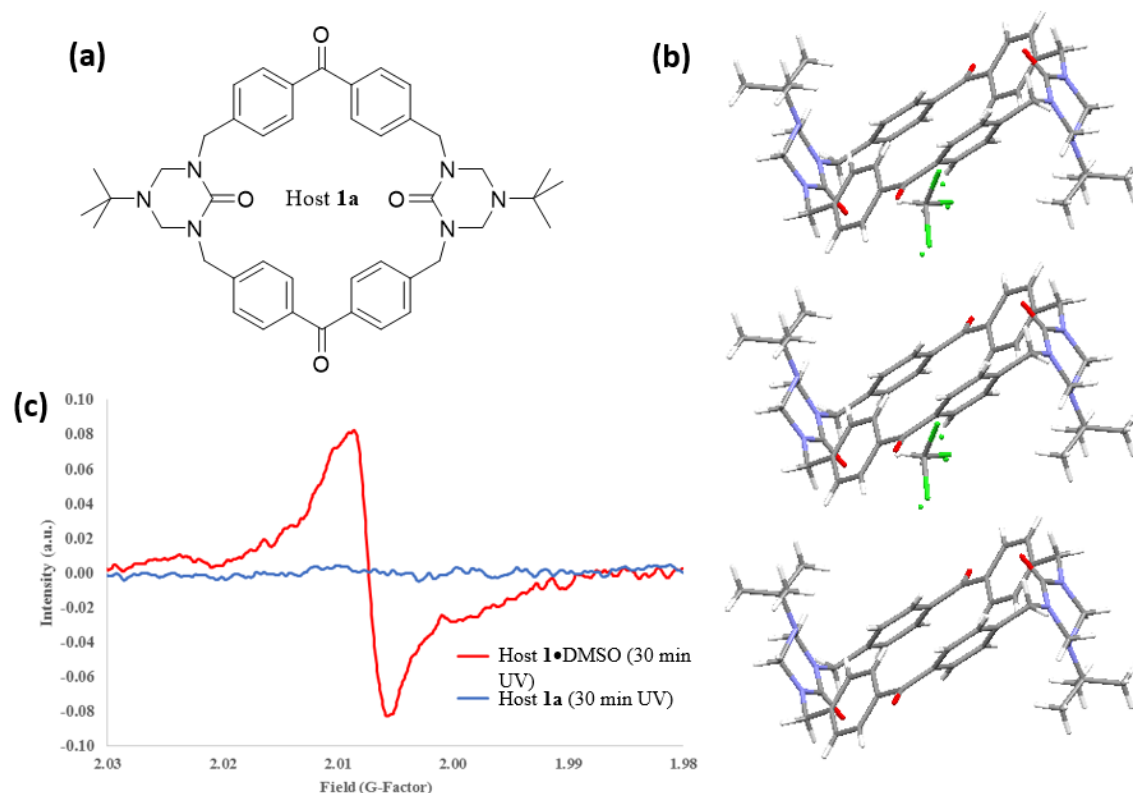


Figure 2.12. (a) Structure of host **1a**, (b) Dewal and Smith's host **1a** crystal structure²⁴ showing a staggered columnar assembly with disordered chloroform molecules in the interstitial space and (c) EPR comparison between UV irradiated host **1** and host **1a**.

The precipitated host **1** (5mg) was placed in an EPR tube and purged with argon for 5 min. Sample was then UV irradiated for 30 min followed by EPR analysis (Figure 2.13b). The resulting EPR spectra was extremely weak with a possible signal at $g = 2.0059$ however, the weak nature of the signal suggests that the precipitated host possesses very limited radical character. In summary, comparison of the EPR spectra from the different degrees of assembly of the benzophenone bis-urea macrocycle and the urea protected

macrocycle, suggest that columnar assembly may play a role in the stabilization of the radical of host **1**.

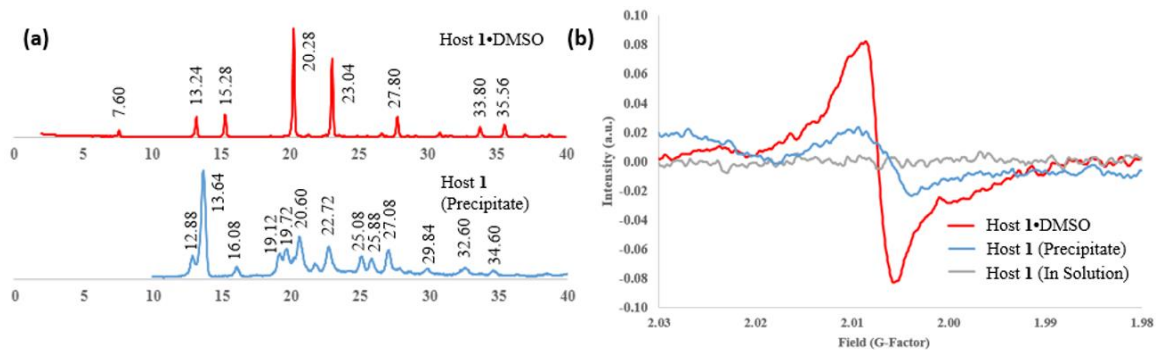


Figure 2.13. (a) PXRD comparison of host **1** (DMSO) and host **1** (precipitate) and (b) EPR comparison of unassembled, precipitate, and assembled host **1** after UV irradiation

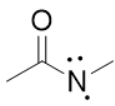
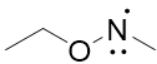
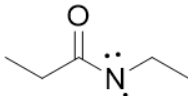
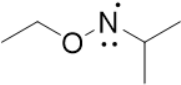
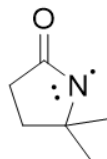
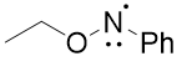
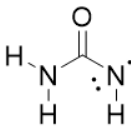
2.10 ^{15}N Labeled Host **1** EPR Comparison

To probe whether a radical is formed on the urea or near the urea nitrogen by the typical H-abstraction process, which would afford the benzophenone ketyl, we synthesized host **1** with an ^{15}N label. Urea with an ^{15}N label is commercially available with 98% ^{15}N enrichment and was used to synthesize the triazinanone, using the reported procedure.⁶⁵ We repeated the procedure in Scheme 2.2 (page 17) using the triazinanone stirring it with NaH in dry THF at reflux, then adding the dibromide to yield the protected macrocycle in 18% yield (75 mg). The macrocycle was deprotected in acidified diethanol amine/methanol mixture to afford ^{15}N Labeled host **1**, which was crystallized hot DMSO (130 °C) upon cooling to room temperature at rate of 1 °C/hour.

Several nitrogen centered radicals have been reported in the literature and their g-values are close to what we observed in the UV irradiated host **1**. For example, Ingold reported a series of amidyl radicals, observed at low temperatures (138-209 K), varying in

functionality with g-values ranging from 2.0044 for an *N*-methylpivalamide radical to 2.0063 for a 1,5,5-trimethylpyrrolidin-2-one (lactam-like) radical.⁶⁶ Ingold also reported a series of *N*-alkoxyamino radicals, which were also observed at low temperatures similar to the amidyl radicals, with g-values ranging from 2.0050 – 2.0044.⁶⁷ Bowers even reported a urea nitrogen based radical, which was observed at 77K, with a g-value of 2.0061 (Table 2.2).⁵⁰

Table 2.1. Nitrogen centered radicals, their g-values, and the temperatures at which they were observed.

Radical	G-Value	Temp. Observed (K)	Radical	G-Value	Temp. Observed (K)
	2.0055	151		2.0050	213
	2.0052	109		2.0046	213
	2.0063	209		2.0044	213
	2.0061	77			

Molecules with unpaired electrons are known to interact with applied external magnetic fields, but they are also known to be sensitive to the fine magnetic moments expressed by their nuclei.⁶⁸ Isotope variations of the same atom have different fine magnetic moments to which nearby radicals will respond differently. These differences are observable via EPR analysis through signal broadening and can be used to study the

locations of radical. Isotope labeling has previously been applied in the characterization of radicals. For example, Rakvin performed EPR experiments comparing L- α -alanine- ^{14}N to an ^{15}N analogue to analyze the one of the three known alanine radicals observed after UV irradiation; the $\text{NH}_3\text{C}(\text{CH}_3)\text{COO}^-$ radical.⁵² These studies resulted in the first report of the nitrogen hyperfine coupling tensors to the alanine carbon centered radical. This example highlights how isotope labeling can be used to identify radicals through labeling an adjacent nucleus. Another example was demonstrated by Brezova who enriched titania nanopowders with ^{17}O to characterize an oxygen centered radical.⁵¹ When comparing the EPR spectra of ^{16}O titania to ^{17}O enriched titania, significant signal broadening was observed for the ^{17}O rich sample thus proving that oxygen was the radical center. Brezova's strategy of direct isotope labeling was applied to host **1**. If the observed radical for UV irradiated host **1** is urea centered, we should see similar signal broadening when comparing the EPR spectra of our ^{14}N host to its ^{15}N analogue.

Freshly evacuated crystals of host **1** and ^{15}N host **1** (5 mg) were loaded into separate EPR tubes and purged with argon for 5 min. EPR analysis was then performed on both samples before UV exposure. As expected, neither sample yielded a positive EPR signal upon ambient light exposure. Crystals were then UV irradiated for 30 min using a Rayonet reactor equipped with 16 x 120 W lamps (350 nm) followed by EPR analysis. The EPR spectra show a single peak in both cases with a g-value of 2.0061 for host **1** and a g-value of 2.0059 for ^{15}N labeled host **1** (Figure 2.14b). No signal broadening was observed for the UV irradiated ^{15}N labeled analogue EPR spectra. This suggests that the observed radical for host **1** is not urea nitrogen centered and that a radical center is not attached to this nitrogen, as it should show altered hyperfine coupling due to the presence of the ^{15}N label.

However, it is possible that such hyperfine coupling is obscured by the broadness of the signal.

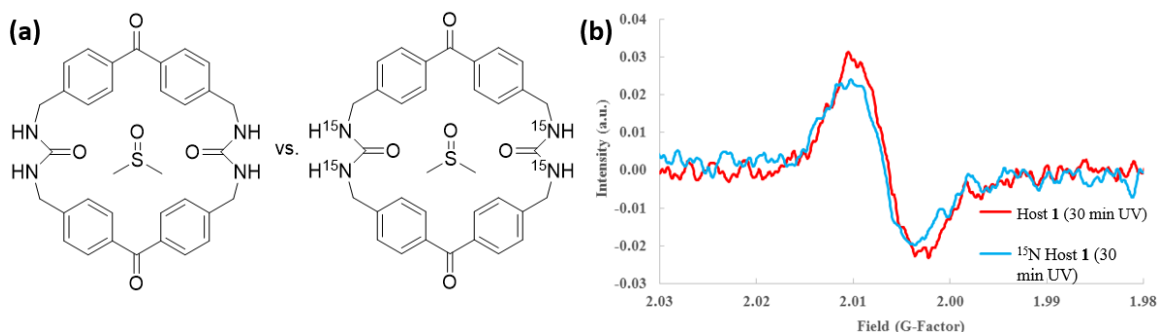


Figure 2.14. (a) Host **1** and its ^{15}N labeled analogue with the (b) resulting EPR spectra after 30 min UV irradiation

2.11. Variable Temperature EPR Studies

As discussed in section 2.10, no difference in EPR spectra was observed for UV irradiated host **1** (empty) when compared ^{15}N host **1** (empty) at room temperature. This data suggests that the radical is not urea nitrogen centered. However, the broadness of the EPR signal is problematic. Therefore, we next turned to variable temperature EPR to investigate if change in the hyperfine coupling could be observed as a function of temperature. Changes in coupling have been previously observed in variable temperature EPR experiments. For example, Chestnut and Phillips use variable temperature EPR analysis to study the temperature-dependent exchange interactions observed for crystalline $(\phi_3\text{PCH}_3)^+(\text{TCNQ})_2^-$ and $(\phi_3\text{AsCH}_3)^+(\text{TCNQ})_2^-$ salts.⁶⁹ They observed via EPR analysis that at -25°C these salts display a single uncoupled narrow signal. Upon EPR analysis at -140°C , the single uncoupled signal split into two sharp defined doublets spaced 112 gauss apart. By comparing the splitting observed at low temperature to the splitting of P^{31} and As^{75} nuclei reported in the literature,⁶⁹ Chestnut and Phillips were able to conclude that P^{31} and

As⁷⁵ nuclei were not correlated to the observed doublet. This led to the conclusion that the observed doublet represents zero-field splitting as a result of the dipolar interaction of two electrons in a triplet state. Another example was demonstrated by Hamwi who applied variable temperature EPR analysis to investigate the local environment of dangling C-F bonds in fluorinated graphite.⁷⁰ EPR analysis of fluorinated graphite at temperatures up to 400° C showed a single broad uncoupled signal. EPR analysis at temperatures higher than 400° C (450 – 680° C) caused the single broad signal to split into seven lines. They concluded that this splitting was a result of hyperfine interactions between dangling bond electrons and the neighboring fluorine nuclei present in the fluorinated graphite sample.⁷¹

Variable temperature EPR analysis can provide valuable characterization data as demonstrated by the previous examples. For host **1** and ¹⁵N labeled host **1**, variable temperature EPR could uncover splitting not observed at room temperature EPR analysis. This data would provide valuable characterization data and could be evidence for a benzophenone or urea centered radical within host **1**. In collaboration with the Forbes group at the University of North Carolina at Chapel Hill, variable temperature EPR experiments were performed. Freshly evacuated host **1** and ¹⁵N labeled host **1** (5 mg), which were purified by 3 and 1 recrystallization cycles respectively, were UV irradiated for 30 min and analyzed via EPR at 20, 50, and 100°C. Figure 2.15 left shows the temperature data for host **1**. Although the intensity of the signal decreasing with increasing temperature, no obvious changes the coupling pattern or the g-value was observed. Similarly, the ¹⁵N labeled host **1** (Figure 2.15 right) also shows the intensity of the EPR signal decreases with increasing temperature; however, no obvious changes in the hyperfine coupling or g-value were observed. In the future, we will evaluate the EPR of

these samples at temperatures below 20 °C to probe for shape and coupling changes that could provide characterization information. These experiments will be outlined in a later section.

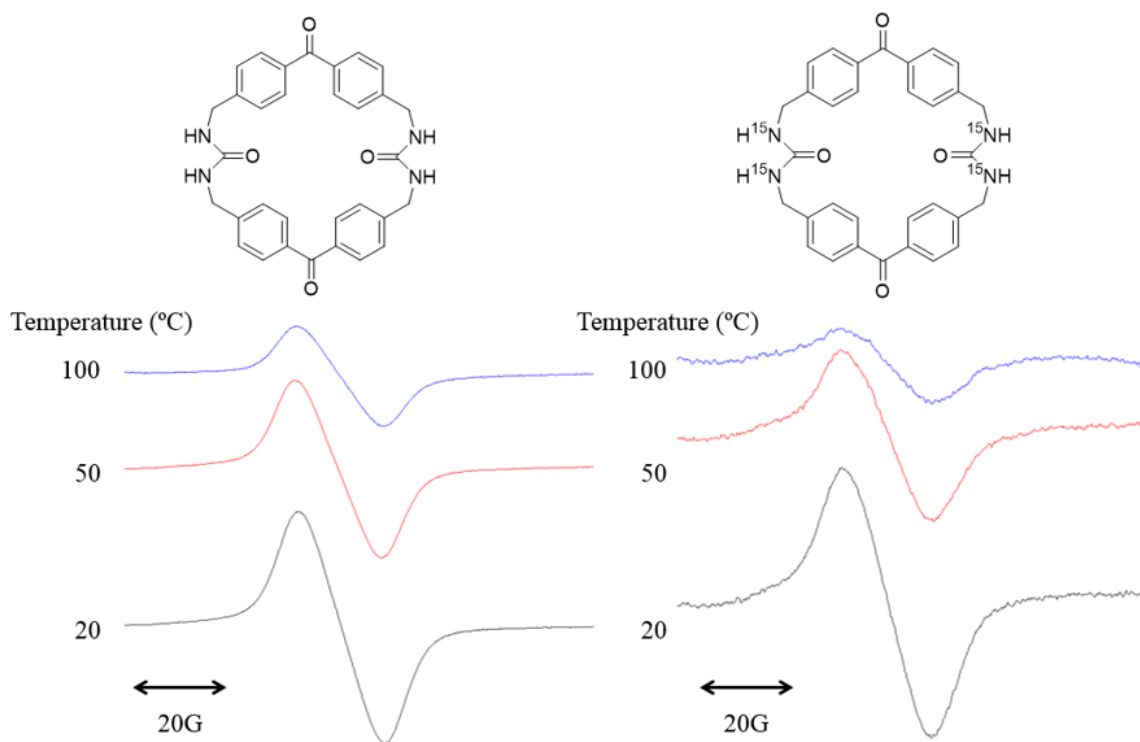


Figure 2.15. EPR comparison at 20, 50, and 100 °C for host **1** (empty) and ¹⁵N labeled host **1**

2.12 IR, UV-Vis, and Emission Analysis of Host 1

In an effort to understand the photophysical properties and to characterize the host **1** radical generated upon UV irradiation, we performed IR, UV-vis, and emission spectroscopy for host **1** before and after UV irradiation. Benzophenone and benzophenone ketyl radical have each distinct absorptions and stretches, which is discussed in the following sections, when analyzed by IR, UV-vis, and emission spectroscopy. Analyzing

host **1** before and after UV irradiation may generate peaks similar to that of a benzophenone ketyl radical which would be indicative of a host **1** ketyl radical.

2.12.1 IR Analysis of Host **1**

We also probed structural changes that occur in the host upon UV-irradiation. One challenge is that we do not have a good measure of how much radical is present upon UV-irradiation. Radical concentration has previously been determined through EPR signal integration.⁷² Zhang et. al. analyzed a bola-form amphiphile with a perylene diimides core (BPDI) supramolecular complex in solution via EPR and found a single uncoupled signal. This signal was integrated and plotted against a standard curve with known radical concentrations. When the data was fit to the standard curve, radical concentration of BPDI was determined to be 0.016 mM. Unfortunately, determination of radical concentration through EPR integration is limited to radicals in solution. As demonstrated in section 2.9, unassembled host **1** in solution shows no significant radical character upon UV irradiation. This makes determination of host **1** radical significantly more challenging and an alternative method for determining radical concentration must be employed.

IR provides a good method for detecting ketyl radicals as well as radical anions. Benzophenone ketyl radicals have been reported to have a distinctive IR absorption band at 1396 cm^{-1} .^{73,74} Alternatively, UV irradiated host **1** could possess benzophenone radical anion character. Benzophenone radical anions are characterized by two IR absorption bands at 1464 cm^{-1} and 1340 cm^{-1} .⁷⁵ The appearance of these IR absorption bands after UV irradiation would indicate that benzophenone is related to the radical observed for host **1**.

Freshly evacuated host **1**, purified by one recrystallization cycle, was analyzed via solid state IR spectroscopy. Sample was then collected and UV irradiated for 30 mins as

previously described using a Rayonet reactor. UV irradiated host **1** was analyzed via EPR spectroscopy to confirm presence of radical then was again analyzed via solid state IR spectroscopy. Figure 2.16 (black spectra) shows the IR spectra for host **1** (empty) before UV irradiation. Three bands at 1426, 1414 and 1356 cm^{-1} appear in this key 1300-1500 cm^{-1} region, which is of interest for benzophenone ketyl radicals. In the parent benzophenone, the ketyl radical are observed at 1396 cm^{-1} but could be shifted in the host **1**, which is a substituted benzophenone derivative. As seen with infrared studies with diketone anion radical derivatives, key peak absorptions such as the C=O stretch are known to shift irregularly between derivatives.⁷⁶ For example, the C=O stretch for benzophenone and benzil radical anions are 1590 cm^{-1} and 1683 cm^{-1} respectively.⁷⁶ In comparison, the IR spectra (in red) after UV-irradiation, does not show any obvious increase or changes in the bands at 1426, 1414 and 1356 cm^{-1} . Since both spectra are identical despite the EPR signal for the radical, which is observed after UV-irradiation, we concluded that the amount of radical or radical anion generated by UV-irradiation is small and does not significantly impact the IR of host **1**. These experiments further highlight the need to quantify the amount of radical present.

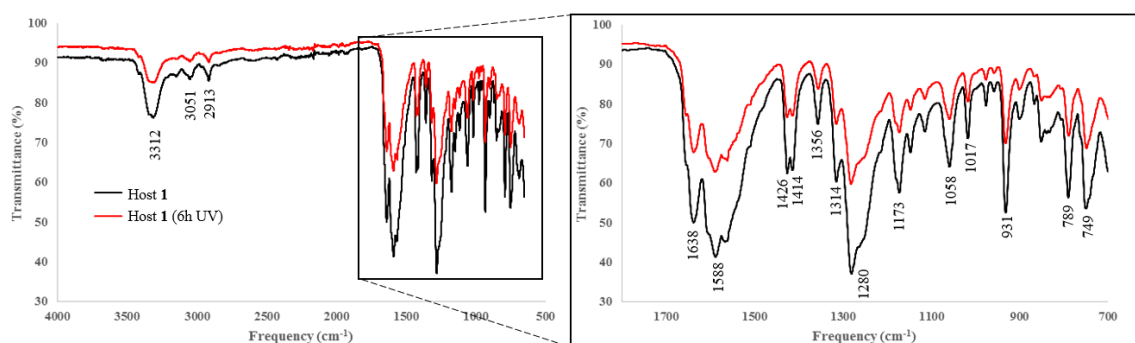


Figure 2.16. IR comparison of solid host **1** (empty) before (black line) and after (red line) UV irradiation

2.12.2 UV-vis Analysis of Host 1

Next, we investigated the absorption and emission of host **1** before and after UV-irradiation. UV-vis spectroscopy is more sensitive than IR and has been known to detect sample at concentrations as low as 10^{-5} M.⁷⁷ We tested if UV-vis could detect changes induced in host **1** from the formation of the radical. Freshly evacuated host **1**, purified by one recrystallization cycle, was analyzed via solid state UV-vis spectroscopy (Figure 2.17, black line). The spectra shows a broad absorption with the typical pi-pi* excitation at $\lambda_{\max} = 301$ nm. We see the more intense n-pi* excitation and $\lambda_{\max} = 355$ nm. Next, the sample was collected and UV irradiated for 30 min using a Rayonet reactor. UV irradiated host **1** was analyzed via EPR spectroscopy to confirm presence of radical. Next, the sample was analyzed via solid state UV-vis spectroscopy using a Perkin Elmer Lambda 35. After UV irradiation (Figure 2.17, red line) host **1** displays a nearly identical spectra with the initial host but generally showed higher signal intensity. The broad pi-pi* excitation absorption was slightly shifted at $\lambda_{\max} = 304$ nm. The more intense n-pi* excitation was identical to that of the before UV-irradiation of the sample at $\lambda_{\max} = 355$ nm. However, a very weak absorption in the noise can be seen at $\lambda_{\max} = 588$ nm. This new absorption is in the range one would expect for a ketyl radical. Benzophenone ketyl radicals have been reported to have λ_{\max} values at 330 and 545 nm.⁷⁸ These absorption bands are reported to shift to longer wavelengths as bulky substituents are attached. This can be seen through comparison ketyl radical derivatives such as benzophenone, naphthylphenylketone, 2-benzoylbiphenyl, and bis(bisphenyl-2-yl)methanone. These analogous possess λ_{\max} absorptions relating to ketyl radical at 545, 585, 585, and 630 nm respectively.⁷⁸ Host **1** structure or assembly motif may similarly shift the ketyl radical. The exceedingly small intensity may be in the noise

level and suggests that the amount of the ketyl radical is very small. Thus more work is needed to confirm if the weak absorption band at 545 nm is real.

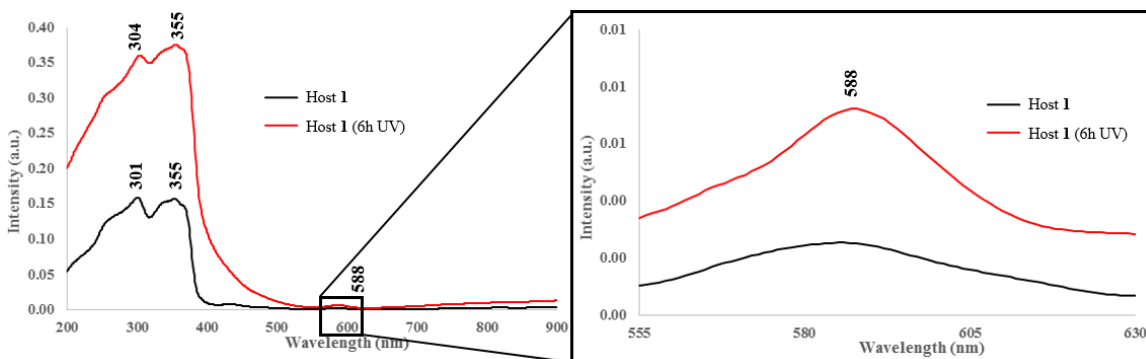


Figure 2.17. UV-vis comparison of solid host **1** (empty) before (black line) and after (red line) UV irradiation. UV irradiated host **1** shows similar λ_{\max} values at 304 and 355 nm but may display a new band with λ_{\max} at 588 nm.

2.12.3 Emission Analysis of Host 1

Emission spectroscopy has previously been applied in the analysis of benzophenone ketyl radicals and ketyl radical derivatives. Benzophenone, naphthylphenylketone, 2-benzoylbiphenyl, and bis(bisphenyl-2-yl)methanone ketyl radicals display emissions at 345, 450, 389, and 462 nm respectively using an excitation wavelength of 355 nm.^{78,79} Similar to UV-vis spectroscopy, emission wavelengths tend to shift to longer wavelength in solution when bulky groups are appended on the ketyl radical. Emission spectroscopy was performed on host **1** to test if host **1** shows a similar lengthening of emission value in the solid state. Freshly evacuated host **1**, purified by one recrystallization cycle, was analyzed via solid state emission spectroscopy with an excitation wavelength of $\lambda_{\text{ex}}=355$. Figure 2.18 shows the normalized emission spectra from 375 to 525 nm with a lambda max of $\lambda_{\text{max}} = 463$ nm. The sample was then collected and UV irradiated for 30 mins as previously described using a Rayonet reactor. UV

irradiated host **1** was analyzed via EPR spectroscopy to confirm presence of radical. Next, solid state emission spectroscopy was obtained with an excitation wavelength of $\lambda_{\text{ex}}=355$ (Figure 2.18, red line). We observed a similar broad peak with a slight shift of the lambda max $\lambda_{\text{max}} = 462$ nm.

UV-vis and emission data was used to calculate host **1** Stokes shift (ν_{ss}) value, which is characterized by the difference between band maxima of absorption and emission.⁷⁸ Calculation of ν_{ss} for host **1** could provide insight into radical lifetime. Benzophenone ketyl radical and its derivatives show that in an increase of radical lifetime can be observed with a decrease of Stokes shift value.⁸⁰⁻⁸² As demonstrated in section 2.8 via EPR dark decay experiments, the host **1** radical has been shown to persist for up to eight days after initial UV irradiation. A low ν_{ss} value would support the unusually long lifetime observed for host **1** radical and would suggest that this radical is a ketyl radical derivative.

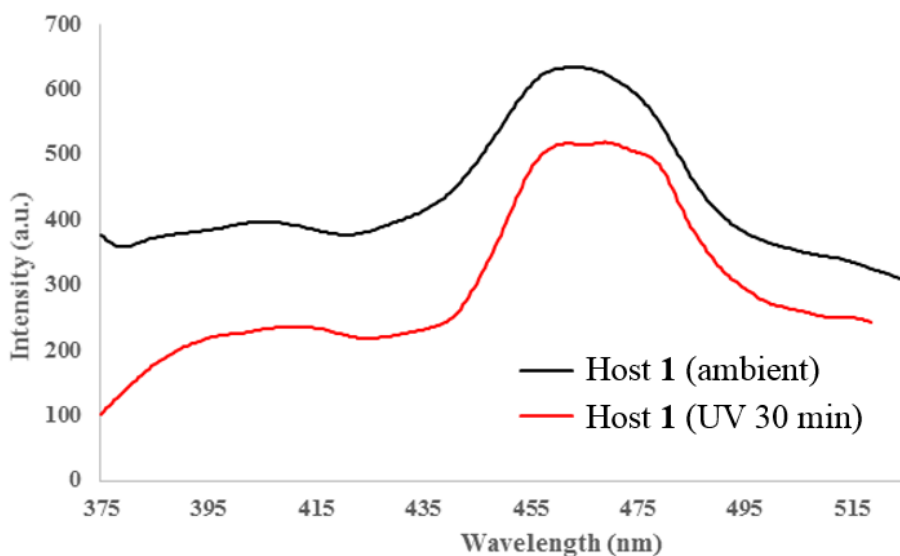
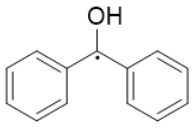
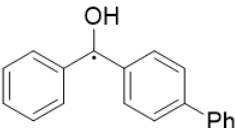
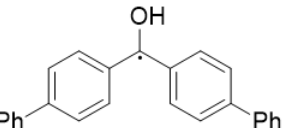


Figure 2.18. Emission spectra comparison of solid host **1** (empty) before (black line) and after (red line) UV irradiation. Scan range was 375 to 525 nm using $\lambda_{\text{ex}}=355$ nm as the excitation wavelength

The value of $\lambda_{\max} = 462$ nm was used to determine ν_{ss} . Using the tentative $\lambda_{\max} = 588$ nm from UV-vis analysis, the Stokes shift value for host **1** was estimated to be $\nu_{ss}/10^3 = 1.16$ cm⁻¹. This value is slightly less than the shift of $\nu_{ss} = 1.18$ for the benzophenone ketyl radical (**1H**[•]). Host **1** Stokes shift value is significantly less than that of 4-benzoylbiphenyl (**2H**[•]) and *bis*(biphenyl4-yl)methanone (**3H**[•]) ketyl radicals that are $\nu_{ss} = 1.82$ and $\nu_{ss} = 1.56$ respectively as seen in Table 2.3.⁷⁴ As expected, the ν_{ss} calculated for host **1** was low which supports the long lifetime observed for the radical. Additionally, ketyl radical excited states have also been shown to have longer lifetimes if they belong to a structure that prevents the conformational change between ground state (D_0) and ketyl radical state (D_1).⁸⁰⁻⁸² Despite the ν_{ss} value being similar between benzophenone and host **1**, the significantly longer lifetime for host **1** radical could potentially be attributed to its structure preventing conformational change between the D_0 and D_1 state.

Table 2.2. Stokes shift (ν_{ss}) for benzophenone, 4-benzoylbiphenyl, *bis*(biphenyl4-yl)methanone, and host **1** ketyl radicals.

Ketyl Radical Variation				Host 1 ketyl radical
Stokes Shift $\nu_{ss}/10^3$ [cm ⁻¹]	1.18	1.82	1.56	1.16

2.13. Computational Comparison of Benzophenone and Host 1

Since the observed radical was a result of UV irradiated assembled host **1**, computational analysis was applied to analyze the stability of a possible host **1** benzophenone ketyl radical. Previously, benzophenone radicals have been reported in the literature through radical trapping with nitroxides,^{43,44} through H-abstraction,⁴⁵ and at low

temperature.^{46,48} Benzophenone, upon UV irradiation, is excited to a short lived singlet state that rapidly undergoes intersystem crossing to a triplet excited state. If there is a suitable proton in close proximity, benzophenone in the triplet excited state will abstract a hydrogen atom resulting in a benzophenone ketyl radical that is in the doublet excited state. While benzophenone radicals are well understood, they generally cannot be examined at room temperature due to their high reactivity and extremely short lifetime. So what factors are contributing to the stability of host **1** radical? Geer suggests that inclusion of benzophenone within columnar assembled host **1** stabilizes the benzophenone radical allowing it to be observed at room temperature after UV irradiation. Does inclusion of benzophenone within a single macrocycle unit, as seen in host **1**'s structure, make higher excitation states and benzophenone ketyl radicals more energetically favorable? We used Spartan (reference) to calculate and compare the energies for ground singlet, singlet excited, triplet excited, and doublet excited (H-abstraction radical) states as outlined in Figure 2.19. Benzophenone, benzophenone ketyl radical, host **1** and host **1** ketyl radical were drawn in Spartan and energetically minimized. These are outlined in Figure 2.19. Next density functional theory studies were performed on each of these structures with Spartan using B3LYP 6-31G* calculations under vacuum with the corresponding multiplicity and energetic states on molecules in their lowest energy conformations. Energy values for the highest occupied molecular orbital (E-HOMO) were generated by each calculation. These calculations can be easily be performed and can provide reliable information to the stability of each of these energetic states. Next, the E-HOMO values for host **1** and benzophenone were compared. By understanding the differences in energy

between these two systems at different excited states, we hoped to gain insight on why the host **1** radical is so unusually stable at room temperature.

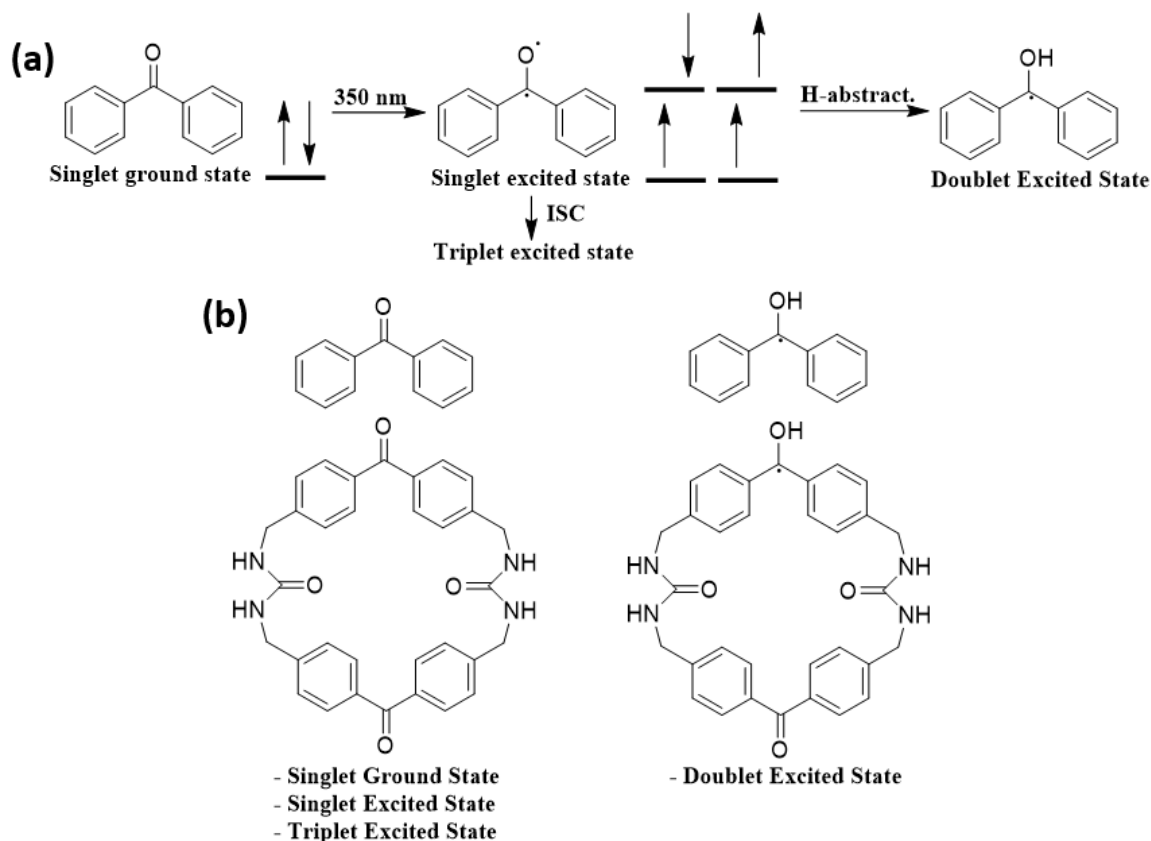


Figure 2.19. (a) Schematic representation of benzophenone radical generation with the corresponding excited states and (b) the energetic states computationally compared between benzophenone and host **1**.

Phillips *et al.* previously used B3LYP/6-311G** DFT calculations to computationally predict Raman shifts for the benzophenone ketyl radical. Included with Raman prediction, energy calculations were performed for ground and triplet state benzophenone and the benzophenone ketyl radical.⁸³ No E-HOMO data was reported by Phillips so our calculations were compared using the total energy data (a.u.) to test the validity of our calculations. As seen in table 2.3, literature values for benzophenone ground singlet state, excited state, and benzophenone ketyl radical are -576.77678, -576.67183,

and -577.34571 a.u. respectively.⁸³ These values are very close to our calculated energies for benzophenone ground singlet state, excited state, and benzophenone ketyl radical which are -576.63030, -576.48293, and -577.04081 a.u. respectively. Our calculations seem reasonable given the small difference in energy between our data and the literature data reported by Phillips.

Energy comparisons between benzophenone and host **1** are based off of the E-HOMO energy (kcal/mol) and are represented in Table 2.1. The ground singlet state and singlet excited state for benzophenone and host **1** was -149.89 kcal/mol and -147.17 kcal/mol respectively. No energy difference was observed between the ground singlet state and singlet excited state for both systems. This could be a result of the extremely short lifetime of the singlet excited state because it quickly undergoes intersystem crossing to the more stable triplet excited state. This also indicates that B3LYP 6-31G* calculations may not be sufficient for detecting these energy differences.

For both benzophenone and host **1**, calculations were reported as E-HOMO energy and are graphically represented in figure 2.20a and 2.20b respectively. Calculations indicate that the triplet excited state was the highest energy state for both systems. Benzophenone in the triplet excited state was calculated at -82.56 kcal/mol. Host **1** in the triplet excited state -62.49 kcal/mol. The difference between the lowest energetic state (ground singlet state) and the highest energetic state (triplet excited state) was 67.3373 kcal/mol for benzophenone and 84.6319 kcal/mol for host **1**. Ketyl radical, which is represented as the doublet excited state, was -111.613 kcal/mol for benzophenone and -137.21 kcal/mol for host **1** ketyl. Calculations indicate that host **1** ketyl radical is 25.60 kcal/mol lower in energy than benzophenone ketyl radical. The triplet excited state was

calculated to be 29.06 kcal/mol and 74.72 kcal/mol higher in energy than the doublet excited state for benzophenone and host **1** respectively. Our calculations indicate that the doublet excited state for host **1** is lower in energy. This suggests that host **1** ketyl radicals are more stable than the corresponding benzophenone ketyl radicals. This could be one of the factors contributing to unusual stability of the radical observed for upon UV irradiated host **1**.

Table 2.3. Energetics of ground singlet, singlet excited, triplet excited, and doublet excited states using B3-LYP 6-31 G* calculations for a.) benzophenone and b.) host **1**

Molecule	State	Energy (a.u.)	Energy Lit. (a.u.)	E-HOMO (kcal/mol)
Benzophenone (BP)	Ground Singlet State	-576.630295	-576.77687	-149.894
	Singlet Excited State	-576.52099		-149.894
	Triplet Excited State	-576.482926	-576.67183	-82.5567
BP Ketyl Radical	Doublet Excited State	-577.040806	-577.34571	-111.613
Host 1	Ground Singlet State	-1756.22439		-147.126
	Singlet Excited State	-1756.11569		-147.126
	Triplet Excited State	-1756.10614		-62.4941
Host 1 Ketyl Radical	Doublet Excited State			-137.21

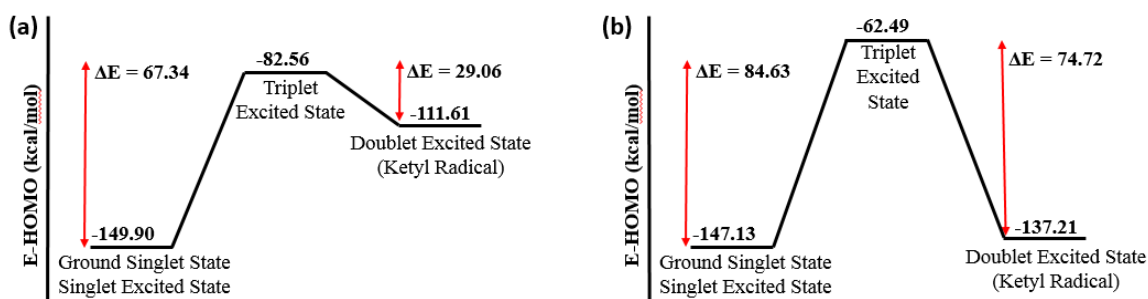


Figure 2.20. Energetics of ground singlet, singlet excited, triplet excited, and doublet excited states for a.) benzophenone and b.) host **1**

2.15. Host **1** analysis by magnetic measurements.

One method to characterize the amount of radical present in a solid state sample is by magnetic measurements using superconducting quantum interference device (SQUID)

analysis. SQUID analysis has previously been applied by Ahn to determine free radical concentration in the polyimide polymer PMR-15.⁸⁴ This polymer has been shown to display stable room temperature radical character after exposure to temperatures above 573 K.⁸⁵ The EPR spectra shows a single broad uncoupled signal at $g = 2.0039$. Magnetic susceptibility (X) of PMR-15 polymer was measured via SQUID analysis between the temperatures 2-320 K upon heating at 1 T magnetic field.⁸⁶ Magnetic susceptibility is temperature dependent meaning that it can be characterized by Curie-Weiss parameters in order to distinguish paramagnetic and diamagnetic effects allowing for the derivation of free-radical concentration.^{87,88} At low temperatures, magnetic susceptibility (X) follows the Curie-Weiss law demonstrated by the equation $X = \{P/(T + \Theta)\} + X_0$ with $P = N_g^2 \mu_B^2 S(S+1)/3k_B$.⁸⁹ Using the second equation, Ahn determined the free-radical concentration (N) to be 6.3×10^{18} radicals per gram of PMR-15.⁸⁴

In addition to probing the paramagnetic properties of host **1**, SQUID analysis could be used to determine the radical concentration of host **1**. The sample was prepared by placing host **1** crystals into a sample container made from a drinking straw as schematically represented by Figure 2.21a. It is important to note that DMSO (solvent of recrystallization) was chosen as a guest for magnetic analysis because it forms the most ordered complex with host **1**. Ambient light exposed host **1**•DMSO (10 mg) complex was placed into a sample container just described and was analyzed via SQUID upon heating. Ambient light exposed host **1**•DMSO showed no paramagnetic character (Figure 2.21b). Next, host **1**•DMSO crystals were removed from the sample container and UV irradiated at 355 nm for 30 min via Rayonet reactor. Host **1**•DMSO radical was verified by EPR then sample was again prepared as represented by Figure 2.21a. UV irradiated host **1**•DMSO complex

was then analyzed via SQUID upon heating (Figure 2.21c). No magnetic character correlating to host **1** was observed despite the radical being detected by EPR suggesting that the amount of radical in host **1** is very low. However, the appearance of a slight bump between the temperatures of 50 – 150 K was observed, which correlates to molecular oxygen. Molecular oxygen in the sample can produce additional magnetic susceptibility variations due to paramagnetic to antiferromagnetic oxygen transitions at 57 K.⁹⁰ This experiment highlights the importance of removing oxygen from the sample prior to analysis. UV irradiated Host **1** (empty) (10 mg) was also prepared as described and analyzed via SQUID upon heating (Figure 2.21d) to probe the effect of DMSO inclusion on magnetic character. No magnetic character was observed for host **1** (empty).

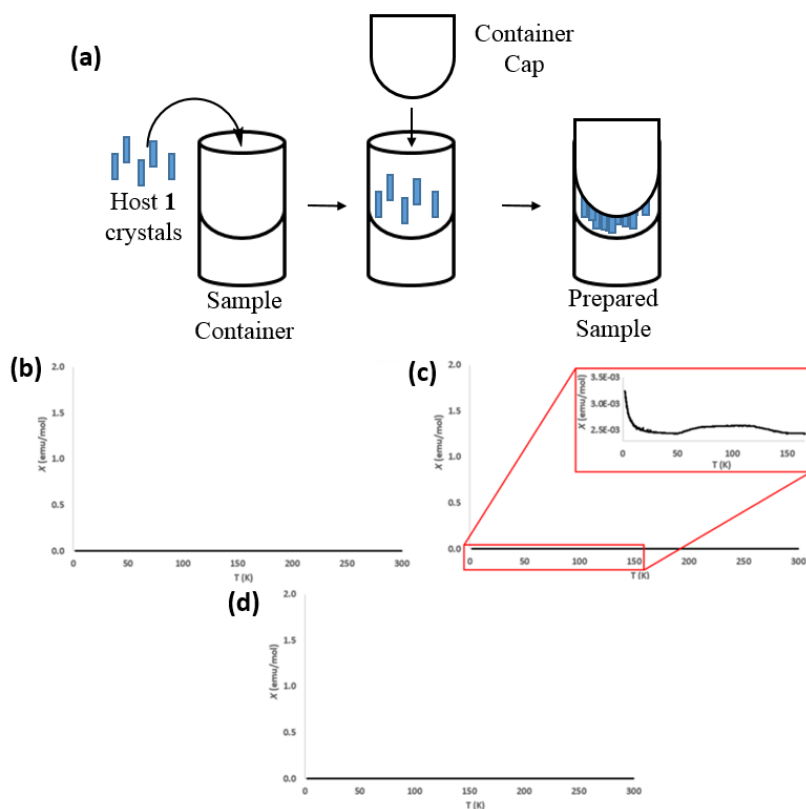


Figure 2.21. (a) Schematic representation of sample preparation and magnetic data from SQUID analysis for (b) ambient light exposed host **1** •DMSO complex, (c) UV irradiated host **1** •DMSO complex, (d) and UV irradiated host **1** (empty) complex

Surprisingly, all of our SQUID experiments showed extremely weak diamagnetic character, which suggests that the percentage of free radical in our host **1** complex is quite low, despite the presence of radical being verified by EPR analysis. Although the SQUID has high sensitivity, the instrument is unable to detect magnetic fields smaller than the flux noise produced by the magnetometer.⁹¹ The lack of paramagnetic character observed for both host **1**•DMSO and host **1** (empty) suggests that the amount of radical produced by our 30 min UV-irradiation is low or it is quenched by the molecular oxygen, or the strength of the possible magnetic field for host **1** is weaker than the flux noise produced by the SQUID. Other methods of UV irradiation will be explored in an effort to increase radical concentration. Additionally, prepared samples will either be pulled under vacuum or prepared in an oxygen free environment prior to SQUID analysis to remove molecular oxygen. Alternative approaches using nano-SQUID analysis, which are known to have higher sensitivity and lower flux noise levels, are briefly discussed in Section 2.13.

2.16 Future Experiments

Additional EPR analysis could help to further elucidate the radical present in host **1** after UV-irradiation. The slight broadening of signal (Figure 2.15, page 71) was upon decreasing temperature to 20 °C. Thus, EPR analysis at lower temperatures may show further broadening and perhaps hyperfine coupling may be observed. In particular, we will examine the EPR spectra at -55, -140, and -270 °C. As mentioned in section 2.10, changes in coupling have been previously observed in variable temperature EPR experiments. Chestnut and Phillips use variable temperature EPR analysis to study the temperature-dependent exchange interactions observed for crystalline $(\phi_3\text{PCH}_3)^+(\text{TCNQ})_2^-$ and $(\phi_3\text{AsCH}_3)^+(\text{TCNQ})_2^-$ salts.⁶⁹ At lower temperature EPR analysis, coupling that was not

observable at room temperature was seen resulting in valuable information that led to characterization of the radical.

We carried out preliminary work to examine the scope and utility of host **1** to facilitate selective oxidations of guests containing allylic and benzylic sites. The first guest examined was 1-methylcyclohexene, which has been previously been oxidized via singlet oxygen and peroxide reduction in moderate to good yields with relatively unselective product distribution (Figure 2.22).^{92,93} First, we examined the loading of 1-methylcyclohexene in host **1** and then tested if the confined nanochamber assisted in the selective oxidation.

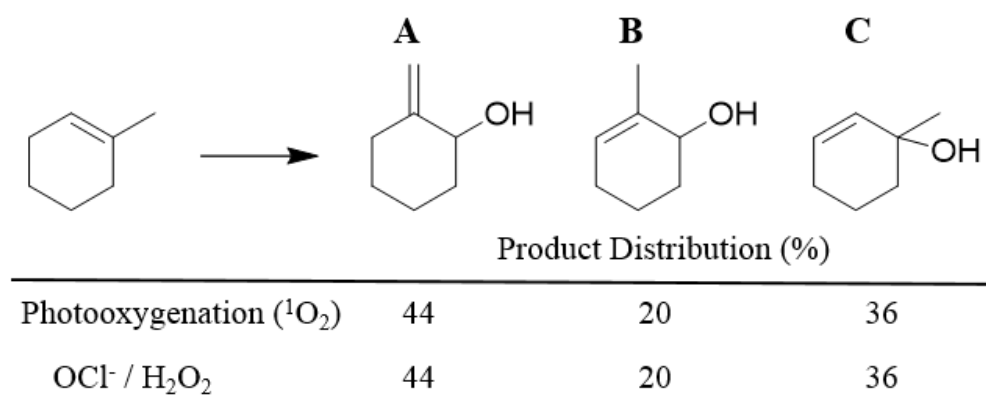


Figure 2.22. Comparison of product distribution of 1-methylcyclohexene oxidation via photooxygenation and $\text{OCl}^-/\text{H}_2\text{O}_2$

Freshly evacuated host **1** crystals (5 mg) were soaked in pure 1-methylcyclohexene (.5 mL) for 6 hours. Crystals were collected via Millipore vacuum filtration and left to dry on the apparatus for 5 min to remove excess 1-methylcyclohexene. Host: guest ratio was determined via TGA analysis to be 2:1 (Figure 2.23). This loading ratio was an average of two loading experiments. Loaded crystals were UV irradiated for 6 hours as previously described. Product was extracted from host **1** nanochamber with δ -chloroform and

analyzed via GC-FID. GC-FID integration suggests moderate conversion and mass spec shows a product with a mass of 100 amu but the products were not isolated or further characterized. Future plans include repeating this on a larger scale and isolating and fully characterizing the oxidation products.

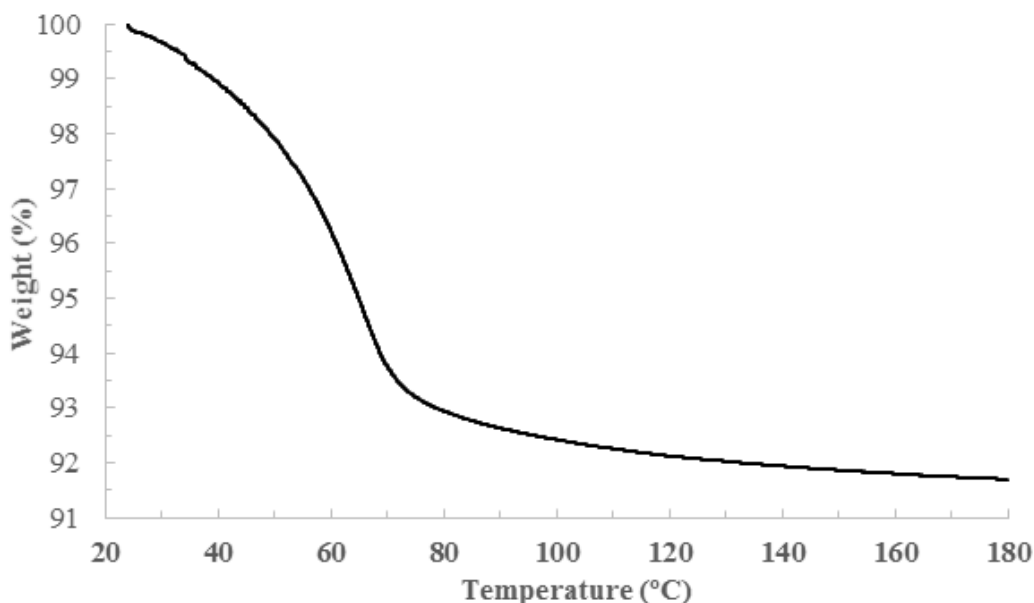


Figure 2.23. Desorption of 1-methylcyclohexene from host **1** nanochamber via TGA. Host: guest ratio was determined to be 2:1.

Polymerization of isoprene within host **1** nanochamber will also be investigated and optimized. Preliminary polymerization attempts were performed as represented by Figure 2.24. Freshly evacuated host **1** crystals (15 mg) were vapor loaded under vacuum with isoprene degassed by three freeze pump thaw cycles for 48 hours. Loaded crystals were UV irradiated at 355 nm as previously described with a Rayonet reactor for 16h. Polymer was then extracted with chloroform (1 mL) and crashed out of solution as a white solid using cold methanol (10 mL). Unfortunately, not enough isoprene was prepared to be characterized by gel permeation chromatography (GPC). This polymerization will be

optimized by using different loading apparatuses, longer loading times, and scaling up the reaction.

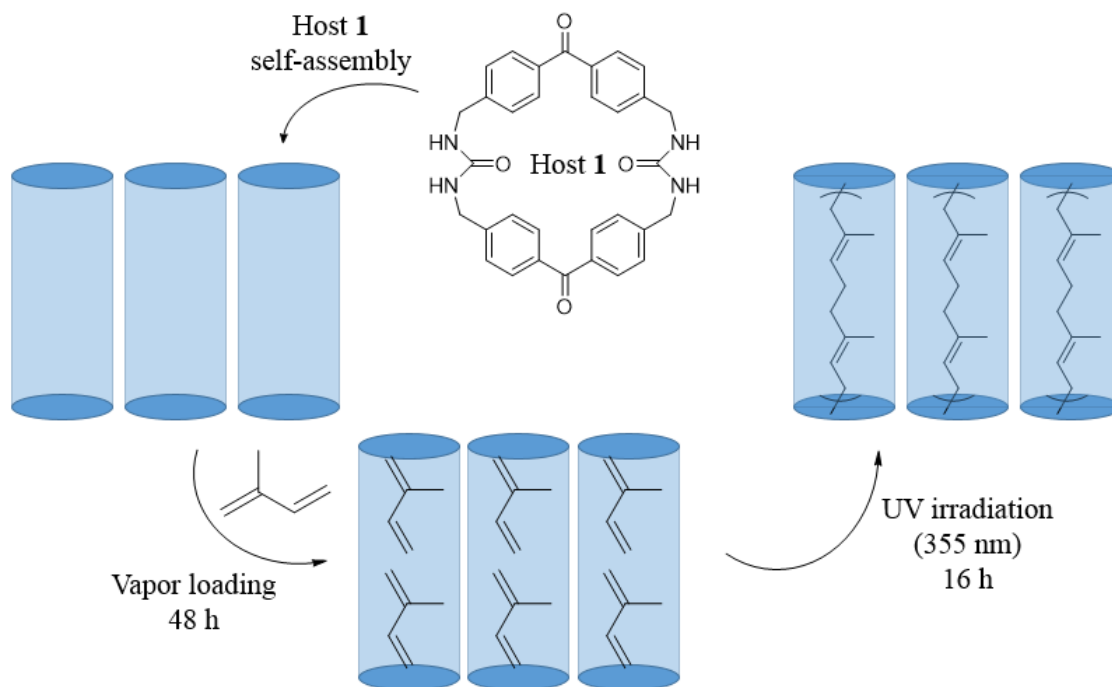


Figure 2.24. Desorption of 1-methylcyclohexene from host 1 nanochamber via TGA. Host: guest ratio was determined to be 2:1.

Preliminary SQUID magnetic studies revealed that host **1** after 30 min of UV irradiation did not form significant percentage of radical and no magnetic properties were observed but oxygen was a problem in the measurement. We will investigate other methods for preparing the samples under Ar(g). As mentioned previously, molecular oxygen can produce magnetic susceptibility variations due to paramagnetic to antiferromagnetic oxygen transitions.⁹⁰ As the paramagnetic character is likely weaker than the flux noise produced by the SQUID, future SQUID experiments could be performed using a nano-SQUID. These devices have been shown to have an extremely low flux noise of $50n\Phi_0\text{Hz}^{-1/2}$ and a spin sensitivity of down to $0.38 \mu_B\text{Hz}^{-1/2}$ at 1 T.⁹⁴⁻⁹⁷ The lower noise level and higher sensitivity of nano-SQUIDs may be sensitive enough to detect magnetic properties

for UV irradiated host **1**. In addition to using a more sensitive SQUID instrument, alternative methods of irradiation will be investigated to increase radical concentration of host **1**. This could potentially allow for analysis of magnetic properties without the use of a nano-SQUID device.

Attempts at characterizing will also be performed by reduction and isolation of host **1** radical followed by analysis via single crystal diffraction. Benzophenone ketyl radicals have previously been isolated using alkali-metals and metals such as Sm³⁺, Ca²⁺, and Na⁺ with the assistance of solvent molecules to stabilize the metal centers.⁹⁸⁻¹⁰⁰ Solvent free isolation and characterization of benzophenone ketyl radicals has also been achieved through one electron reduction using potassium followed by single-crystal X-ray diffraction analysis.⁴⁸ Since host **1** radical is likely benzophenone centered, it may be amenable to characterization by similar strategies.

2.17 Conclusion

This chapter outlined our investigation into the mechanism of the unusual and selective photooxidation observed by Geer for host **1**•2-methyl-2-butene upon UV-irradiation under an oxygen atmosphere. We focused on trying to understand the properties of the host and specifically the radical observed upon UV-irradiation of host **1** and its ¹⁵N labeled analogue to probe the structure and origin through EPR analysis, IR, UV-vis, fluorescence, and computational analysis. EPR analysis of assembled host **1** revealed that the unusually stable room temperature radical was only generated upon UV irradiation. EPR spectra of host **1** (empty), purified by three recrystallization cycles from host DMSO, showed a single broad uncoupled signal at $g = 2.0060 \pm 0.0001$. Host **1**•DMSO crystals were also analyzed via EPR before and after UV irradiation to understand the relationship

between guest inclusion and radical. Similar to host **1** (empty), EPR analysis host **1**•DMSO showed no signal from ambient light exposure but 30 min UV exposure generated a single uncoupled signal at $g = 2.0060$. This result, further supports that guest inclusion does not affect host **1** radical character. X-ray analysis of host **1** before and after UV irradiation was performed to see if any structural changes could be observed that would indicate the structure of the radical. Unfortunately, no changes were observed but X-ray crystal analysis of host **1**•DMSO single crystals showed that DMSO guests are extremely ordered within the host nanochamber with 90% of DMSO molecules facing in the same direction. The lifetime of host **1** radical was also probed through dark decay EPR experiments. Host **1**•DMSO radical persists for eight days after initial UV irradiation. EPR analysis of unassembled host **1** (in solution) and randomly assembled host **1** lacked significant radical character upon UV irradiation further indicating that assembly is related to radical stability.

As the urea nitrogen or the benzophenone moiety in host **1**'s structure were potential sites for the radical center, we synthesized the ^{15}N analogue and investigated it by variable temperature EPR at 100, 50 and 20 °C. The EPR spectra of host **1** and ^{15}N labeled analogue at room temperature, 50° C, and 100° C were nearly identical, indicating the urea nitrogen is not the radical center. IR, UV-vis, and fluorescence spectroscopy was performed on host **1** (empty) before and after UV irradiation in an attempt to characterize the observed radical. The UV-vis analysis of host **1** after UV irradiation revealed a weak new absorption with $\lambda_{\text{max}} = 588$ nm. More work is needed to determine if this band can be correlated to a host **1** ketyl radical. Using the emission value at $\lambda_{\text{max}} = 462\text{nm}$ for host **1** after UV irradiation, the Stokes shift value for host **1** was estimated to be $\nu_{\text{ss}}/10^3 = 1.16$ cm^{-1} . This lower ν_{ss} value could explain why host **1** radical has such an usually long lifetime

after UV irradiation. To investigate the benzophenone ketyl radical in host **1** further, we turned to computational studies using (what method add info). The computations suggest that the host **1** ketyl radical is significantly lower in energy (25.60 kcal/mol) than the benzophenone ketyl radical. This data suggests that inclusion of benzophenone with host **1** macrocycle structure makes the ketyl radical more thermodynamically accessible. In summary, preliminary evidence suggest that host **1** radical is likely a benzophenone ketyl radical derivative.

2.18 Experimental

2.18.1 Materials and Methods

All chemicals were purchased from Sigma Aldrich, VWR, or TCI Inc. and were used without further purification. ¹H-NMR and ¹³C-NMR spectroscopy was performed on Varian Mercury/VX 300 NMR spectrometers. UV-irradiation was carried out in a Rayonet RPR-200 reactor equipped with RPR-3500 lamps. X-ray powder diffraction data was obtained using a Rigaku Dmax- 2 100 & 2200 powder X-ray diffractometers using Bragg-Brentano geometry with CuK α radiation with step scans of 0.05 over range 2-40 ° 2 θ . Thermometric analysis (TGA) was carried out using TA instruments SDT-Q600 simultaneous DTA/TGA at a rate of 4°/min from 25-180°C with 5 min isotherms before and after temperature increase. Electron paramagnetic resonance (EPR) spectroscopy was performed using a Bruker EMX plus equipped with a Bruker X-band microwave bridgehead and Xenon software (v 1.1b.66). All variable temperature EPR analysis were performed at the University of North Carolina at Chapel Hill in collaboration with the Dr. Forbes group on a JEOL USA Inc. JES-RE1X X-band EPR spectrometer equipped with a wide bandwidth preamplifier and a low-noise GaAsFET microwave amplifier. All IR

analysis was performed using a Perkin Elmer Spectrum 100 IR Spectrometer. All UV-vis analysis was performed using a Perkin Elmer Lambda 35 UV-vis spectrometer with UV Winlab software. All Fluorescence analysis was performed using a Perkin Elmer LS 55 fluorescence spectrometer with FL Winlab software.

2.16.3 Synthesis of host 1:

Synthesis of 4,4'-bis (bromomethyl) benzophenone

4,4'-Benzophenone (5.00 g, 23.28 mmol) was reacted with *N*-bromo succinimide (8.919 g, 50.11 mmol) and azobisisobutyronitrile (0.039 g, .2372 mmol) in carbon tetrachloride (80 mL) at reflux for 18 h. The reaction was cooled to room temperature and solvent was removed under vacuum. Product was isolated via flash silica gel column chromatography (1:9 ethyl acetate: hexanes) to yield a white solid (7.527 g, 85%). $^1\text{H-NMR}$: (300 MHz; CDCl_3) $\delta=7.78$ (4H, d, $J=8.1$), 7.51 (4H, d, $J=8.4$), 4.54 (4H, s); $^{13}\text{C-NMR}$: (75 MHz, CDCl_3) $\delta= 195.46, 142.52, 137.45, 130.75, 129.25, 32.43$.

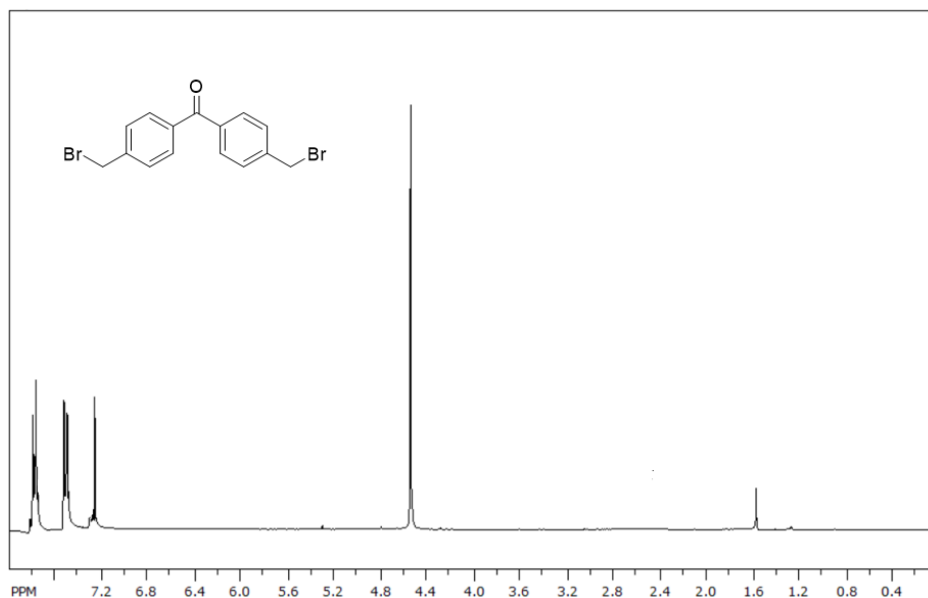


Figure 2.25. $^1\text{H-NMR}$ (300 MHz, CDCl_3) of 4,4'-bis (bromomethyl) benzophenone

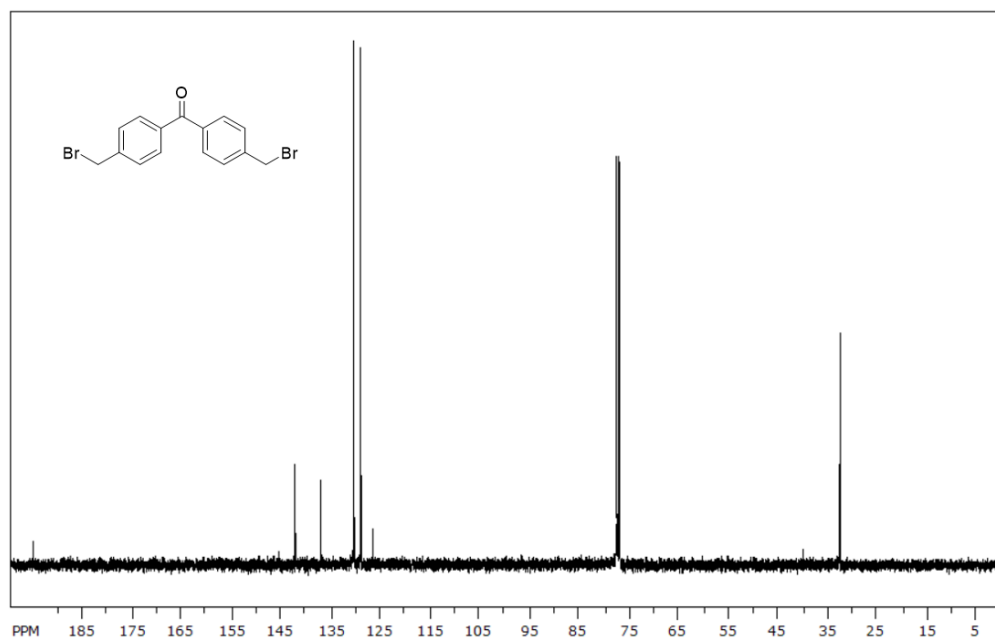


Figure 2.26. ^{13}C -NMR (75 MHz, CDCl_3) of 4,4'-*bis* (bromomethyl) benzophenone

Synthesis of triazinanone protected *bis*-urea benzophenone macrocycle

All glassware and the stir bars were oven dried prior to use. Triazinanone (0.8547 g, 5.43 mmol) and NaH (60 % suspension in mineral oil, 0.8600 g, 21.72 mmol) were refluxed in dry THF (400 mL) under N_2 atmosphere for 2 h. The suspension was cooled to room temperature and a solution of 4,4'-bis(bromomethyl)benzophenone (2.000 g, 5.43 mmol) in dry THF (100 mL) was added all at once. The reaction was heated back to reflux for 48 h. Upon completion, the reaction was cooled to room temperature and the excess NaH was neutralized with 1N HCl (10 mL). The solution was then diluted with water (100 mL). Solvent was removed under vacuum until an aqueous suspension remained. Crude product was extracted with methylene chloride (3 x 100 mL). Combined organic layers were washed with brine (150 mL) and dried over anhydrous Na_2SO_4 . Product was purified via flash silica gel column chromatography (1:19 methanol: ethyl acetate) to yield a white solid

(0.140 g, 3.5%). $^1\text{H-NMR}$: (300 MHz; CDCl_3) $\delta=7.81$ (8H, d, $J=8.4$), 7.45 (8H, d, $J=8.1$), 4.36 (8H, s), 1.10 (18H, s); $^{13}\text{C-NMR}$: (75 MHz, CDCl_3) $\delta= 196.02, 155.69, 143.52, 136.62, 131.00, 127.35, 62.99, 54.35, 49.24, 28.45$.

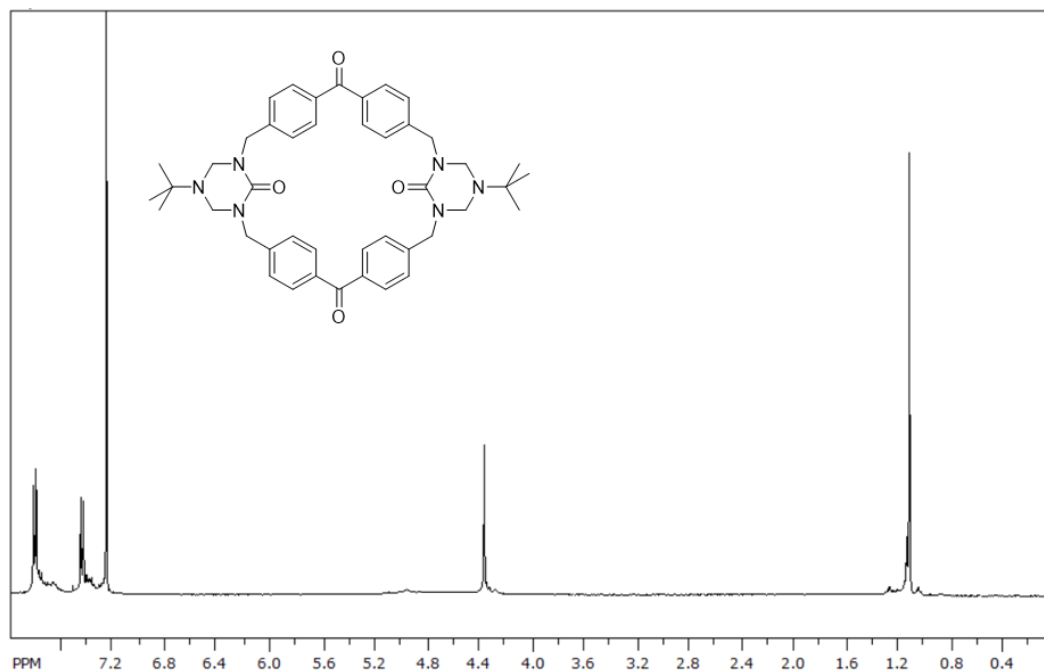


Figure 2.27. $^1\text{H-NMR}$ (300 MHz, CDCl_3) of host **1a**

Deprotection of triazinanone protected benzophenone macrocycle

Triazinanone protected bis-urea benzophenone macrocycle (0.200 g, 0.275 mmol) was heated to reflux in 1:1 20% diethanol amine (pH 2 with conc. HCl)/ water: methanol solution (140 mL) for 48 h. Product precipitated out of solution as a white powder. Product was collected via vacuum filtration. The product was washed with 1N HCl (20 mL) and distilled water (3 x 100 mL) when dried under vacuum (0.135 g, 92%). $^1\text{H-NMR}$: (300 MHz; $(\text{CD}_3)_2\text{SO}$) $\delta=7.73$ (8H, d, $J=8.1$), 7.41 (8H, d, $J=8.1$), 6.81 (4H, t, $J=6.0$), 4.36 (8H, d, $J=5.4$) $^{13}\text{C-NMR}$: (75 MHz, $(\text{CD}_3)_2\text{SO}$) $\delta= 196.02, 155.69, 143.52, 136.62, 131.00, 127.35, 62.99, 54.35, 49.24, 28.45$.

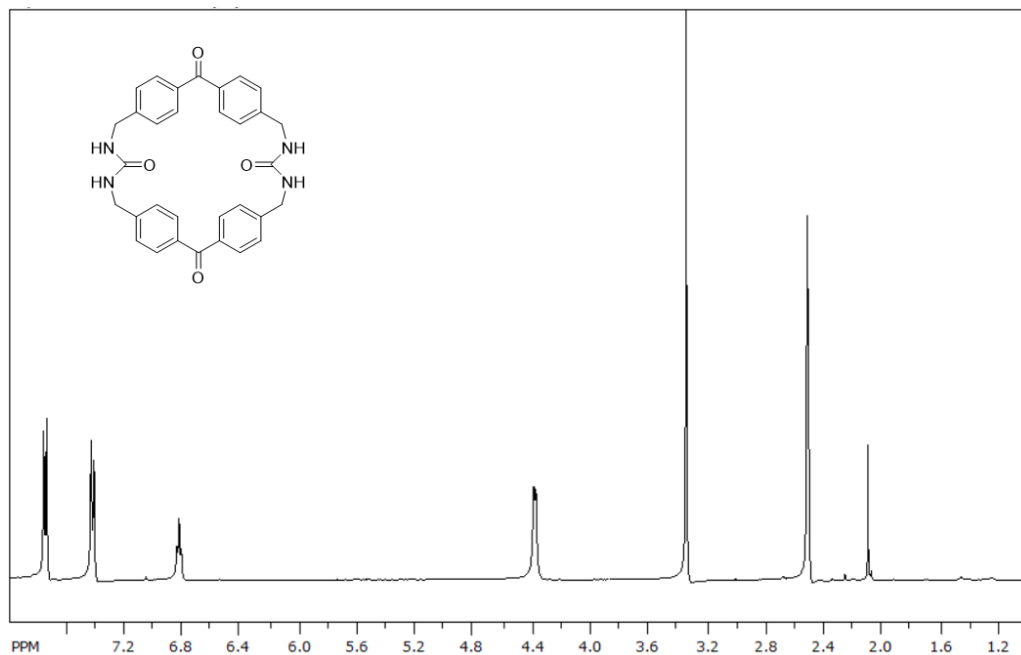
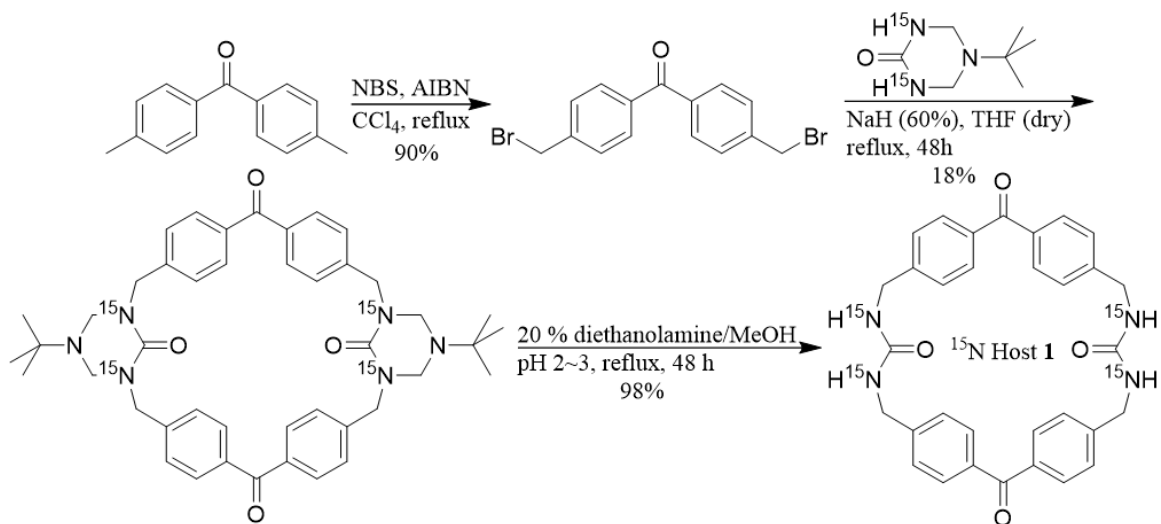


Figure 2.28. ^1H -NMR (300 MHz, δ_6 -DMSO) of ^{15}N labeled host **1**.

2.16.2 Synthesis of ^{15}N labeled host **1**:



Scheme 2.3. Synthesis of ^{15}N labeled *bis*-urea benzophenone macrocycle (host **1**). Reagents and Conditions: 4,4-dimethylbenzophenone was brominated using N-bromosuccinimide (NBS) and 2,2'-azobis(isobutyronitrile) (AIBN) in CCl_4 to produce 4,4'-*bis*-(bromomethyl)benzophenone. The dibromide was then reacted with ^{15}N labeled triazinanone and NaH in dry THF at reflux to yield protected macrocycle. The protected macrocycle was deprotected in acidified diethanol amine/methanol mixture resulting in the ^{15}N labeled *bis*-urea benzophenone macrocycle (^{15}N host **1**).

2.16.3 Synthesis of ^{15}N labeled triazinanone protected host 1:

^{15}N labeled triazinanone (0.183 g, 1.15 mmol) and NaH (0.182 g, 4.59 mmol) were heated to reflux in freshly distilled dry THF (200 mL) for 2 h. The solution was then cooled to room temperature and 4,4' bis(bromomethyl)benzophenone (0.423 g, 1.15 mmol) dissolved in dry THF (100 mL) was added all at once. The reaction mixture was brought back to reflux for 48 h. Upon completion, the reaction was quenched with 1N HCl (5 mL) and H_2O (100 mL) and reduced in *vacuo* down to an aqueous mixture. The mixture was extracted with methylene chloride (3 x 100 mL). Combined organic layers were washed with brine and dried over anhydrous MgSO_4 . Crude reaction mixture was purified by flash silica gel chromatography using methanol: ethyl acetate (1:9) yielding pure product as a white solid (0.075 g, 17.94%). ^1H -NMR (300 MHz, CDCl_3) δ 7.75 (d, $J = 8.1$, 8H), 7.38 (d, $J = 8.1$, 4H), 4.30 (s, 8H), 1.06 (s, 18H). ^{13}C -NMR: (75 MHz, CDCl_3) $\delta =$ 196.02, 155.69, 143.52, 136.62, 131.00, 127.35, 62.99, 54.35, 49.24, 28.45.

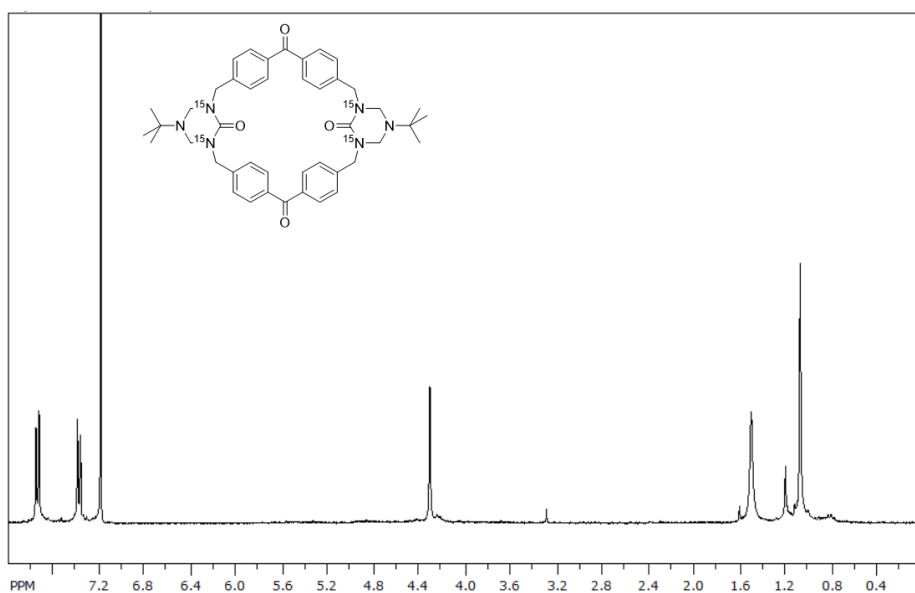


Figure 2.29. ^1H -NMR (300 MHz, δ_6 -DMSO) of ^{15}N labeled host **1a**

2.16.4 Deprotection of ^{15}N labeled triazinanone protected host **1**

^{15}N labeled triazinanone protected host **1** (0.075 g, .103 mmol) was heated to reflux in 1:1 20% $[\text{NH}(\text{CH}_2\text{CH}_2\text{OH})_2/\text{H}_2\text{O}]$ pH ~ 2 with Conc. HCl : MeOH (54 mL) for 48 h. The reaction was cooled to room temperature and the white precipitate was collected via vacuum filtration and washed with 20 mL 1N HCl, 20 mL of H_2O , and 20 mL of methylene chloride. The filtrate was dried in vacuo yielding pure product in the form of a white powder (0.050 g, 0.093 mmol, 92%). ^1H -NMR (300 MHz, $\text{DMSO}-d_6$) δ 7.75 (d, $J=8.0$, 8H), 7.43 (d, $J=7.9$, 8H), 6.82 (d, $J=90.6$, 4H), 4.384 (d, $J=5.5$, 8H) ^{13}C -NMR (75 MHz, $\text{DMSO}-d_6$) δ 195.36, 158.62, 158.42, 147.21, 135.74, 130.38, 126.70.

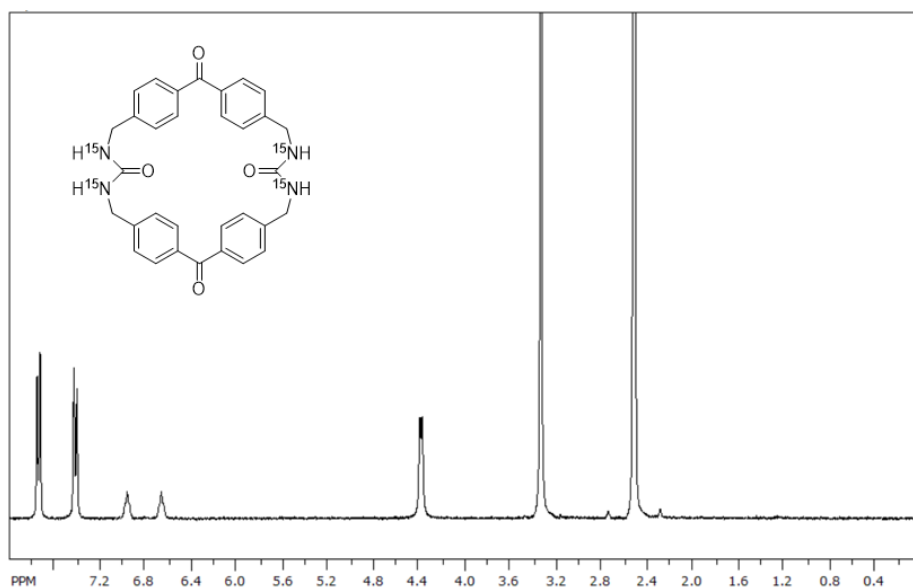


Figure 2.30. ^1H -NMR (300 MHz, δ_6 -DMSO) of ^{15}N labeled host **1**.

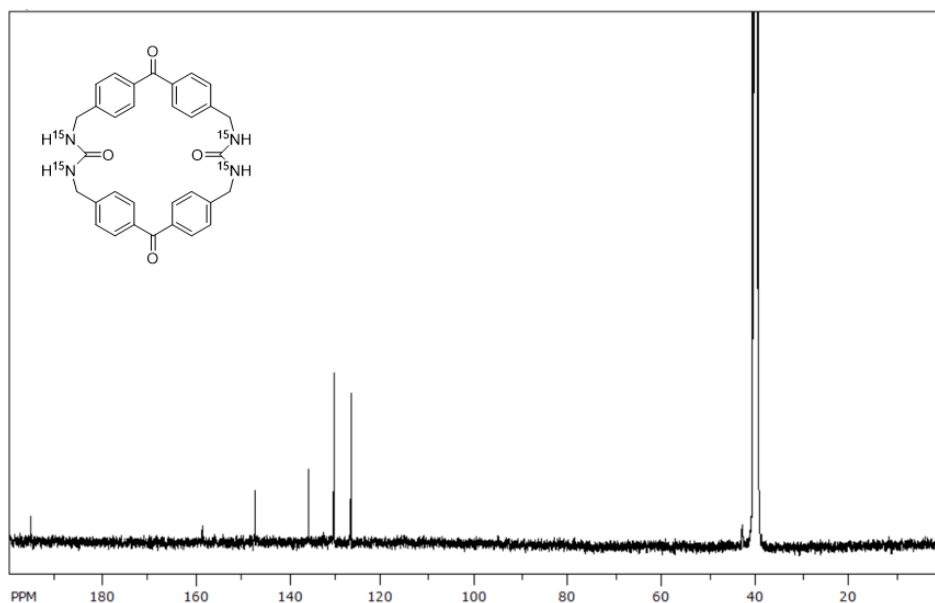


Figure 2.31. ^{13}C -NMR (75 MHz, δ_6 -DMSO) of ^{15}N labeled host **1**.

2.16.5. EPR studies

EPR experiments were performed using 5-10 mg of empty, randomly assembled, DMSO filled, or ^{15}N labeled host **1**. EPR analysis was performed using a Bruker EMX plus equipped with a Bruker premium X X-band microwave bridgehead and Xenon software version 1.1b.66. at USC.

Solution experiments: Freshly recrystallized host **1** crystals (1 mg) were dissolved in DMSO (1 mL) by heating with a heat gun. Solution was transferred into an EPR tube and purged with argon gas (99.99% purity) for 5 min and the EPR was recorded. Sample was then irradiated in a Rayonet UV reactor equipped with 3500 Å bulbs for 30 min and the EPR was again recorded.

DMSO loaded experiments: Host **1**•DMSO crystals (5-10 mg), purified via 3x recrystallization cycles, were collected via Millipore vacuum filtration. Sample was then washed with CH_2Cl_2 (25 mL) and left to pull on the vacuum filtration apparatus for 30 min.

Crystals were then loaded into an EPR tube, then purged with Argon for 5 min, and the EPR spectra was recorded. Sample was then transferred to the Rayonet UV reactor and irradiated for 30 min and the EPR spectra were again recorded.

EPR experiments on the precipitate: Host **1** precipitate collected directly from the deprotection step was collected via Millipore vacuum filtration and washed with H₂O (25 mL) and CH₂Cl₂ (25 mL). Sample was left to dry on the vacuum filtration apparatus for 30 min, and then the purity was verified via ¹H-NMR spectroscopy. Sample was then submitted for PXRD analysis. The precipitated host **1** (5 mg) was loaded into an EPR sample tube and purged with argon for 5 min then EPR spectra was recorded. Sample was then transferred to the Rayonet UV reactor and irradiated for 30 min and the EPR spectra was again recorded.

¹⁵N labeled experiments: Freshly evacuated ¹⁵N labeled Host **1** crystals (5 mg), purified via 1x recrystallization cycle, were loaded into an EPR tube. Sample was then purged with Argon for 5 min and the EPR spectra were recorded. Sample was then transferred to the Rayonet UV reactor and irradiated for 30 min and the EPR spectra were recorded.

Dark decay experiments: Host **1**•DMSO crystals (5 mg), purified via 1x recrystallization cycle, were collected, washed, and pulled on a Millipore vacuum filtration apparatus as previously described. Sample was then purged with argon for 5 min then transferred to the Rayonet UV reactor and irradiated for 30 min followed by recording of the EPR spectra. Sample was then wrapped in aluminum foil and stored in the dark. Every 24 hours, sample was loaded into the sample holder in the dark and any exposed parts of the EPR tube was wrapped in foil. EPR spectra were recorded then in the dark, sample was once again

wrapped in foil and stored in the dark. This process was repeated until the EPR signal was completely quenched.

Variable temperature studies: Evacuated host **1** crystals (5 mg), purified via 3x recrystallization cycles, and evacuated ¹⁵N labeled host **1** crystals (5 mg) were UV irradiated for 30 min. EPR spectra was recorded at 20, 50, and 100°C. All variable temperature EPR analysis were performed at the University of North Carolina at Chapel Hill in collaboration with the Dr. Forbes group on a JEOL USA Inc. JES-RE1X X-band EPR spectrometer equipped with a wide bandwidth preamplifier and a low-noise GaAsFET microwave amplifier.

2.16.16 Superconducting Quantum Interference Device Analysis:

Host **1**•DMSO, host **1** empty, host **1**•DMSO (30 min UV), and host **1** empty (30 min UV) (5 mg of each) were analyzed for magnetic properties using a Quantum Design MDMS 3 SQUID. Each sample was purified via one recrystallization cycle. Samples were analyzed upon heating from 2K up to room temperature.

2.16.17. Powder X-ray diffraction studies

Empty host **1** crystals, host **1**•DMSO crystals, and host **1** precipitate (~30 mg) were ground to a powder and examined by PXRD. Diffraction data was collected on a Rigaku DMAX-2100 and DMAX-2200 powder X-ray diffractometers using CuK α radiation. The step-scans were collected at +0.05° steps at angular range 2-40 °2 θ at ambient conditions.

2.16.18. IR spectroscopy studies

IR spectroscopy was performed on freshly evacuated host **1** crystals purified by one recrystallization cycle both before and after 30 min UV irradiation. Irradiation was

performed as previously described using a Rayonet reactor. All IR analysis was performed using a Perkin Elmer Spectrum 100 IR Spectrometer.

2.16.19. UV-vis studies

UV-vis spectroscopy was performed on freshly evacuated host **1** (10 mg) crystals purified by one recrystallization cycle both before and after 30 min UV irradiation. Sample was analyzed using a 4 mm quartz well with a quartz cover plate. All UV-vis analysis was performed using a Perkin Elmer Lambda 35 UV-vis spectrometer with UV Winlab software.

2.16.19. Fluorescence studies

Fluorescence spectroscopy was performed on freshly evacuated host **1** (10 mg) crystals purified by one recrystallization cycle both before and after 30 min UV irradiation. Sample was analyzed using a 4 mm quartz well with a quartz cover plate. Solid-state fluorescence analysis was performed using a Perkin Elmer LS 55 fluorescence spectrometer with FL Winlab software with integrating sphere. Sample was analyzed over 375 – 525 nm range using an excitation wavelength of $\lambda_{\text{ex}} = 355$ nm.

2.16.20. X-ray crystal structure determination

Bis-urea benzophenone macrocycle (host **1**•DMSO) $\text{C}_{32}\text{H}_{28}\text{N}_4\text{O}_4$, $\text{C}_2\text{H}_6\text{OS}$

Monoclinic:

145 X-ray intensity data from a colorless block-like crystal were collected at 100(2) K using a Bruker SMART APEX diffractometer (Mo $K\alpha$ radiation, $\lambda = 0.71073$ Å).¹⁵ The raw area detector data frames were reduced with the SAINT+ program. Final unit cell parameters were determined by least-squares refinement of 83073 reflections from the data set. Direct methods structure solution, difference Fourier calculations and full-matrix least-

squares refinement against F^2 were performed with SHELXS/L16. The compound crystallizes in the monoclinic space group $P2_1/n$ as determined by the pattern of systematic absences in the intensity data. The asymmetric unit consists of half of one molecule, which is located on a crystallographic inversion center. Nonhydrogen atoms were refined with anisotropic displacement parameters. Hydrogen atoms were placed in geometrically idealized positions and included as riding atoms

2.16.21. Crystal data structure and refinement [$C_{32}H_{28}N_4O_4$, C_2H_6OS]

Identification code	akbpmc_uv_0m
Empirical Formula	$C_{32}H_{28}N_4O_4$, C_2H_6OS
Temperature (K)	100 (2)
Formula Weight	532.60, 78.13
Space group	$P 2_1$
$a/\text{\AA}$	9.4285 (7)
$b/\text{\AA}$	23.0859 (15)
$c/\text{\AA}$	13.2392 (9)
Volume/ \AA^3	2879.76
Z, Z'	4,0
Density (calculated)	1.322 Mg/m^3
Absorption coefficient	0.090
$F(000)$	1288.0
Crystal size/ mm^3	0.44 x 0.08 x 0.06
Theta range for data collection	4.322 to 55.146
Index ranges	$12 \leq h \leq 12, -30 \leq k \leq 30, -17 \leq l \leq 17$

Reflections collected	83073
Independent reflections	13329 [$R_{\text{int}} = 0.0339$, $R_{\text{sigma}} = 0.0240$]
Completeness to theta	100.0%
Absorption correction	None
Refinement method	Full matrix least-squares on F^2
Data / restraints / parameters	13329/13/856
Goodness-of-fit on F^2	1.065
Final R indices [$I > 2\sigma(I)$]	$R_1 = 0.0350$, $wR_2 = 0.0864$
R indexes (all data)	$R_1 = 0.0420$, $wR_2 = 0.0910$
Largest diff. peak and hole	0.26/-0.42

2.17 References

1. Geer, M. F.; Walla, M. D.; Solntsev, K. M.; Strassert, C. A.; Shimizu, L. S. *J. Org. Chem.* **2013**, *78*, 5568-5578.
2. Congzhi, Z.; Lei, F. *Curr. Org. Chem.* **2014**, *18*, 1957-1964.
3. Fiedler, D.; Leung, D. H.; Bergman, R. G.; Raymond, K. N. *Acc. Chem. Res.* **2005**, *38*, 349-358.
4. Gibbs, C. L. D.; Sundaresan, A. K.; Ramamurthy, V.; Gibb, B. C. *J. Am. Chem. Soc.* **2008**, *130*, 4069-4080.
5. Schimidtchen, F. P. *Chem. Ber.*, **1981**, *114*, 597-607.
6. Parac, T. N.; Caulder, D. L.; Raymond, K. N. *J. Am. Chem. Soc.* **1998**, *120*, 8003-8004.
7. Fiedler, D.; Pagliero, D.; Brumaghim, J. L.; Bergman, R. G.; Raymond, K. N. *Inorg. Chem.* **2004**, *43*, 846-848.
8. Verbiest, T.; Elshocht, S. V.; Kauranen, M.; Hellemans, L.; Snauwaert, J.; Nuckolls, C.; Katz, T. J.; Persoons, A. *Science* **1998**, *282*, 913-915.
9. Stupp, S. I.; LeBonheur, V.; Walker, K.; Li, L.; Huggins, K. E.; Keser, M.; Amstutz, A. *Science* **1997**, *276*, 384-389.
10. Percec, V.; Glodde, M.; Bera, T.; Miura, Y.; Shiyanovskaya, I.; Singer, K. D.; Balagurusamy, V.; Heiner, P.; Schnell, I.; Rapp, A.; Spiess, H.; Hudson, S.; Duan, H. *Nature* **2002**, *417*, 384-387.
11. Beer, P. D.; Gale, P. A.; Smith, D. K. *Supramolecular Chemistry*, Oxford University Press, **1998**.
12. Fujita, M.; Nagao, S.; Ogura, K. *J. Am. Chem. Soc.* **1995**, *117*, 1649-1650.

13. Fujita, M.; Ogura, D.; Miyazawa, M.; Oka, H.; Yamaguchi, K.; Ogura, K. *Nature* **1995**, *378*, 469-471.
14. Raynal, M.; Ballestwer, P.; Vidal-Ferran, A.; van Leeuwen, P. W. *Chem. Soc. Rev.* **2014**, *43*, 1734-1787.
15. Samanta, S. R.; Parthasarathy, A.; Ramamurthy, V. *Photochem. Photobiol. Sci.* **2012**, *11*, 1652-1660.
16. Ramamurthy, V.; Gupta, S. *Chem. Soc. Rev.* **2015**, *44*, 119-135.
17. Sanghamitra, N. J.; Inab, H.; Kitagawa, S.; Ueno, T. J. *Inorg. Organomet. Polym.* **2013**, *13*, 50-60.
18. Cook, T. R.; Zheng, Y-R.; Stang, P. J. *J. Chem. Rev.* **2013**, *113*, 734-777.
19. Koblenz, T. S.; Wassenaar, J.; Ree, J. M. H. *Chem. Soc. Rev.* **2008**, *37*, 247-262.
20. Bossart, O.; DeCola, L.; Welter, S.; Calzaferri, G. *Chem. Eur. J.* **2004**, *10*, 5771-5775.
21. Ravanat, J-L.; Cadet, J.; Araki, K.; Toma, H. E.; Medeiros, M. G.; Mascio, P. D. *Photochem. Photobio.* **1998**, *68*, 689-702.
22. Dilling, W. L. *J. Org.Chem.* **1966**, *31*, 1045-1050.
23. Turro, N. J., *Modern Molecular Photochemistry* 1 ed.; University Science Books: CA, 1991; p 628.
24. Shimizu, L. S.; Salpage, S. R.; Korous, A. A. *Acc. Chem. Res.* **2014**, *47*, 2116-2127.
25. Dewal, M. B.; Xu, Y.; Yang, J.; Mohammed, F.; Smith, M. D.; Shimizu, L. S. *Chem. Commun.* **2008**, 3909-3911.
26. Block, H.; Ledwith, A.; Taylow, A. R. *Polymer*, **1971**, *12*, 271-288.
27. Greenstock, C. L.; Johns, H. E. *Biochem. Biophys. Res. Commun.* **1968**, *30*, 21-27.

28. Foote, C. S. *Acc. Chem. Res.* **1968**, *1*, 104-110.
29. Geer, M. F. (2013) Self-Assembled Benzophenone bis-urea macrocycles facilitate selective oxidation by singlet oxygen. (Ch. 2).
30. Arai, T.; Sakuragi, J.; Tokumaru, K. *Bull. Chem. Soc. Jpn.* **1982**, *55*, 2204-2207.
31. Rocklye, M.G.; Salisbury, K. *J. Chem. Soc., Perken. Trans.* **1973**, *2*, 1582-1585.
32. Bryant, J. R.; Matsuo, T.; Mayer, J. M. *Inorg. Chem.* 2004, *43*, 1587-1592.
33. Zhang, M.; Wang, L.; Ji, H.; Wu, B.; Zeng, X. *J. Nat. Gas. Chem.* **2007**, *16*, 393-398.
34. Silverman, S. K.; Foote, C. S. *J. Am. Chem. Soc.* **1991**, *113*, 7672-7675.
35. Foote, C. S. *Photochem. Photobiol.* **1991**, *54*, 659.
36. Stephenson, L. M.; Grdina, M. J.; Orfanopoulos, M. *Acc. Chem Res.* **1980**, *13*, 419-425.
37. Gomberg, M. *J. Am. Chem. Soc.* **1900**, *22*, 757-771.
38. Nakatsuji, S.; Anzai, H. *J. Mater. Chem.* **1997**, *7*, 2161-2174.
39. Rawson, J. M.; Alberola, A.; Whalley, A. E. *J. Mater. Chem.* **2006**, *16*, 2560-2575.
40. Hicks, R. G. *Org. Biomol. Chem.* **2007**, *5*, 1321-1338.
41. Barash, L.; Wasserman, E.; Yager, W. A. *J. Am. Chem. Soc.* **1967**, *89*, 3931-3932.
42. Bowers, H.; McRae, J.; Symons, M. C. R. *J. Chem. Soc. (A)*, **1971**, 2400-2402.
43. Lin, T.-S. *J. Chem. Phys.* **1972**, *57*, 2260-2264.
44. Qu, B.; Xu, Y.; Shi, W.; Raanby, B. *Macromolecules* **1992**, *25*, 5220-5224.
45. Tsierkezos, N. G.; Ritter, U. *Phys. Chem. Liq.* **2011**, *49*, 729-742.
46. Murai, H.; Imamura, T.; Obi, K. *Chem. Phys. Lett.* **1982**, *87*, 295-298.

47. Woodward, J. R.; Lin, T-S.; Sakaguchi, Y.; Hayashi, H. *Mol. Phys.* **2002**, *100*, 1235-1244.
48. Hisao, M. *Chem. Phys. Lett.* **1982**, *87*, 295-298.
49. Scott, T. A.; Ooro, B. A.; Collins, D. J.; Shatruk, M.; Yakovenko, A.; Dunbar, K. R.; Zhou, H-C. *Chem. Commun.*, **2009**, *1*, 65-67.
50. Bowers, H.; McRai, J.; Symons, M. C. R. *J. Chem. Soc. A* **1971**, 2400-2402.
51. Brezova, V.; Barbierikova, Z.; Zukalova, M.; Dvoranova, D.; Ladislav, K. *Catal. Today* **2014**, *230*, 112-118.
52. Maltar-Strmecki, N.; Rakvin, B. *J. Magn. Reson.* **2012**, *222*, 81-87.
53. Hicks, R. G. *Stable Radicals*; John Wiley & Sons, **2010**.
54. Matsuda, K.; Irie, M. *J. Am. Chem. Soc.* **2000**, *122*, 8309-8310.
55. Hamachi, K.; Matsuda, K.; Itoh, T.; Iwamura, H. *Bull. Chem. Soc. Jpn.*, **1998**, *71*, 2937-2943.
56. Sato, O.; Iyoda, T.; Fujishima, A.; Hashimoto, K. *Science*, **1996**, *272*, 704-705.
57. Ratera, I.; Ruiz-Molina, D.; Vidal-Gancedo, J.; Novoa, J. J.; Wurst, K.; Letard, J.; Rovira, C.; Veciana, J. *Chem. Eur. J.* **2004**, *10*, 603-616.
58. MasPOCH, D.; Domingo, N.; Ruiz-Molina, D., Wurst, K., Vaughan, G., Tejada, J., Rovira, C., Veciana, J. *J. Angew. Chem.*, **2004**, *116*, 1864-1866.
59. Otsuka, T.; Okuno, T.; Awage, K.; Inabe, T. *J. Mater. Chem.* **1998**, *8*, 1157-1163.
60. Akita, T.; Mazakati, Y.; Kobayashi, K. *J. Chem. Soc. Chem. Commun.* **1995**, 1861-1865.
61. Cirujeda, J.; Ochando, L. E.; Amigo, J. M.; Rovira, C.; Ruis, J.; Veciana, J. *Angew. Chem.* **1995**, *107*, 99-103.

62. Romero, F. M.; Ziessel, R.; Bonnet, M.; Pontillon, Y.; Ressouche, E.; Schweitzer, J.; Delley, B.; Grand, A.; Paulsen, C. *J. Am. Chem. Soc.* **2000**, *122*, 1298-1309.
63. MasPOCH, D.; Domingo, D.; Roques, N.; Wurs, K.; Tejada, J.; Rovira, C.; Ruiz-Molina, D.; Veciana, J. *Chem. Eur. J.* **2007**, *13*, 8153-8163.
64. Kawana, M.; Sano, T.; Aloe, J.; Ohashi, Y. *J. Am. Chem. Soc.* **1999**, *121*, 8106-8107.
65. Mitchell, A. R.; Pagoria, P. F.; Coon, C. L.; Jessop, E.S.; Poco, J. F.; Tarver, C. M.; Breithaupt, R.D.; Moody, G. L. *Propellants, Explos. Pyrotech.* **1994**, *19*, 232-239.
66. Suttcliffe, R.; Griller, D.; Lessard, J.; Ingold, K. U. *J. Am. Chem. Soc.* **1981**, *103*, 624-628.
67. Kaba, R. A.; Ingold, K. U. *J. Am. Chem. Soc.* **1976**, 7375-7380.
68. Freed, J. H. *Annu. Rev. Phys. Chem.*, **1972**, *23*, 265-310.
69. Chestnut, D. B.; Phillips, W. D. *J. Chem. Phys.* **1961**, *35*, 1002-1010.
70. Dubois, M.; Guerin, K.; Pinheiro, J. P.; Fawal, Z.; Masin, F.; Hamwi, A. *Carbon* **2004**, *42*, 1931-1940.
71. Panich, A. M.; Shames, A. I.; Nakajima, T. *J. Phys. Chem. Solids* **2001**, *62*, 959-964.
72. Jiao, Y.; Liu, K.; Wang, G.; Wang, Y.; Zhang, X. *Chem. Sci.* **2015**, *6*, 3975-3980.
73. Juchnovski, I.; Kolev, T.; Rashkov, I. *Spectrosc. Lett.* **1985**, *18*, 171-178.
74. Jchnovski, I.; Raschkov, I.; Panayotov, I. *Monatsh, Chem.* **1970**, *101*, 1712-1713.
75. Pons, S.; Davidson, T.; Bewick, A. *J. Am. Chem. Soc.* **1983**, *105*, 1802-1805.
76. Eargle, D. H. *J. Org. Chem.*, **1974**, *39*, 1295-1297.
77. Spectrophotometry and Light-Scattering, *Physical Tests*, *851*, 1-6.

78. Sakamoto, M.; Cai, X.; Fujitsuka, M.; Majima, T. *Chem. Eur. J.* **2006**, *12*, 1610-1617.
79. Johnston, L. J.; Lougot, D. J.; Wintgens, V.; Scaiano, J. C. *J. Am. Chem. Soc.*, **1988**, *110*, 518-524.
80. Yang, F.; Wilkinson, M.; Austin, E. J.; O'Donnell, K. P. *Phys. Rev. Lett.* **1993**, *70*, 323.
81. Hiratsuka, H.; Yamazaki, T.; Maekawa, T.; Hikida, T.; Mori, Y. *J. Phys. Chem.* **1986**, *90*, 774-778.
82. Sakamoto, M.; Cai, X.; Hara, M.; Tojo, S.; Fujisuka, M.; Majima, T. *J. Phys. Chem. A* **2004**, *108*, 8147-8150.
83. Du, Y.; Ma, C.; Kwok, W. M.; Xue, J.; Phillips, D. L. *J. Org. Chem.* **2007**, *72*, 7148-7156.
84. Ahn, M. K. *Macromolecules* **1995**, *28*, 7026-7028.
85. Wilson, D. *Br. Polym. J.* **1988**, *20*, 405-416.
86. Ahn, M. K.; Stringfellow, T.; Fasano, M.; Bowles, K.; Meador, M. A. *J. Polym. Sci. Part B* **1993**, *31*, 831-841.
87. Smirnov, T. I.; Smirnov, A. I.; Clarkson, R. B.; Belford, R. L. *J. Phys. Chem.* **1994**, *98*, 2464-2468.
88. Auteri, F. P.; Belford, R. L.; Boyer, S.; Motsegood, K.; Smirnov, A.; Smirnova, T.; Vahidi, N.; Clarkson, R. B. *Appl. Magn. Reson.* **1994**, *6*, 287-308.
89. Van Fleck, H. H. *The Theory of Electronic and Magnetic Susceptibilities*; Oxford University press: oxford, 1952.
90. Gregory, S. *Phys. Rev. Lett.* **1987**, *40*, 723-725.

91. Vasyukov, D.; Anahory, Y.; Embon, L.; Halbertal, D.; Cuppens, J.; Neeman, L.; Finkler, A.; Segev, Y.; Myasoedov, Y.; Rappaport, M. L.; Huber, M. E.; Zeldov, E. *Nat. Nanotechnol.* **2013**, *8*, 639-644.
92. Jefford, C. W.; Rimbault, C. G. *Tetrahedron. Lett.* **1981**, *22*, 91-94.
93. Foote, C. S. *Acc. Chem. Res.* **1968**, *1*, 104-110.
94. Nagel, J. *Appl. Phys. Lett.* **2011**, *99*.
95. Veauvy, C.; Haselbach, K.; Maily, D. *Rev. Sci. Instrum.* **2002**, *73*, 3825-3830.
96. Hao, L.; Macfarlane, J. C.; Gallop, J. C.; Cox, D.; Beyer, J.; Drung, D.; Schurig, T. *Appl. Phys. Lett.* **2008**, *92*, 192507.
97. Finkler, A. *Nano, Lett.* **2010**, *10*, 1046-1049.
98. Hou, Z.; Miyano, T.; Yamazaki, H.; Wakasuki, Y. *Kidorui*, **1995**, *26*, 314-315.
99. Hou, Z.; Jia, X.; Hoshino, M.; Wakatsuki, Y. *Angew. Chem., Int. Ed. Engl.*, **1998**, *36*, 1292-1294.
100. Hou, Z.; Jia, X.; Fujita, A.; Texuka, H.; Yamazaki, H.; Wakatsuke, Y. *Chem. Eur. J.*, **2000**, *6*, 2994-3000.

BIBLIOGRAPHY

1. Ercolani, G. *J. Phys. Chem. B* **1998**, *102*, 5699-5703.
2. Seeman, N. C. *Angew. Chem.*, **1998**, *110*, 3408-3428.
3. Seeman, N. C. *Angew. Chem.*, **1998**, *37*, 3220-3238.
4. Lehn, J. -M. *Angew. Chem. Int. Ed. Engl.*, **1988**, *27*, 89-112.
5. Schneider, H. -J.; Yatsimirsky, A. Principles and Methods in Supramolecular Chemistry, *VCH, Weinheim*, **2000**.
6. Steed, J. W.; Atwood, J. L. Supramolecular Chemistry, *Wiley, Chichester*, **2000**.
7. Lehn, J.-M. Supramolecular Chemistry: Concepts and Perspectives, *VCH, Weinheim*, **1995**.
8. Rehm, T.; Schmuck, C. *Chem. Commun*, **2008**, 810-813.
9. Tsivadze, A. Y.; Ionova, G. V.; Kostrubov, Y. N. *Russ. Chem. Rev.* **2007**, *76*, 213-233.
10. Marie, R-L.; Christian, P. *Science China Chem.* **2013**, *56*, 24-32.
11. Chi, X.; Xu, D.; Yan, X.; Chen, J.; Zhang, M.; Hu, B.; Yu, Y.; Huang, F. *Polym. Chem.*, **2013**, *4*, 2767-2772.
12. Park, S.; Li, X.; Kim, H. M.; Singh, C. R.; Tian, G.; Hoyt, M. A.; Lovell, S.; Battaile, K. P.; Zolkiewski, M.; Coffino, P.; Roelofs, J.; Cheng, Y.; Finley, D. *Nature*, **2013**, *479*, 512-516.
13. Glusker, J. P. *Top. Curr. Chem.*, **1998**, *198*, 1-56.

14. Israelachvili, J. *Intermolecular & Surface Forces*, Academic Press, London, 2nd edn, **1992**.
15. Kelly, T. R.; Kim, M. H. *J. Am. Chem. Soc.*, **1994**, *116*, 7072-7080.
16. Jeffrey, G. A., *An Introduction to Hydrogen Bonding*, Oxford University Press, New York, **1997**.
17. Legon, A. C.; Millen, D. J. *Chem. Soc. Rev.*, **1987**, *16*, 467-498.
18. Rebek, Jr. J. *Chem. Commun.*, **2007**, 2777-2789.
19. Wang, F.; Ma, N.; Chen, Q.; Wang, W.; Wang, L. *Langmuir* **2007**, *23*, 9540-9542.
20. Takwale, M. G.; Pant, L. M., *Acta. Crystallogr. Sect. B*, **1971**, *27*, 1152-1158.
21. Shimizu, L. S.; Salpage, S. R.; Korous. A. A. *Acc. Chem. Res.*, **2014**, *47*, 2116-2127.
22. Schneider, H. J. *Angew. Chem. Int. Ed.* **2009**, *48*, 3924-3977.
23. Allen, F. H.; Baalham, C. A.; Lommerse, J. P. M.; Raithby, P. R. *Acta Crystallogr. Sect. B.* **1998**, *54*, 320-329.
24. Hunter, C. A.; Sander, J. K. M. *J. Am. Chem. Soc.*, **1990**, *112*, 5525-5534.
25. Battaglia, M. R.; Buckingham, A. D.; Williams, J. H. *Chem. Phys. Lett.*, **1981**, *75*, 421-423.
26. Waters, M. L. *Curr. Opin. Chem. Biol.*, **2002**, *6*, 736-741.
27. Hunter, C. A.; Lawson, K. R.; Perkins, J.; Urch, C. J. *J. Chem. Soc. Perkin. Trans. 2*, **2001**, 651-669.
28. Hwang, J.; Li, P.; Carroll, W. R.; Smith, M. D.; Pellechia, P. J.; Shimizu, K. D. *J. Am. Chem. Soc.* **2014**, *136*, 14060-14067.

29. West, J.; Mecozzi, S.; Dougherty, D. A. *J. Phys. Org. Chem.* **1997**, *10*, 347-350.
30. Cox, E. G.; Cruickshank, D. W. J.; Smith, J. A. S. *Proc. R. Soc. London*, **1958**, *247*, 1-21.
31. Burley, S. K.; Petsko, F. A. *Science* **1985**, *229*, 23-28.
32. Burley, S. K.; Petsko, G. A. *Adv. Protein Chem.* **1988**, *39*, 125-189.
33. Spirko, V.; Engkvist, O.; Soldan, P.; Selzle, H. L.; Schlag, E. W.; Hobza, P., *J. Chem. Phys.* **1999**, *111*, 572-582.
34. Lewis, G. N.; Randall, M. *J. Am. Chem. Soc.* **1921**, *43*, 1112-1154.
35. Gokel, G. W.; Barbour, L. J.; Ferdani, R.; Hu, J. X. *Accounts Chem. Res.* **2002**, *35*, 878-886.
36. Krygowski, T. M.; Fawcett, W. R. *J. Am. Chem. Soc.* **1975**, *97*, 2143-2148.
37. Lauher, J. W. *J. Am. Chem. Soc.*, **1978**, *100*, 5305-5315.
38. Hermes, S.; Witte, T.; Hikov, T.; Zacher, D.; Bahnmuller, S.; Langstein, G.; Huber, L. Fischer, R. A., *J. Am. Chem. Soc.* **2007**, *129*, 5324-5325.
39. Jung, S. H.; Lee, J-H.; Forster, P. M.; Ferey, G.; Cheetham, A. K.; Chang, J-S. *Chem. Eur. J.* **2006**, *12*, 7899-7905.
40. Koshland, D. E. *Angew. Chem. Int. Ed. Engl.* **1995**, *33*, 2375-2378.
41. Hirschberg, J. H. K.; Brunsveld, L.; Ramzi, A.; Vekemans, J. A.; Sibesma, R. P.; Meijer, E. W. *Nature*, **2000**, *407*, 167-170.
42. Beijer, F. H.; Kooijman, J.; Spek, A. L.; Sijbesma, R. P.; Meijer, E. W. *Angew. Chem. Int. Edn. Engl.*, **1998**, *37*, 75-78.
43. Sangeetha, N. M.; Maitra, U. *Chem. Soc. Rev.* **2005**, *34*, 821-836.
44. Sergeev, S.; Pisula, W.; Geerts, Y. H. *Chem. Soc. Rev.* **2007**, *36*, 1902-1929.

45. Li, Z.; Barnes, J. C.; Bosoy, A.; Stoddard, J. F.; Zink, J. I. *Chem Soc. Rev.* **2012**, *41*, 2590-2605.
46. Beer, P. D.; Gale, P. A.; Smith, D. K. *Supramolecular Chemistry*, Oxford University Press, **1998**.
47. Murray-Rust, P.; Glusker, J. P. *J. Am. Chem. Soc.*, **1984**, *106*, 1018-1025.
48. Cram, D. J.; Choi, H.-J.; Bryant, J. A.; Knobler, C. B. *J. Am. Chem. Soc.* **1992**, *114*, 7748-7765.
49. Rebek, Jr, J. *Chem. Commun.*, **2007**, 2777-2789.
50. Vriezema, D. M.; Aragonés, M. C.; Elemans, J. A.; Cornelissen, J. J.; Rowan, A. E.; Nolte, R. J. *Chem. Rev.* **2005**, *105*, 1445-1490.
51. Gibb, C. L. D.; Sundaresan, A. K.; Ramamurthy, V.; Gibb, B. C. *J. Am. Chem. Soc.* **2008**, *130*, 4069-4080.
52. Gunderson, V. L.; Conron, S. M. M.; Wasielewski, M. R. *Chem. Commun.*, **2010**, *46*, 401-403.
53. Flamigni, L.; Ventura, B.; Oliva, A. I.; Ballester, P. *Chem.-Eur. J.*, **2008**, *14*, 4214-4224.
54. Hunter, C. A.; Meah, M. N.; Sanders, J. K. M. *J. Am. Chem. Soc.*, **1990**, *112*, 5773-5780.
55. Fujita, M.; Oguro, D.; Miyazawa, M.; Oka, H.; Yamaguchi, K.; Ogura, K. *Nature* **1995**, *378*, 469-471.
56. Kusukawa, T.; Nakai, T.; Okano, T.; Fujita, M. *Chem. Lett.* **2003**, *32*, 284-285.
57. Haycock, R. A.; Yartsev, A.; Michelsen, U.; Sundstrom, V.; Hunter, C. A. *Angew. Chem. Int. Ed.*, **2000**, *39*, 3616-3619.

58. Moorthy, J. N.; Natarajan, R.; Venugopalan, P. *Angew. Chem. Int. Ed.*, **2002**, *14*, 4317-4320.
59. Brunsveld, L.; Folmer, B. J. B.; Meijer, E. W.; Sijbesma, R. P. *Chem. Rev.* **2001**, *101*, 4071-4097.
60. Li, G.; McGown, L. B. *Science* **1994**, *264*, 249-251.
61. Lee, J. Y.; Painter, P. C.; Coleman, M. M. *Macromolecules* **1988**, *21*, 954-960.
62. Appella, D. H.; Christianson, L. A.; Klein, D. A.; Powell, D. R.; Huang, X.; Barchi, J. J.; Gellman, S. H. *Nature*, **1997**, *387*, 381-384.
63. Nelson, J. C.; Saven, J. G.; Moore, J. S.; Wolynes, P. G., *Science*, **1997**, *277*, 1793-1796.
64. Sakai, N.; Majumdar, N.; Matile, S. *J. Am. Chem. Soc.* **1999**, *121*, 4294-4295.
65. Clark, T. D.; Buriak, J. M.; Kobayashi, K.; Isler, M. P.; McRee, D. E.; Ghadiri, M. R. *J. Am. Chem. Soc.* **1998**, *120*, 8949-8962.
66. Semetey, V.; Didierjean, C.; Briand, J-P.; Aubry, A.; Guichard, G. *Angew. Chem.*, **2002**, *114*, 1975-1978.
67. Nelson, J. C.; Saven, J. G.; Moore, J. S.; Wolynes, P. G. *Science*, **1997**, *277*, 1793-1796.
68. De Santis, P.; Morosetti, S.; Rizzo, R. *Macromolecules*, **1974**, *7*, 52- 58.
69. Clark, T. D.; Buriak, J. M.; Kobayashi, K.; Isler, M. P.; McRee, D. E.; Ghadiri, M. R. *J. Am. Chem. Soc.* **1998**, *120*, 8949-8962.
70. Ghadiri, M. R.; Granja, J. R.; Milligan, R. A.; McRee, D. E.; Khazanovich, N. *Nature*, **1993**, *366*, 324-327.

71. Etter, M. C.; Urbanczyk-Lipkowska, Z.; Zia-Ebrahimi, M.; Panunto, T. W. *J. Am. Chem. Soc.*, **1990**, *112*, 8415-8426.
72. Etter, M. C.; Panunto, T. W. *J. Am. Chem. Soc.*, **1988**, *110*, 5896-5897.
73. Shimizu L. S.; Smith, M. D.; Hughes, A. D.; Shimizu, K. D. *Chem. Commun.*, **2001**, 1592-1593.
74. Mayer, M. F.; Nakashima, S.; Zimmerman, S. C. *Org. Lett.*, **2005**, *14*, 3005-3008.
75. Simic, V.; Bouteiller, L.; Jalabert, M. *J. Am. Chem. Soc.*, **2003**, *125*, 13148-13154.
76. Ranganathan, D.; Lakshmi, C.; Karle, I. L. *J. Am. Chem. Soc.* **1999**, *121*, 6103-6107.
77. Roy, K.; Wibowo, A. C.; Pellechia, P. J.; Ma, S.; Geer, M. F.; Shimizu, L. S. *Chem. Mater.* **2012**, *24*, 4773-4781.
78. Roy, K.; Wang, C.; Smith, M. D.; Pellechia, P. J.; Shimizu, L. S. *J. Org. Chem.* **2010**, *75*, 5453-5460.
79. Dawn, S.; Dewal, M. B.; Sobransingh, D.; Paderes, M. C.; Wibowo, A. C.; Smith, M. D.; Krause, J. A.; Pellechia, P. J.; Shimizu, L. S. *J. Am. Chem. Soc.* **2011**, *133*, 7025-7032.
80. Dawn, S.; Salpage, S. R.; Koscher, B. A.; Bick, A.; Wibowo, A. C.; Pellechia, P. J.; Shimizu, L. S. *J. Phys. Chem. A* **2014**, *118*, 10563-10574.
81. Dewal, M. B.; Xu, Y.; Yang, J.; Mohammed, F.; Smith, M. D.; Shimizu, L. S. *Chem. Commun.* **2008**, 3909-3911.
82. Geer, M. F.; Walla, M. D.; Solnstev, K. M.; Strassert, C. A.; Shimizu, L. S. *J. Org. Chem.* **2013**, *78*, 5568-5578.

83. Arai, T.; Sakuragi, J. Tokumaru, K. *Bull. Chem. Soc. Jpn.*, **1982**, *55*, 2204-2207.
84. Rocklye, M. G.; Salisbury, K. *J. Chem. Soc., Perken. Trans.* **1972**, *2*, 158215-85.
85. Foote, C. S. *Acc. Chem. Res.* **1968**, *1*, 104-110.
86. Geer, M. F.; Walla, M. D.; Solntsev, K. M.; Strassert, C. A.; Shimizu, L. S. *J. Org. Chem.* **2013**, *78*, 5568-5578.
87. Congzhi, Z.; Lei, F. *Curr. Org. Chem.* **2014**, *18*, 1957-1964.
88. Fiedler, D.; Leung, D. H.; Bergman, R. G.; Raymond, K. N. *Acc. Chem. Res.* **2005**, *38*, 349-358.
89. Gibbs, C. L. D.; Sundaresan, A. K.; Ramamurthy, V.; Gibb, B. C. *J. Am. Chem. Soc.* **2008**, *130*, 4069-4080.
90. Schimidtchen, F. P. *Chem. Ber.*, **1981**, *114*, 597-607.
91. Parac, T. N.; Caulder, D. L.; Raymond, K. N. *J. Am. Chem. Soc.* **1998**, *120*, 8003-8004.
92. Fiedler, D.; Pagliero, D.; Brumaghim, J. L.; Bergman, R. G.; Raymond, K. N. *Inorg. Chem.* **2004**, *43*, 846-848.
93. Verbiest, T.; Elshocht, S. V.; Kauranen, M.; Hellemans, L.; Snauwaert, J.; Nuckolls, C.; Katz, T. J.; Persoons, A. *Science* **1998**, *282*, 913-915.
94. Stupp, S. I.; LeBonheur, V.; Walker, K.; Li, L.; Huggins, K. E.; Keser, M.; Amstutz, A. *Science* **1997**, *276*, 384-389.
95. Percec, V.; Glodde, M.; Bera, T.; Miura, Y.; Shiyanovskaya, I.; Singer, K. D.; Balagurusamy, V.; Heiner, P.; Schnell, I.; Rapp, A.; Spiess, H.; Hudson, S.; Duan, H. *Nature* **2002**, *417*, 384-387.

96. Beer, P. D.; Gale, P. A.; Smith, D. K. *Supramolecular Chemistry, Oxford University Press, 1998.*
97. Fujita, M.; Nagao, S.; Ogura, K. *J. Am. Chem. Soc.* **1995**, *117*, 1649-1650.
98. Raynal, M.; Ballestwer, P.; Vidal-Ferran, A.; van Leeuwen, P. W. *Chem. Soc. Rev.* **2014**, *43*, 1734-1787.
99. Samanta, S. R.; Parthasarathy, A.; Ramamurthy, V. *Photochem. Photobiol. Sci.* **2012**, *11*, 1652-1660.
100. Sanghamitra, N. J.; Inab, H.; Kitagawa, S.; Ueno, T. *J. Inorg. Organomet. Polym.* **2013**, *13*, 50-60.
101. Cook, T. R.; Zheng, Y-R.; Stang, P. *J. Chem. Rev.* **2013**, *113*, 734-777.
102. Koblenz, T. S.; Wassenaar, J.; Ree, J. M. H. *Chem. Soc. Rev.* **2008**, *37*, 247-262.
103. Bossart, O.; DeCola, L.; Welter, S.; Calzaferri, G. *Chem. Eur. J.* **2004**, *10*, 5771-5775.
104. Ravanat, J-L.; Cadet, J.; Araki, K.; Toma, H. E.; Medeiros, M. G.; Mascio, P. D. *Photochem. Photobio.* **1998**, *68*, 689-702.
105. Dilling, W. L. *J. Org. Chem.* **1966**, *31*, 1045-1050.
106. Turro, N. J., *Modern Molecular Photochemistry* 1 ed.; University Science Books: CA, 1991; p 628.
107. Shimizu, L. S.; Salpage, S. R.; Korous, A. A. *Acc. Chem. Res.* **2014**, *47*, 2116-2127.
108. Block, H.; Ledwith, A.; Taylow, A. R. *Polymer*, **1971**, *12*, 271-288.
109. Greenstock, C. L.; Johns, H. E. *Biochem. Biophys. Res. Commun.* **1968**, *30*, 21-27.

110. Foote, C. S. *Acc. Chem. Res.* **1968**, *1*, 104-110.
111. Geer, M. F. (2013) Self-Assembled Benzophenone bis-urea macrocycles facilitate selective oxidation by singlet oxygen. (Ch. 2).
112. Arai, T.; Sakuragi, J.; Tokumaru, K. *Bull. Chem. Soc. Jpn.* **1982**, *55*, 2204-2207.
113. Rocklye, M.G.; Salisbury, K. *J. Chem. Soc., Perkin. Trans.* **1973**, *2*, 1582-1585.
114. Bryant, J. R.; Matsuo, T.; Mayer, J. M. *Inorg. Chem.* 2004, *43*, 1587-1592.
115. Zhang, M.; Wang, L.; Ji, H.; Wu, B.; Zeng, X. *J. Nat. Gas. Chem.* **2007**, *16*, 393-398.
116. Silverman, S. K.; Foote, C. S. *J. Am. Chem. Soc.* **1991**, *113*, 7672-7675.
117. Foote, C. S. *Photochem. Photobiol.* **1991**, *54*, 659.
118. Stephenson, L. M.; Grdina, M. J.; Orfanopoulos, M. *Acc. Chem Res.* **1980**, *13*, 419-425.
119. Gomberg, M. *J. Am. Chem. Soc.* **1900**, *22*, 757-771.
120. Nakatsuji, S.; Anzai, H. *J. Mater. Chem.* **1997**, *7*, 2161-2174.
121. Rawson, J. M.; Alberola, A.; Whalley, A. E. *J. Mater. Chem.* **2006**, *16*, 2560-2575.
122. Hicks, R. G. *Org. Biomol. Chem.* **2007**, *5*, 1321-1338.
123. Barash, L.; Wasserman, E.; Yager, W. A. *J. Am. Chem. Soc.* **1967**, *89*, 3931-3932.
124. Bowers, H.; McRae, J.; Symons, M. C. R. *J. Chem. Soc. (A)*, **1971**, 2400-2402.
125. Lin, T.-S. *J. Chem. Phys.* **1972**, *57*, 2260-2264.
126. Qu, B.; Xu, Y.; Shi, W.; Raanby, B. *Macromolecules* **1992**, *25*, 5220-5224.
127. Tsierkezos, N. G.; Ritter, U. *Phys. Chem. Liq.* **2011**, *49*, 729-742.

128. Murai, H.; Imamura, T.; Obi, K. *Chem. Phys. Lett.* **1982**, *87*, 295-298.
129. Woodward, J. R.; Lin, T-S.; Sakaguchi, Y.; Hayashi, H. *Mol. Phys.* **2002**, *100*, 1235-1244.
130. Hisao, M. *Chem. Phys. Lett.* **1982**, *87*, 295-298.
131. Scott, T. A.; Ooro, B. A.; Collins, D. J.; Shatruk, M.; Yakovenko, A.; Dunbar, K. R.; Zhou, H-C. *Chem. Commun.*, **2009**, *1*, 65-67.
132. Bowers, H.; McRai, J.; Symons, M. C. R. *J. Chem. Soc. A* **1971**, 2400-2402.
133. Brezova, V.; Barbierikova, Z.; Zukalova, M.; Dvoranova, D.; Ladislav, K. *Catal. Today* **2014**, *230*, 112-118.
134. Maltar-Strmecki, N.; Rakvin, B. *J. Magn. Reson.* **2012**, *222*, 81-87.
135. Hicks, R. G. *Stable Radicals*; John Wiley & Sons, **2010**.
136. Matsuda, K.; Irie, M. *J. Am. Chem. Soc.* **2000**, *122*, 8309-8310.
137. Hamachi, K.; Matsuda, K.; Itoh, T.; Iwamura, H. *Bull. Chem. Soc. Jpn.*, **1998**, *71*, 2937-2943.
138. Sato, O.; Iyoda, T.; Fujishima, A.; Hashimoto, K. *Science*, **1996**, *272*, 704-705.
139. Ratera, I.; Ruiz-Molina, D.; Vidal-Gancedo, J.; Novoa, J. J.; Wurst, K.; Letard, J.; Rovira, C.; Veciana, J. *Chem. Eur. J.* **2004**, *10*, 603-616.
140. MasPOCH, D.; Domingo, N.; Ruiz-Molina, D., Wurst, K., Vaughan, G., Tejada, J., Rovira, C., Veciana, J. *J. Angew. Chem.*, **2004**, *116*, 1864-1866.
141. Otsuka, T.; Okuno, T.; Awage, K.; Inabe, T. *J. Mater. Chem.* **1998**, *8*, 1157-1163.
142. Akita, T.; Mazakati, Y.; Kobayashi, K. *J. Chem. Soc. Chem. Commun.* **1995**, 1861-1865.

143. Cirujeda, J.; Ochando, L. E.; Amigo, J. M.; Rovira, C.; Ruis, J.; Veciana, J.
Angew. Chem. **1995**, *107*, 99-103.
144. Romero, F. M.; Ziessel, R.; Bonnet, M.; Pontillon, Y.; Ressouche, E.;
Schweitzer, J.; Delley, B.; Grand, A.; Paulsen, C. *J. Am Chem. Soc.* **2000**, *122*,
1298-1309.
145. Maspoch, D.; Domingo, D.; Roques, N.; Wurs, K.; Tejada, J.; Rovira, C.; Ruiz-
Molina, D.; Veciana, J. *Chem. Eur. J.* **2007**, *13*, 8153-8163.
146. Kawana, M.; Sano, T.; Aloe, J.; Ohashi, Y. *J. Am. Chem. Soc.* **1999**, *121*, 8106-
8107.
147. Mitchell, A. R.; Pagoria, P. F.; Coon, C. L.; Jessop, E.S.; Poco, J. F.; Tarver, C.
M.; Breithaupt, R.D.; Moody, G. L. *Propellants, Explos. Pyrotech.* **1994**, *19*, 232-
239.
148. Suttcliffe, R.; Griller, D.; Lessard, J.; Ingold, K. U. *J. Am. Chem. Soc.* **1981**, *103*,
624-628.
149. Kaba, R. A.; Ingold, K. U. *J. Am. Chem. Soc.* **1976**, 7375-7380.
150. Freed, J. H. *Annu. Rev. Phys. Chem.*, **1972**, *23*, 265-310.
151. Chestnut, D. B.; Phillips, W. D. *J. Chem. Phys.* **1961**, *35*, 1002-1010.
152. Dubois, M.; Guerin, K.; Pinheiro, J. P.; Fawal, Z.; Masin, F.; Hamwi, A. *Carbon*
2004, *42*, 1931-1940.
153. Panich, A. M.; Shames, A. I.; Nakajima, T. *J. Phys. Chem. Solids* **2001**, *62*, 959-
964.
154. Jiao, Y.; Liu, K.; Wang, G.; Wang, Y.; Zhang, X. *Chem. Sci.* **2015**, *6*, 3975-3980.
155. Juchnovski, I.; Kolev, T.; Rashkov, I. *Spectrosc. Lett.* **1985**, *18*, 171-178.

156. Jchnovski, I.; Raschkov, I.; Panayotov, I. *Monatsh, Chem.* **1970**, *101*, 1712-1713.
157. Pons, S.; Davidson, T.; Bewick, A. *J. Am. Chem. Soc.* **1983**, *105*, 1802-1805.
158. Eargle, D. H. *J. Org. Chem.*, **1974**, *39*, 1295-1297.
159. Spectrophotometry and Light-Scattering, *Physical Tests*, *851*, 1-6.
160. Sakamoto, M.; Cai, X.; Fujitsuka, M.; Majima, T. *Chem. Eur. J.* **2006**, *12*, 1610-1617.
161. Johnston, L. J.; Lougot, D. J.; Wintgens, V.; Scaiano, J. C. *J. Am. Chem. Soc.*, **1988**, *110*, 518-524.
162. Yang, F.; Wilkinson, M.; Austin, E. J.; O'Donnell, K. P. *Phys. Rev. Lett.* **1993**, *70*, 323.
163. Hiratsuka, H.; Yamazaki, T.; Maekawa, T.; Hikida, T.; Mori, Y. *J. Phys. Chem.* **1986**, *90*, 774-778.
164. Sakamoto, M.; Cai, X.; Hara, M.; Tojo, S.; Fujisuka, M.; Majima, T. *J. Phys. Chem. A* **2004**, *108*, 8147-8150.
165. Du, Y.; Ma, C.; Kwok, W. M.; Xue, J.; Phillips, D. L. *J. Org. Chem.* **2007**, *72*, 7148-7156.
166. Ahn, M. K. *Macromolecules* **1995**, *28*, 7026-7028.
167. Wilson, D. *Br. Polym. J.* **1988**, *20*, 405-416.
168. Ahn, M. K.; Stringfellow, T.; Fasano, M.; Bowles, K.; Meador, M. A. *J. Polym. Sci. Part B* **1993**, *31*, 831-841.
169. Smirnov, T. I.; Smirnov, A. I.; Clarkson, R. B.; Belfod, R. L. *J. Phys. Chem.* **1994**, *98*, 2464-2468.

170. Auteri, F. P.; Belford, R. L.; Boyer, S.; Motsegood, K; Smirnov, A.; Smirnova, T.; Vahidi, N.; Clarkson, R. B. *Appl. Magn. Reson.* **1994**, *6*, 287-308.
171. Van Fleck, H. H. *The Theory of Electronic and Magnetic Susceptibilities*; Oxford University press: oxford, 1952.
172. Gregory, S. *Phys. Rev. Lett.* **1987**, *40*, 723-725.
173. Vasyukov, D.; Anahory, Y.; Embon, L.; Halbertal, D.; Cuppens, J.; Neeman, L.; Finkler, A.; Segev, Y.; Myasoedov, Y.; Rappaport, M. L.; Huber, M. E.; Zeldov, E. *Nat. Nanotechnol.* **2013**, *8*, 639-644.
174. Jefford, C. W.; Rimbault, C. G. *Tetrahedron. Lett.* **1981**, *22*, 91-94.
175. Foote, C. S. *Acc. Chem. Res.* **1968**, *1*, 104-110.
176. Nagel, J. *Appl. Phys. Lett.* **2011**, *99*.
177. Veauvy, C.; Haselbach, K.; Maily, D. *Rev. Sci. Instrum.* **2002**, *73*, 3825-3830.
178. Hao, L.; Macfarlane, J. C.; Gallop, J. C.; Cox, D.; Beyer, J.; Drung, D.; Schurig, T. *Appl. Phys. Lett.* **2008**, *92*, 192507.
179. Finkler, A. *Nano, Lett.* **2010**, *10*, 1046-1049.
180. Hou, Z.; Miyano, T.; Yamazaki, H.; Wakasuki, Y. *Kidorui*, **1995**, *26*, 314-315.
181. Hou, Z.; Jia, X.; Hoshino, M.; Wakatsuki, Y. *Angew. Chem., Int. Ed. Engl.*, **1998**, *36*, 1292-1294